Investigating the Mode(s) of Action of Human B7-1 Small-Molecule Inhibitors

by

Rui Chen

A thesis submitted in partial fulfillment of the requirements for the degree of

Master of Science

in

Pharmaceutical Sciences

Faculty of Pharmacy and Pharmaceutical Sciences
University of Alberta

ABSTRACT

Human B7-1 (hB7-1) is the first and most characterized costimulatory protein from the B7 family, which plays a key role in regulating T-cell functions. It is, therefore, regarded as an important target for the treatment of autoimmune diseases and, potentially, cancers. Given the promising clinical benefits of targeting hB7-1, several hB7-1 specific small-molecule modulators were developed and characterized. However, the binding sites and the mode(s) of action of these molecules are not fully understood and relatively unexplored. Identifying the binding locations and understanding their mode(s) of action may help develop more selective and potent modulators rationally. This thesis, therefore, aimed at closing this knowledge gap, by studying the interactions of hB7-1 and two known small-molecule B7-1 inhibitors, namely inhibitors 1 and 2.

Towards this goal, I established a workflow utilizing various advanced modelling tools. In this workflow, molecular dynamics (MD) simulations were initially performed to relax the hB7-1 protein structures and to reach a low energy state, suitable for further studies. Then I used root mean square deviation (RMSD)-based clustering methods to capture the dominant B7-1 conformations visited by the protein during the MD simulations for subsequent molecular docking studies. Following molecular docking, several docked poses were selected to closely investigate their interactions with B7-1. In this context, MD simulations of the protein/compound complexes were used to refine the structures of the generated complexes and to analyze the interactions between the protein and each tested compound. By studying the stability of the formed complexes and the compounds' binding affinities, I identified two binding sites that were suitable for compounds' binding within B7-1. Inhibitor 1 binds to one site with two orientations, while inhibitor 2 binds to a second site. The hydrogen bond (H-bond) analyses and the binding free

energy decompositions allowed me to understand the interactions of the final selected complexes and to further confirm the findings.

To experimentally validate the modelling results, I expressed and purified the extracellular domain of hB7-1 using an *E. coli* expression system in the form of inclusion bodies as an initial step. Then I recovered the biological function of the aggregated B7-1 through denaturing the proteins followed by refolding them slowly. Two protein purification tools were used to improve the purity of the recombinant proteins, including the immobilized metal affinity chromatography (IMAC) and the size exclusion chromatography (SEC). The preliminary binding assays proved that the recombinant hB7-1 has a limited cytotoxic T-lymphocyte-associated protein 4 (CTLA-4) binding activity, compared to a commercial human B7-1. This could be in part due to the recombinant proteins not correctly folding because of the lack of mammalian chaperons in the bacterial expression system. Expressing the extracellular domain of hB7-1 through the mammalian expression system will be a future direction. Furthermore, using mutagenesis assays to confirm the key residues important for compounds binding predicted through modelling studies will be another future direction.

To my knowledge, this thesis revealed the possible binding site(s) and potential mode(s) of action of hB7-1 small-molecule compounds for the first time. These findings can be used as a good starting point to guide the development of novel hB7-1 small-molecule modulators in the future.

PREFACE

A version of Chapter 1 has been published as a review article: Chen R, Ganesan A, Okoye I, Arutyunova E, Elahi S, Lemieux M Joanne and Barakat K. “Targeting B7-1 in immunotherapy.” Med Res Rev. 2020;40(2):654-682. Chen R and Ganesan A devoted equally.

A version of Chapter 2 will be submitted to the Journal of Molecular Graphics and Modelling.

A version of Chapter 3 will be submitted to the Journal of Membrane Biology.

ACKNOWLEDGMENTS

I would like to express my gratitude to my supervisors, Dr. Khaled Barakat and Dr. Joanne Lemieux who enabled my research and for their support and contribution throughout the course of my degree. I also would like to thank my committee members Dr. John Ussher, Dr. Arno Siraki and Dr. Carlos A. Velázquez-Martínez. Without them, I couldn't achieve my goals.

I wish to thank my lab members, Dr. Aravindhan Ganesan, Dr. Marawan Ahmed, Dr. Subha Kalyaanamoorthy, and Horia Jalily Hasani for their patience and help. I also acknowledge my other lab members Dr. Suryanarayanan Chandrasekaran, Tianhua Feng, Yasser Tabana, and Farag Mosa. Special thanks go to Dr. Tae Chul Moon and Dr. Elena Arutyunova who helped me with my experiments. I would like also to thank Dr. Joydeb Kundu, who performed the surface plasmon resonance assays and analyzed the data. I also appreciate my parents and my brother's encouragement and support, because of them I have the courage to explore the colorful world and enjoy the wonderful life.

In the end, I wish to thank the financial support from the Alberta Cancer Foundation and the Shoppers Drug Mart Graduate Scholarships.

TABLE OF CONTENTS

LIST OF TABLES

LIST OF FIGURES

LIST OF ABBREVIATIONS

TCR	T-cell Receptor
CTLA-4	Cytotoxic T-Lymphocyte-Associated Protein 4
PD-1	Programmed Cell Death 1
APC	Antigen-Presenting Cells
NF-κB	Nuclear Factor-κB
MAP	Mitogen-Activated Protein
IL-2	Interleukin-2
TNF	Tumor Necrosis Factor
IFN	Interferon
MIP	Macrophage Inflammatory Protein
SLE	Systemic Lupus Erythematosus
RA	Rheumatoid Arthritis
TNFRSF	Tumor Necrosis Factor Receptor Superfamily
irAE	Immune Related Adverse Event
mAb	Monoclonal antibody
LCMV	Lymphocytic Choriomeningitis Virus
Treg	Regulatory T-cell
NHL	Non-Hodgkin's Lymphoma
R-EAE	Relapsing-Remitting Experimental Autoimmune Encephalomyelitis
STZ	Streptozotocin
IgV	Ig variable
IgC	Ig constant
hB7-1	Human B7-1
hB7-2	Human B7-2
H-bond	Hydrogen bond
hCTLA-4	Human CTLA-4
hCD28	Human CD28
BMS	Bristol-Myers Squibb
FDA	Food and Drug Administration

HTS	High Throughput Screening
SAR	Structure-Activity Relationships
SPA	Scintillation Proximity Assay
HTRF	Homogenous Time-Resolved Fluorescence
SPR	Surface Plasmon Resonance
TR-FRET	Time Resolved-Fluorescence Resonance Energy Transfer
MHC	Major Histocompatibility Complex
IgSF	Immunoglobulin Superfamily
IS	Immunological Synapse
PD-L1	Programmed Death Ligand 1
MD	Molecular Dynamics
RMSD	Root Mean Square Deviation
MM-GBSA	Molecular Mechanics-Generalized Born Surface Area
3D	Three-Dimensional
PBC	Periodic Boundary Conditions
VDW	Van Der Waals
PME	Particle Mesh Ewald
RMSF	Root Mean Square Fluctuation
MOE	Molecular Operating Environment
PLB	Propensity for Ligand Binding
GAFF	General AMBER Force Field
SASA	Solvent-Accessible Surface Area
VMD	Visual Molecular Dynamics
DBI	Davies-Bouldin Index
SSR/SST	the Sum of Squares Regression) /the Total Sum of Squares
FDA	Food and Drug Administration
E. coli	Escherichia Coli
PTM	Post-Translational Modification
TEV	Tobacco Etch Virus
IB	Inclusion Body
LB	Lysogeny Broth

LBA	LB agar
OD	Optical Density
IPTG	Isopropyl β-D-1-thiogalactopyranoside
SDS-PAG	Sodium Dodecyl Sulfate Polyacrylamide Gel Electrophoresis
Ni-NTA	Nickel Nitrilotriacetic Acid
IMAC	Immobilized Metal Affinity Chromatography
βME	β-mercaptoethanol
SEC	Size Exclusion Chromatography
PVDF	Polyvinylidene Fluoride
BCA	Bicinchoninic Acid
HRP	Horseradish Peroxidase
TMB	3,3′,5,5′-Tetramethylbenzidine
GSH	Reduced Glutathione
GSSG	Oxidized Glutathione
SLS	Sodium Lauryl Sulfate
HEK	human embryonic kidney

CHAPTER 1: TARGETING B7-1 IN IMMUNOTHERAPY[a]

1.1 Introduction

T-cells are major components of the adaptive immune system and include $CD4^+$ helper T-cells and cytotoxic $CD8^+$ T-cells. Both subsets possess antigen-recognition T-cell receptors (TCRs) generated by genetic recombination, which promotes the diversity of T-cell responses against pathogens, self-antigens and mutated tumor epitopes.[1,2] Consequently, T-cells are at the center of many therapeutic interventions in immuno-oncology[3] and autoimmunity.[4] Notably, the blockade of inhibitory receptors such as cytotoxic T lymphocyte antigen-4 (CTLA-4) and programmed cell death 1 (PD-1) using monoclonal antibodies have revolutionized metastatic melanoma and lung cancer treatment.[5,6]

The activation of naïve T-cells is achieved through the interaction of the TCRs with cognate antigen-loaded major histocompatibility complexes (MHC) on the surface of activated professional antigen-presenting cells (APCs, *e.g.*, dendritic cells) (Fig. 1.1).[7]

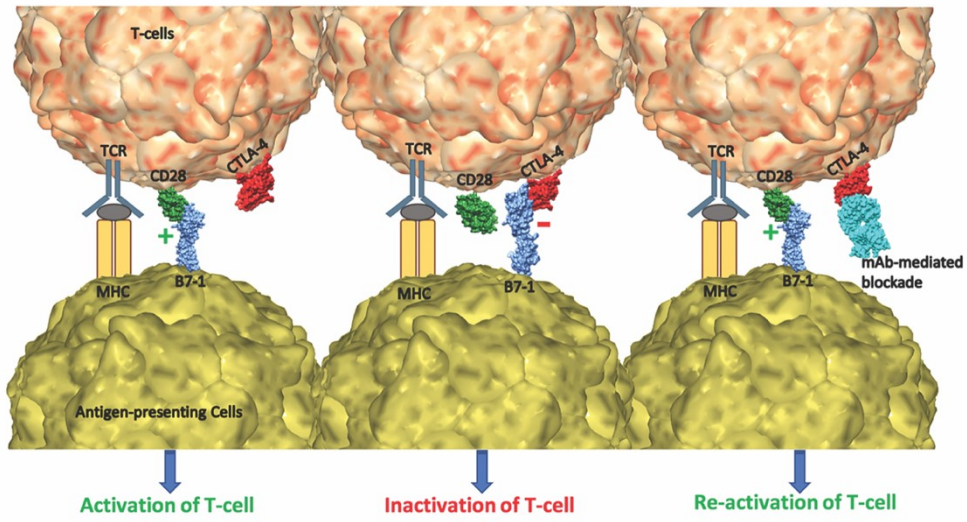

Figure 1. 1 Schematic representation of T-cell-mediated immunological regulation.

Briefly, in the immunological synapse, the T-cells are activated by interactions of the TCR and MHC (signal 1) and CD28 and B7-1 (signal 2 or costimulatory signal). When T-cells are activated, CTLA-4 is transported to the cell surface and outcompetes CD28 to bind with B7-1. The interaction of CTLA-4 and B7-1 results in T-cell inactivation. Therefore, the blockade of B7-1: CTLA-4 interface using mAbs helps in T- cell reactivation. CTLA-4, cytotoxic T lymphocyte antigen-4; MHC, major histocompatibility complex; TCR, T-cell receptor [Color figure can be viewed at wileyonlinelibrary.com]

---

[a]A version of this chapter has been published as a review article: *Chen R, Ganesan A, Okoye I, Arutyunova E, Elahi S, Lemieux M Joanne and Barakat K. "Targeting B7-1 in immunotherapy." Med Res Rev. 2020;40(2):654-682.*

In addition, two secondary signals provided by constitutively expressed positive co-stimulatory molecules and inflammatory cytokines are integral of T-cell proliferation and effector function.[8-10] CD28, mainly expressed by $CD4^+$ helper T-cells, provides a co-stimulatory signal through binding to its ligands (*i.e.* B7-1 or CD80 and B7-2 or CD86), presented on the surface of professional APCs.[11-17] This event, which also drives B-cell activation,[18] serves as a control to maintain self-tolerance. The surface binding of B7-1/2 and CD28, in tandem with the primary TCR signal, activates the nuclear factor-κB (NF-κB), mitogen-activated protein (MAP) kinase and the calcium-calcineurin pathways that elicit the production of numerous factors, including interleukin-2 (IL-2), the α–chain of its receptor, CD25, and the CD40 ligand by T-cells.[19] In addition, the production of other cytokines involved in T-cell function (tumor necrosis factor (TNF)-α, TNF-β and interferon-γ (IFN-γ)) is also induced.[20] Furthermore, these interactions upregulate chemokines (such as macrophage inflammatory proteins (MIP)-α and MIP-β), induce anti-apoptotic protein expression (*e.g.*, Bcl-X and Bcl-2)[20-22] and enhance cell-cycle progression by upregulating the expression levels of D-cyclin.[23,24] Thus, the interactions between CD28 and B7-1/2 are associated with enhanced and sustained T-cell activation. The cells that undergo activation in the absence of co-stimulation become anergic. It must be noted that cytotoxic $CD8^+$ T-cells, on the other hand, rely less on CD28 for co-stimulation and require the interaction of other molecules such as CD27 and 4-1BB with their ligands (CD70 and 4-1BBL respectively) to facilitate stimulation and effector cell differentiation.[25,26] Other co-stimulatory molecules such as ICOS and OX40 consolidate effector T-cell responses once stimulated by their corresponding ligands expressed by APCs.[27-35]

In addition to the expression of constitutive and inducible co-stimulatory molecules, expression of negative regulators or co-inhibitory receptors such as CTLA-4, PD-1, BTLA, TIM-3, LAG-3, and TIGIT is induced in response to T-cell stimulation and activity.[36-55] In particular, the CD28-B7 interaction is counteracted by CTLA-4, a negative co-stimulatory molecule and a structural homolog of CD28, which competes for binding to B7-1 and B7-2, at a much higher affinity.[44,56-58] In contrast to CD28, the interactions between CTLA-4 and B7-1/2 trigger an inhibitory signal that negatively regulates T-cell responses. The up-regulation of co-inhibitory receptors serves an important role in maintaining the balance between chronic T-cell activation and the onset of gross immunopathology.[2,59-61] The associations of B7-1 with CD28 and CTLA-4, therefore, are crucial for immune responses against viral/microbial infections, cancers, autoimmunity, and graft rejection.[62-66] Apart from CD28 and CTLA-4, B7-1 has also been reported

to interact with PD-L1 expressed by T-cells, B-cells, DCs and macrophages.[67] The interaction between B7-1 and PD-L1 *in vitro* provides an inhibitory signal, depicted by reduced T-cell activation and cytokine production.[67] Binding of PD-L1 to B7-1 provides another level of T-cell regulation during anti-tumor responses and graft versus host disease.[68,69] Interestingly, a few studies have demonstrated that PD-L1 and B7-1 can interact in *cis* on the same cell as a mechanism to block interaction with PD-1 or CTLA-4 and corresponding T-cell inhibition.[70,71] Therefore, the molecules of B7-CD28 family play crucial roles in regulating T-cell mediated immune responses, which make them potential immunotherapy targets.[12-15,17,27-31,44-46,57,58,67,72-85] In support of this are observations of increased expression of B7 family members in various cancers.[86,87] For example, there is evidence that certain solid tumors express low levels of B7-1 and B7-2, leading to concomitant binding by CTLA-4 and inhibition of anti-tumor responses.[88,89] Other studies have shown that differential expression of B7-1 and B7-2 by cells in hematological malignancies corresponds with disease prognosis.[90,91] Unsurprisingly, B7 pathways are also implicated in autoimmune diseases such as systemic lupus erythematosus (SLE) and rheumatoid arthritis (RA).[92] In agreement, strategies to alleviate the lymphoproliferative disease by targeting the interactions of CD28 with B7-1/2 have implemented in SLE mouse models.[93,94] In addition, a number of new immune checkpoint proteins associated with the B7-CD28 family and other families (tumor necrosis factor receptor superfamily or TNFRSF,[33-35,95-107] for example) have been discovered (Table 1). Thus, developing novel strategies for targeting immune checkpoints remains an important focus of research in immunotherapy. Nevertheless, it should be acknowledged that there are also important challenges in such immunotherapy strategies such as the development of immune-related adverse events (irAEs).[108,109]

In this chapter, I present a comprehensive overview of B7-1, as an example of the B7 family of co-stimulatory molecules. I focus on the structures of B7-1 and its modes of interaction with CD28 and CTLA-4. Subsequently, I summarize the previous efforts and the implications of targeting B7-1 with specific inhibitors. As discussed in this review, earlier B7-1 drug discovery campaigns focused on B7-1 as a target for the treatment of autoimmune diseases to facilitate organ transplantation.[110,111] These efforts were centered on blocking the interaction between B7-1 and CD28, hence, suppressing T-cell responses. In this regard, all known drugs targeting B7-1 are summarized in this review. The application of B7-1 inhibitors in cancer is limited to hematological

malignancies and current strategies and research directions are also discussed. Finally, I discuss the challenges and perspectives facing the design of potent small-molecule inhibitors of B7-1.

Table 1. 1 Selected immune checkpoint proteins that modulate T cell functions.

Ligands	Receptors	Roles	References
Immune checkpoints from B7 Family			
B7-1 (CD80)	CD28	Co-stimulation	13-15,44,58,67
	CTLA-4	Co-inhibition	
	B7-H1	Co-inhibition	
B7-2 (CD86)	CD28	Co-stimulation	12,17,57
	CTLA-4	Co-inhibition	
B7-DC (PD-L2, CD273)	PD-1(CD279)	Co-inhibition	45,46,72
	Unknown	Co-stimulation	
B7-H1 (PD-L1, CD274)	PD-1 (CD279)	Co-inhibition	45,67,73,74
	B7-1	Co-inhibition	
	Unknown	Co-stimulation	
B7-H2 (ICOSL, CD275)	ICOS (CD278)	Co-stimulation	27-31
	CD28	Co-stimulation	
	CTLA-4	Unknown	
B7-H3 (CD276)	Unknown	Co-inhibition	75,76
B7-H4 (VTCN1, B7x)	Unknown	Co-inhibition	77,78
B7-H5 (VISTA, PD-1H)	Unknown	Co-inhibition	79,80
B7-H7 (HHLA2)	TMIGD2 (CD28H)	Co-stimulation	81-85
	Unknown	Co-inhibition	
Other immune checkpoints from Ig superfamily			
MHC-II	LAG-3 (CD223)	Co-inhibition	36-39
LSECtin		Co-inhibition	
Gal-3		Co-inhibition	
Gal-9	TIM-3 (HAVCR2)	Co-inhibition	40-43
HMGB1		Co-inhibition[a]	
CEACAM-1		Co-inhibition	
CD155 (PVR)	TIGIT (WUCAM)	Co-inhibition	51-53
CD112 (PVRL2)		Co-inhibition	
HVEM (TR2, CD270)	BTLA (CD272)	Co-inhibition	47-50
Immune checkpoints from tumor necrosis factor (TNF) receptor family			
GITRL	GITR (CD357)	Co-stimulation	95-97
4-1BBL(CD137L)	4-1BB (CD137)	Co-stimulation	98-100
CD70	CD27	Co-stimulation	101-104
CD40L (CD154)	CD40	Co-stimulation	105-107
OX40L (CD252)	OX40 (CD134)	Co-stimulation	33-35

[a]: TIM-3 binds to HMGB1 and interferes with the nucleic acids-mediated activation in innate immunity. Except for modulating T-cells' function, several immune checkpoint proteins also regulate the function of other immune cells.

1.2 The Significance of B7-1/2-CD28/CTLA-4 Interactions in Immunity

B7-1 antigen was first identified on a subpopulation of human splenic B-cells that responded rapidly to activation and proliferation signals.[13] Shortly thereafter CD28 and CTLA-4 were identified as receptors for B7-1.[44] The discovery of B7-2 stemmed from experiments that demonstrated that mice deficient of B7-1 were able to induce co-stimulation and interact with CTLA-4.[17] In early studies, the expression of B7-1 and B7-2 were demonstrated in B-cells, T-cells, dendritic cells and APCs.[13,112,113] Expression of B7-1 and B7-2 by APCs was shown to be sequential, where B7-2 being constitutively expressed and upregulated in response to stimulation, whilst B7-1 was detected at later time points. This highlights the differences in the abilities of B7-1 and B7-2 to initiate or promote T-cell responses.[112-114] Indeed, previous studies have documented differential expression of B7-1 and B7-2 by APCs such as B-cells and monocytes; correlating with the mediation of co-stimulation, subsequent T-cell proliferation, and IFN-γ production.[112,113] However, in previous studies (carried out *in vitro* using human peripheral blood mononuclear cells or splenocytes),[112,113] there were contrasting conclusions regarding the specific roles of B7-1 and B7-2 in the induction of T-cell activation and proliferation. Results were dependent on differences in epitope affinity of B7-1/2 monoclonal antibodies (mAbs), stimuli and type of APC used for induction of T-cell activation[112,113]. These studies indicate that the kinetics of B7-1 and B7-2 expression are required for the maintenance and initiation of T-cell responses, respectively.[115,116]

The role of these ligands in mediating various aspects of T-cell activity (proliferation, trafficking, memory cell differentiation, cytotoxicity, T helper cell differentiation, *etc.*) in response to various pathogens, tumor development, and autoimmunity have been studied.[117,118] Other studies imply that antigen-load, exposure, T-cell subsets and their dependence on other co-stimulatory pathways govern the necessity for B7-1/2.[114] For instance, the differential impact of B7-1 and B7-2 on T-cell activation and subsequent effector function was investigated using a mouse model of allergic rhinitis.[119] In this model, blockade of B7-1 inhibited Th2-associated responses, which included IgE production, nasal eosinophilia, and the production of IL-4 and IL-5 by nasal lymphocytes.[119] These observations indicate that distinct requirements for B7-1 and B7-2 may be dependent on expression in sites of tissue tropism or effector cells and the nature of the stimulus. For instance, the absence of B7-1 and B7-2 in both chronically and acutely infected mice with lymphocytic choriomeningitis virus (LCMV) correlated with impaired virus-specific T-cell memory and viral persistence in the lungs.[120] In contrast, CD28-deficient mice exhibited less $CD8^+$

T-cell dysfunction and viral persistence.[120] As a matter of fact, several studies have demonstrated the importance of both co-stimulatory ligands in promoting anti-microbial T-cell responses.[117,121,122] Lumsden *et al.* have identified a role for B7-1 in influenza-infected mice treated with anti-B7-1 antibody (Y100F-Ig).[123] Compared with mice treated with CTLA-4Ig, Y100F-Ig-treated mice had impaired lung effector function characterized by reduced IFN-γ production and decline in virus-specific $CD8^+$ T-cells in the lungs and bronchoalveolar lavage fluids.[123] These results imply that the requirements of B7-1 or B7-2 are mainly driven by the nature of infections and elicited effector cells.

Also of importance is the occurrence of CD28-independent B7 pathways, possibly driven by CTLA-4, which also influences the nature of T-cell responses in certain scenarios.[115] Although studies using B7-1/2 knockout mice demonstrate their requirement for promoting T-cell responses they do not provide information regarding the specific role of T-cell intrinsic B7-1 and B7-2 in shaping T-cell responses. The acquisition of B7-1 by naïve CD4+ T-cells from APCs during activation as shown in a study by Sabzevari *et al.* results in both stimulatory and regulatory responses by T-cells.[124] Naïve $CD4^+$ T-cells were able to present antigens to other T-cells following the acquisition of B7-1 from APCs. The acquisition of B7-1 by T-cells was dependent on its expression by APCs[125]. On the other hand, the acquisition of B7-1 by memory T-cells promoted apoptosis, which was dependent on the strength of TCR signaling.[124] In a study by Taylor *et al.*, the immunoregulatory aspect of activation-induced B7 expression by T-cells, B7-2, in this case, was also demonstrated.[16] In comparison to T-cells from mice deficient in B7-1 and B7-2, T-cells from B7-2 T-cell transgenic mice promoted significantly reduced graft versus host disease-associated mortality.[16] This immunoregulatory mechanism was shown to occur through the interaction of B7-2 with CTLA-4, which is upregulated in response to sustained or exaggerated TCR stimulation.

The interaction of B7-1/2 with CTLA-4 expressed by conventional T-cells is characterized by the triggering of inhibitory signals. Early studies demonstrated that CTLA-4 ligation impacted mainly the amplification of T-cell responses, in the form of IL-2 production and provision of 'help' for antibody production[126] and memory T-cell formation.[127] Its higher affinity for B7-1/2 in comparison to CD28 forms the basis of T-cell tolerance required to control the activity of self-reactive T-cells.[128,129] The upregulation of CTLA-4 by conventional 'exhausted' T-cells in response to sustained antigen exposure provides another level of control against T-cell-induced

immunopathology.[130-132] In addition to CTLA-4, exhausted T-cells co-express multiple inhibitory receptors such as PD-1, TIM-3, and TIGIT, which correlates with defective IL-2 production and cell proliferation.[130,133] Dysregulation of T-cell responses in the absence of CTLA-4 is mirrored by the occurrence of gross autoimmunity in genetically deficient mice.[134] This occurrence is probably due to the synergistic effect of the unregulated activity of conventional T-cells, to a small extent and the absence of regulatory T-cells (Tregs), the major T-cell subset that expresses CTLA-4, to a larger extent.[135]

Notwithstanding the source of CTLA-4 (Tregs or conventional T-cells) that competes with CD28 expressed by conventional T-cells for binding to B7-1/2, the subsequent inhibition of T-cell responses has implications for autoimmunity and the control of pathogens or tumor growth. The existence of such extrinsic inhibitory signaling mechanisms whereby Tregs compete with conventional T-cells for B7-1/2 interaction by expressing increased levels of CTLA-4, preferential aggregation and continual interaction with APCs, or intrinsic inhibition by CTLA-4 present on conventional T-cells,[136] formed the basis of checkpoint blockade strategies for the reinvigoration of T-cell responses. The targeting of CTLA-4 using monoclonal antibodies has revolutionized the immunotherapy of cancers, particularly melanoma and some solid tumors such as renal carcinoma and non-small cell lung cancer.[137,138] Tumor rejection in response to CTLA-4 blockade has been attributed to the restoration of anti-tumor T-cell function in the tumor microenvironment, induction of naïve T-cell stimulation in lymphoid organs[139] in addition to depletion of Tregs in the tumor microenvironment.[140] However, the absence of the "CTLA-4-associated brake" is reflected by the induction of a plethora of irAEs in treated patients ranging from diarrhea and colitis to organ-specific events such as hepatic failure and uveitis.[141-143] Consequently, new strategies for targeting B7-1 (and B7-2) instead will have to account for the predominance of either extrinsic or intrinsic CTLA-4 signaling, which will depend on the strength of antigenic stimulation and the ratio of elicited Tregs to conventional T-cells.[138,144]

1.3 B7 Ligands in Cancer and Autoimmunity

The constitutive expression of B7-1 and B7-2 is a hallmark of hematological malignancies such as non-Hodgkin's lymphoma (NHL), classic Hodgkin's lymphoma, multiple myeloma, and chronic lymphocytic leukaemia.[86,145] The significance of B7-1/2 expression by malignant cells in relation to prognosis is somewhat unclear. According to a study by Pope *et al.,*[146] the expression

of B7-2 by plasma cells from myeloma patients was indicative of poor survival and high tumor load.[146] However, plasma cells from the patients in this study lacked B7-1. This could be explained by the observations from another study by Chaperot *et al.*, in which the authors demonstrated that co-expression of B7-1 and B7-2 by malignant B-cells correlated with effective immunogenicity based on their ability to induce T-cell proliferation in a mixed lymphocyte reaction.[145] Based on these observations one may conclude that the relative expression of B7-1 and B7-2 by malignant cells dictates the prognosis of hematological malignancies. Immune suppression through the interaction between B7-1 expressed by malignant cells and non-malignant cells with PD-L1 has been shown to promote tumor progression in NHL.[67,68] In this regard, it is likely that targeting this interaction will restore anti-tumor responses. Studies that have investigated the cross-linking of B7-1 expressed by lymphoma cells with antibodies *in vitro* reported inhibition of cell proliferation, upregulation of proapoptotic molecules and the induction of antibody-dependent cell-mediated cytotoxicity.[147,148] This has formed the rationale for the development of galiximab, a chimeric, anti-B7-1 monoclonal antibody (section 5).[148]

The autoimmunity landscape is shaped by multiple co-stimulatory and co-inhibitory pathways, which are implicated in priming autoreactive T-cells and inhibition of autoimmune T-cell responses (reviewed in Zhang and Vignali, 2016).[92] Similar to infections, differential expression of B7-1 and B7-2 in different anatomical locations, temporal dynamics, and their function, governs the pathogenesis, regulation and therapeutic strategies associated with autoimmune diseases. For instance, differential upregulation of B7-1 on splenic and CNS-infiltrating B-cells, T-cells and macrophages relative to B7-2, was observed in mice induced with relapsing-remitting experimental autoimmune encephalomyelitis (R-EAE).[149] These phenotypes correlated with the predominance B7-1 to induce T-cell activation in this system. Interestingly, R-EAE induction did affect the predominant expression of B7-2 by lymph node APCs.[149] Kinoshita *et al.*, in their study, have demonstrated a dual requirement for both B7-1 and B7-2 co-stimulatory pathways in the pathogenesis of autoimmune lupus.[94] B7-1 and B7-2 were expressed by kidney-infiltrating leukocytes, which correlated with progressive nephritis in MRL-Fas^{lpr} mice.[94] This phenotype was confirmed by the absence of kidney pathology, proteinuria and increased survival observed in MRL-Fas^{lpr} mice deficient in B7-1 and B7-2.[94] The progressive expression of B7-1 and B7-2 by pancreatic lymph node cells in streptozotocin (STZ) induced insulin-dependent diabetes has been described.[150]

The positive outcomes from pre-clinical studies on targeting CD28 and CTLA-4 have given way to clinical trials and subsequently, FDA approval of CTLA-4Ig (abatacept), which selectively binds to B7-1 and B7-2, for treatment of RA.[110,151] Abatacept is also in clinical trials for SLE arthritis and primary biliary cirrhosis.[48,85,152] In addition, belatacept, a derivative of abatacept, has demonstrated increased potency in inhibition of renal transplant rejection.[153-155] Irrespective of the remarkable progress in the alleviation of various autoimmune syndromes by targeting B7: CD28 "first-line" pathways,[92] understanding the relative roles, kinetics and tissue-specificity of "second-line" pathways are integral to novel therapeutic strategies.

1.4 Structures of B7-1 and its Complexes with CTLA-4 and CD28

B7-1 is a transmembrane glycoprotein, which has a molecular weight of ~45-70 kDa.[20] A mature B7-1 (of 254 residues) includes an extracellular segment (of 208 residues), a transmembrane anchor (of 21 residues) and a short cytoplasmic tail (of 25 residues).[156] The extracellular segment is made of two domains, namely, a membrane-distal Ig variable-like (IgV) domain and a membrane-proximal Ig constant-like (IgC) domain (Fig. 1.2).[13,14] Structurally, the N-terminal IgV domain includes an antiparallel β sheet topology of nine strands, forming AGFCC'C" sheets on one layer and BED sheets on the other layer (Fig. 1.2A). The IgC domain presents a typical C1-set β sandwich topology formed by seven strands, arranged as ABED and GFC layers (Fig. 1.2A).[14,157] The extracellular domains of B7-1 (IgV and IgC) are linked by a short seven-residue long loop. As has been demonstrated in the X-ray crystal structure of soluble B7-1 (PDB ID: 1DR9),[14] this interdomain region buries a surface area of ~670 $Å^2$ and is formed by a hydrophobic core of residues, bordered by electrostatic interactions and interdomain hydrogen bonds (H-bonds) (as shown in Fig. 1.2A). B7-1 is known to exist as a homodimer, which is mainly facilitated by the IgV domains of two B7-1 monomers and particularly through their BED faces and the interconnecting loops (Fig. 1.2B).[14,58] The main inter-monomer interactions of a B7-1 dimer are mediated by hydrophobic residues, Val11, Val22, Gly45, Met47, Ile58, Asp60, Ile61, Thr62 and Leu70 from each monomer.[14] The dimer interface of B7-1 IgV domains buries a large surface area of 1220 Å.[214,57]

B7-1 shares ~25% extracellular domain sequence identity and high structural similarity with its homologous ligand B7-2, which is another type-1 surface protein of APCs. There are 22 conserved residues in human B7-1 (hB7-1) and human B7-2 (hB7-2) IgV domain sequences.

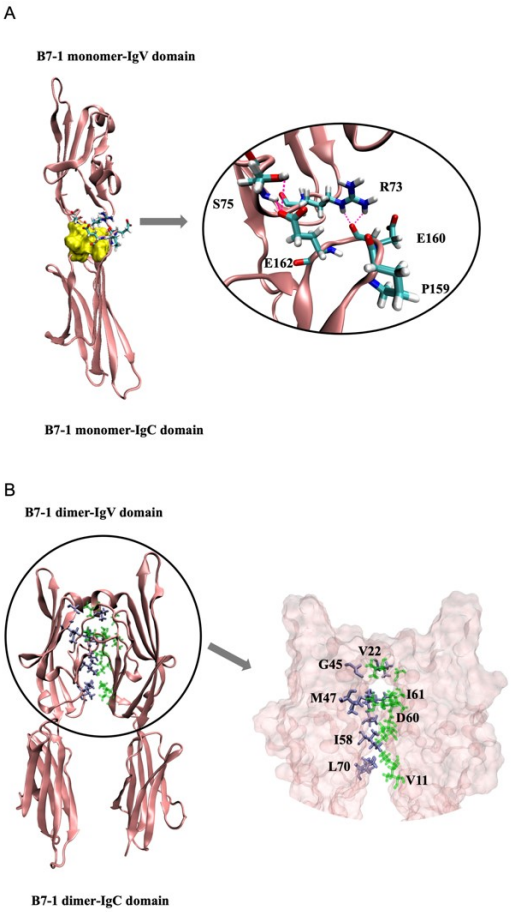

Figure 1. 2 The structures of human B7-1 monomer and a homodimer.

A, The structure of the extracellular domain of a B7-1 monomer (PDB ID: 1DR9) is shown as cartoon representation in pink, and the hydrophobic core within the interdomain area formed by residues Val8, Pro74, Ala106, Phe134, and Leu163 are represented as surface representation in yellow. The key residues engaging in interdomain H-bond interactions (*i.e.*, distance ≤3.2 Å) are shown in stick representations and also in a zoomed-in inset figure. B, The structure of a B7-1 homodimer extracted from PDB ID: 1I8L is shown as a cartoon representation in pink. The zoomed-in inset figure on the right shows only the IgV domains from the two monomers in surface representations and the key residues interacting at the dimer interface are shown in stick representations. The residues from chain A are shown in ice blue color and those in the alternate chain are shown in green. All the structures were generated by visual molecular dynamics version 1.9.4a12. IgV, Ig variable-like; PDB, protein database [Color figure can be viewed at wileyonlinelibrary.com]

From the previous report, eight of them are IgSF IgV domain conserved residues, namely Leu14, Cys16, Trp32, Arg56, Asp76, Gly78, Tyr80, Cys82.[157,158] Despite their high structural similarities, unlike B7-1, B7-2 was found to exist as a monomer on the cell surface.[159] This difference in the oligomer state of B7-1 and B7-2 has been proposed as an important factor in the regulation and

organization of macromolecular complexes with their receptors, CD28 and CTLA-4, at the immune synapse.[159,160]

Previous mutagenesis-based studies[161-164] and X-ray crystal structures[14,57,58,160] confirmed that the IgV domain of B7-1 (and B7-2) is mainly involved in the binding to CD28 and CTLA-4; whereas, the IgC domain is predominantly involved in cell-surface adhesion of B7-1,[58] although possibly having some indirect effects of receptor-ligand binding.[14,163,165] For example, Girard *et al.* explained through a quantitative cytofluorometric method that the presence of the IgC domain in B7-1 (and B7-2) is important for the optimal receptor binding.[165] The deletion of this IgC domain significantly diminished its binding to both CD28 and CTLA-4. An earlier mutagenesis-based study by Peach *et al.* also reported the key hydrophobic residues in the IgC domain of B7-1 that could be involved in the binding of B7-1 to CD28 and CTLA-4.[163] CD28 and CTLA-4 are homologous transmembrane proteins that are expressed on the T-cell surface and are known to exist as homodimers. Their extracellular domains share ~28% sequence-level conservation and a single IgV domain (note that IgC is absent) that exhibit almost similar topology made of two faces: ABED and A'GFCC' strands.[58,162,166,167] The ABED face in the receptors is involved in the homodimer interface, whereas their other layer (*i.e.*, A'GFCC') forms a ligand binding face. In particular, CD28 and CTLA-4 share a 100% conserved FG loop made of the ^{99}MYPPPY^{104} residues, which has been reported to play a significant role in the recognition and binding to the B7 ligands (both B7-1 and B7-2). The X-ray crystal structure of human CTLA-4 (hCTLA-4): B7-1 complex (PDB ID: 1I8L)[58] has revealed their binding mode (Fig. 1.3A) and the key interactions that stabilize their complex. The key residues from B7-1, including Tyr31, Met38, Thr41, Met43, Val83, Leu85, Ala91, Phe92, and Leu97, have been found to interact with CTLA-4 (specifically with its ^{99}MYPPPY^{104} loop (Fig. 1.3B).[58] Site-directed mutagenesis experiments confirmed the importance of Tyr31, Met38 along with a few other residues (*e.g.* Arg29, Gln33, Met47, and Trp50) on the IgV domain of B7-1 in the binding to CD28 and CTLA-4.[163] Since both B7-1 and CTLA-4 are homodimers and bivalent, they tend to pack in a remarkable zipper-like arrangement to form a periodic oligomer complex (see Fig. 1.3C). Therefore, the association between CTLA-4 and B7-1 displays an astonishing complementarity shape, high surface affinity and avidity.[56,58]

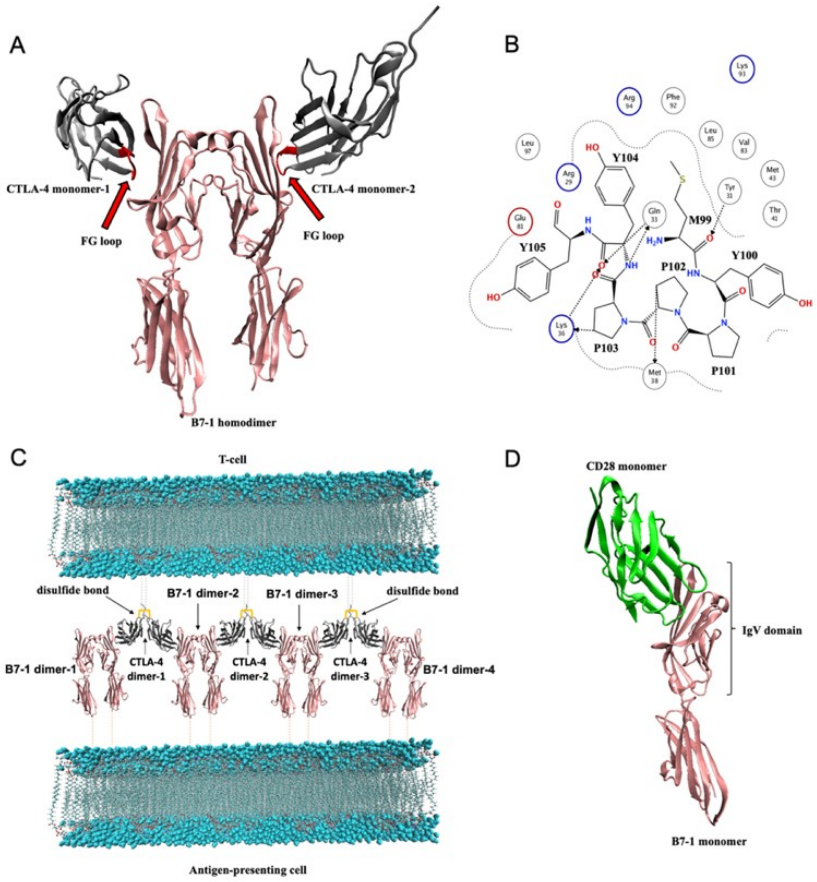

Figure 1. 3 Structures of B7-1: CTLA-4 and B7-1: CD28 complexes.

A, The structure of a B7-1 homodimer (shown in pink) in complex with two CTLA-4 monomers (shown in silver) on their receptor binding faces are presented in a cartoon representation. The $M^{99}YPPPYY^{105}$ motifs forming the FG loop in the CTLA-4 monomers are shown in red and with arrow marks. B, A 2D interaction diagram describing the hydrogen bond interactions between the $M^{99}YPPPYY^{105}$ residues from a CTLA-4 monomer (shown as line representation) and the key residues from its B7-1 binding partner (shown as three-letter amino acid codes and within circles). C, A mock diagram showing a "Zipper-like" arrangement by the association of CTLA-4 (in grey) and B7-1 (in pink) proteins at the immunological synapse formed between a T-cell (shown as lipid layer on the top) and an antigen-presenting cell (shown as a lipid layer at the bottom). Both CTLA-4 and B7-1 are able to form divalent interactions with each other such that a CTLA-4 homodimer is sandwiched between two B7-1 homodimers thereby resulting in a "Zipper-like" chain formation at the synapse. While a B7-1 homodimer is formed by noncovalent interactions, a CTLA-4 homodimer is linked by a disulfide bond formed at the stalk regions of the two monomers (marked in the figure). D, A 3D structural complex of a human CD28 (in green) and a monomer of human B7-1 (in pink). Except for (B), which was generated by molecular operating environment version 2013.08, the other structures were generated by visual molecular dynamics version 1.9.4a12. CTLA-4, cytotoxic T lymphocyte antigen-4 [Color figure can be viewed at wileyonlinelibrary.com]

Nevertheless, in contrast to CTLA-4, CD28 is known to bind the B7 ligands (both B7-1 and B7-2) monovalently.[168] Until now, the experimental structure of B7-1: human CD28 (hCD28): (or B7-2: hCD28) complex was not reported in the literature. Most of the efforts to understand the structures of B7: CD28 complexes were driven through molecular modelling and simulations.[166,167,169] A recent molecular model of B7-1: CD28[167] (Fig. 1.3D) suggested that the key differences between the B7-1: CD28 and B7-1: CTLA-4 complexes were mainly observed on the B7-1 surface.[167] The study also highlighted the key residues such as Thr41, Met43, and Trp50 from B7-1 IgV domain exhibited more significant contributions in binding to the CD28 than that of CTLA-4.[167] Such hotspot differences amongst the two complexes (B7-1: CD28 and B7-1: CTLA-4) could be exploited to develop drugs specific to one of these pathways.

1.5 Fusion Proteins and MAbs Targeting B7-1

The therapeutic benefits of targeting B7-1 interactions have been successfully demonstrated by the use of fusion proteins. By exploiting the strong affinity between CTLA-4 and B7-1, therapeutic proteins were generated by fusing the extracellular IgV domain of hCTLA-4 with a modified human IgG Fc domain in order to specifically target B7-1 and block its interactions with its receptors.[19,170-173] Abatacept, developed by Bristol-Myers Squibb (BMS), became the first-in-class B7-targeted co-stimulation blocker to be approved by the U.S. Food and Drug Administration (FDA) in 2005 for the treatment of RA and Psoriatic arthritis.[151,170] The CTLA-4-Ig in abatacept is the pharmacologically active segment that competes with CD28 and CTLA-4 and binds to B7-1 or B7-2 on APC, thereby blocking the generation of the co-stimulatory signal for T-cell activation. The Fc region in abatacept is constructed by modifying three cysteine residues as well as a proline residue to serine, so as to thwart cytotoxicity effects that are usually mediated by the wild-type human IgG1.[174] A 6-month interim analysis of a 2-year observational trial in Europe and Canada studied the effectiveness, safety and tolerability of intravenously administered abatacept for the treatment of RA.[175] This study concluded that abatacept presents an effective and well-tolerated therapeutic option for RA. In particular, higher retention rates were observed when abatacept treatment was started during the early stage of the disease. Later on, BMS developed a second generation of the fusion protein, namely belatacept, by substituting two amino acids (*i.e.*, L104E and A29Y) in abatacept.[19,176] These specific modifications increased its affinity to B7 ligands and reduced its dissociation rates.[176] Therefore, belatacept was shown to

render more enhanced and longer inhibition of B7-1.[176] Belatacept was approved by the U.S. FDA in 2011 for the treatment of organ transplant, rejection prophylaxis.[19,155,171,172] Belatacept is widely used to avoid rejection in kidney transplantation. However, very recently, Ville and Cantarovich[177] reported that the use of belatacept in their patient who underwent renal transplantation possibly resulted in psoriatic plaques, which progressively disappeared after stopping the use of belatacept. Thus, immunotherapy fusion proteins, despite being mostly clinically efficient, also display adverse effects.[177,178]

Biogen Idec Inc. developed a primatized IgG1 λ mAb, galiximab (or IDEC-114), to target the B7-1 antigen. The variable segment of galiximab was extracted from cynomolgus monkeys and its constant regions were of human nature. It has been demonstrated that galiximab specifically binds to B7-1 and blocks its interactions with CD28 and, to a lesser extent, CTLA-4.[179,180] Therefore, it is proposed that galiximab is able to target B7-1: CTLA-4 interactions and elucidate anti-tumor T-cell immune responses against B-cell lymphomas.[179] Previous *in vitro* and *in vivo* studies have demonstrated that galiximab exhibits promising anticancer activity against different B-cell lymphoma cell lines.[147] In clinical trials, galiximab was mainly tested as a monotherapy or in combination with rituximab (a CD28 mAb) for the treatment of follicular lymphoma.[181] When administered as a single agent, galiximab presented an 11% response rate in follicular lymphoma; whereas, when used in combination with rituximab, the response rate increased to a significant 70% in follicular lymphoma patients.[181,182]

Apart from anti-B7-1 mAbs, many mAbs have been developed to target several other immune checkpoint proteins, such as CTLA-4, PD-1, and PD-L1. For example, the FDA approved mAbs targeting CTLA-4 (ipilimumab), PD-1 (*e.g.*, nivolumab and pembrolizumab) and PD-L1 (*e.g.*, atezolizumab, avelumab and durvalumab) have shown promising effects against metastatic melanoma and/or other cancer types.[6,183,184] In addition, several other mAbs are currently in clinical trials for immune checkpoints therapy. This includes mAbs targeting CTLA-4 (tremelimumab)[185], TIM-3 (LY3321367, MBG453, MEDI9447, TSR-022),[186-189] LAG-3 (BMS-986016, LAG525),[190,191] B7-H3 (enoblituzumab, 8H9),[192,193] GITR (TRX-518, BMS-986156, MK-4166, INCAGN01876, GWN323),[194-198] and OX40 (9B12, MOXR 0916, PF-04518600, MEDI0562, INCAGN01949, GSK3174998)[199-204] to name a few.[205] Despite their significant therapeutic efficacies, mAbs have some important limitations such as their complex production process, instability, high treatment cost, need for intravenous administration, long half-lives, low

bioavailability, immunogenicity, poor localization, inability to penetrate solid tumors, and irAEs.[206-210] Small-molecule inhibitors, on the other hand, can overcome these limitations throughout their high membrane permeability, easy manufacturing, better stability, lower treatment costs, and possibilities for oral administration.[207,211,212] Therefore, there has been growing attraction towards the development of small-molecule inhibitors for immune checkpoints. Nevertheless, it should be noted that developing a specific small-molecule inhibitor is a very complex process and, in many cases, it is not possible to achieve, particularly, for protein-protein interactions. This poses huge limitations and concerns on the use of small-molecule inhibitors in this area. For example, a small molecule that is designed to occupy a specific pocket or a binding site can also interact with many off-targets, such as homologous proteins or ion channel proteins (*e.g.*, the hERG ion channel in the heart) that could induce unwanted side effects. In fact, the inadequate efficiency, toxicity and poor pharmacokinetics of many small-molecule inhibitors have been the main reasons for high attrition rates in pharmaceutical industries.[213-216] Thus, developing small-molecule inhibitors of immune checkpoints with favorable drug-like features, strong efficacy and highly target specificity remain a significant challenge.

1.6 Discovery and Development of Small-Molecule Inhibitors of Human B7-1

Efforts to design small-molecule inhibitors targeting the CD28: B7 interactions began during the late nineties.[217-222] Although initial efforts resulted in either weak[222] or non-specific inhibitors,[218,220,221] a major breakthrough came from Wyeth Research (part of Pfizer Inc.). They reported the discovery and characterization of anti-B7-1 small molecules with nanomolar activity.[217,223] An automated high throughput screening (HTS) assay using the B7-1: CD28 ELISA technique identified two dipyrazolo[3,4-b:3',4'-d] pyridine-3-ones scaffolds, (*i.e.* compound 1 and compound 2) (See Fig. 1.4). The two compounds blocked the B7-1: CD28 interaction with IC_{50} values of 60 ± 17 nM and 30 ± 6 nM, respectively (Fig. 1.4A).[217] The binding of these compounds to hB7-1 was confirmed using equilibrium dialysis experiments, in which a semipermeable membrane separates the protein(s) from the tested small molecule(s). In principle, if a small molecule is a binder to the target protein, it diffuses through the membrane, leading to an increase in the compounds' concentration in the protein side. In this study,[217] the equilibrium dialysis experiments were performed with different Fc chimeras (such as hCTLA-4-Fc, mouse B7-1-Fc, hB7-1-Fc, hB7-2-Fc, and hCD28-Fc) and revealed that the two compounds can bind specifically

to hB7-1. To gain insights on their binding location within hB7-1, the equilibrium dialysis experiments were repeated with different constructs of B7-1. These constructs include the IgV of hB7-1, a B7-1 chimera with human IgV and mouse IgC, a B7-1 chimera with mouse IgV and human IgC, a complex of hB7-1 and IgV-specific antibody, and a complex of hB7-1 and IgC-specific antibody.[217]

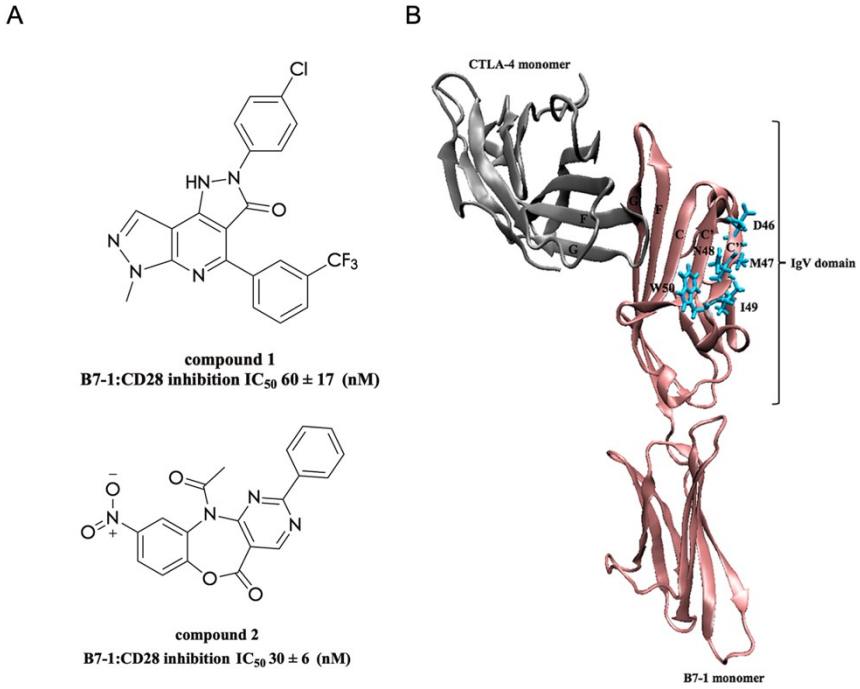

Figure 1. 4 The 2D structures of the most promising small molecule hits targeting human B7-1 (A), along with the probable binding sites for these compounds (B) as reported by Erbe *et al.*

A, Structures of two most promising small-molecule inhibitors (named as compound 1 and compound 2) and their respective IC50 values for the inhibition of B7-1: CD28 interaction are shown. B, The 3D structure of a monomer complex of human B7-1: CTLA-4 complex (from PDB ID: 1I8L) are shown in cartoon representations. The key residues identified to be playing a role in the binding of the reported small molecules through mutagenesis and in vitro binding assays are mapped over the IgV domain of B7-1 in blue. These residues probably form the binding site for the compounds 1 and 2. A, was generated by ChemDraw Prime version 16.0.1.4 (61). B, was generated by visual molecular dynamics version 1.9.4a12. CTLA-4, cytotoxic T lymphocyte antigen-4 [Color figure can be viewed at wileyonlinelibrary.com]

Apparent fold enrichment was seen only in the constructs with an accessible hB7-1 IgV domain, thereby, establishing that both compounds bound to the IgV domain of hB7-1. Subsequently, the binding sites for these compounds on the hB7-1 IgV domain were also explored using mutagenesis and equilibrium dialysis experiments. Of the multiple hB7-1 mutants tested in this study, two

mutants resulted in a loss of binding of the small molecules to hB7-1. These include a mutant in which the wild type ^{46}DMNI^{49} motif was mutated to ^{46}KLKV^{49}; whereas, a single tryptophan residue was mutated to an alanine (W50A) in the other mutant. Mapping them on the surface of hB7-1 (Fig. 1.4B) suggests that these residues are located on the GFCC'C" face of hB7-1 IgV domain in proximity to the B7-1: receptor binding interface. As a result, unsurprisingly, compounds 1 and 2 were found to inhibit the interactions of B7-1 with both CD28 and CTLA-4, although the latter interaction was inhibited with almost 100 times weaker IC_{50} than that of B7-1: CD28 pathway. It was proposed that such differences in inhibition of B7-1: CD28 and B7-1: CTLA-4 interactions were due to the stoichiometry and oligomerization nature of the two complexes. It is known that unlike B7-1:CD28 interaction, B7-1: CTLA-4 complexes are able to form 'zipper-like' arrangements at the immunological synapse (as depicted in Fig. 1.3C). This argument is in correlation with the lack of activity seen for the two compounds when tested in the CHO-cell lines-based cell adhesion assay,[217] which included high avidity protein-protein interactions similar to the physiological conditions.

A follow-up study[219] on understanding the structure-activity relationships (SAR) of the small molecules based dipyrazolo[3,4-b:3',4'-d] pyridine-3-ones was reported. As part of this effort, several derivatives of compound 1 (Fig. 1.4A) were synthesized and their activity towards inhibiting the hB7-1: CD28 interaction was evaluated using the ELISA technique. This study[219] revealed that the core structure of compound 1 (Fig. 1.4A), which encompassed a dipyrazolopyridine group, a chlorophenyl ring, and a trifluoromethylphenyl ring, was important for favorable activity. For example, removal of the chlorophenyl ring or substituting it with alkyl groups led to a complete loss of activity.[219] The chlorophenyl ring was, however, found to be fairly tolerant of functional group changes on its *meta*- and *para*- positions. This study also revealed that the presence of a carboxylate group (CO_2H) at the *meta* position of the chlorophenyl ring along with a *para*-chloro atom exhibited an IC_{50} value of 7 ± 3 nM, which is a ~12-fold increase in the affinity towards the inhibition of B7-1: CD28 interaction. Nevertheless, interchanging the positions of chloro and carboxylate groups exhibited an IC_{50} value of 16 ± 2 nM, which is still better than that of the parent compound (compound 1). Another derivative with a *meta*-methyl ester group and a hydrogen atom at the *para*- position exhibited an IC_{50} of 8 ± 4 nM. Moving the methyl ester group to the adjacent *para*- position, along with the addition of a *meta*-fluoro atom led to a stronger binding to the B7-1 with an IC_{50} value of 12 ± 2 nM. This SAR study[219] also

found that the analogs with longer linear chains and cyclic groups such as morpholine, pyrrolidine, proline acids, and aniline derivatives at either the *para*- or the *meta*-position of the chlorophenyl ring, along with a hydrogen atom at the adjacent site exhibited modest activity (Fig. 1.5A). An analog based on *N*-[3-1-hydroxyethyl) phenyl] group on the chlorophenyl ring exhibited the best activity (IC_{50} = 3 ± 1 nM) towards the inhibition of B7-1: CD28 interaction (Fig. 1.5B). Another simple derivative of compound 1, with a *meta*-fluoro atom in the original chlorophenyl ring along with an electron-withdrawing nitro group (NO_2) in the original trifluoromethylphenyl ring, exhibited potent activity (IC_{50} = 4 ± 1 nM) (Fig. 1.5B). However, most of these potent compounds exhibited low cell-based activity when tested for their ability to block the CD28-PI3 kinase association in Jurkat cells followed by stimulation with CHO-B7-1 cells. Even small cell-based activity was only achieved with relatively high concentrations (50 μM) of the compounds. This suggests that despite having a high affinity towards the target these compounds are unable to compete with highly avid surface interactions of B7-1 and CD28 under physiological conditions.

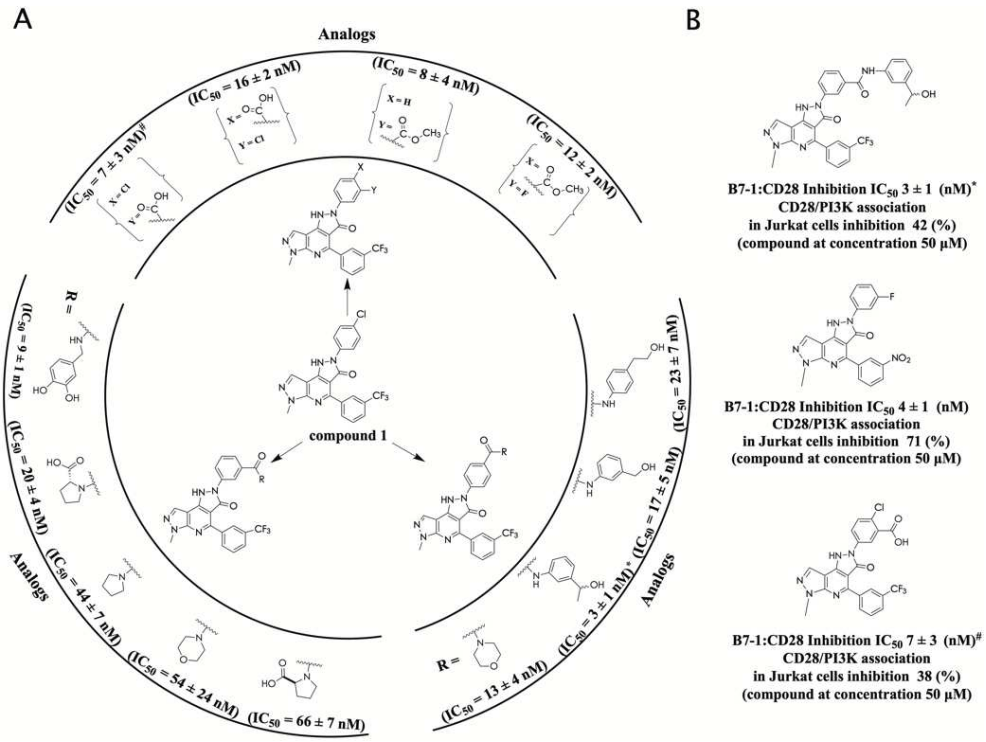

Figure 1. 5 The most active analogs of compound 1 developed through SAR analyses reported by Green *et al*.

A, The 2D structures and activity of some of the most promising analogs toward the inhibition of B7-1: CD28 pathway are shown. B, The cell-based activity of the top 3 inhibitors from this SAR study are shown along with their respective structures and IC50 values. All the structures were generated by ChemDraw Prime version 16.0.1.4 (61). SAR, structure-activity relationship.

Realizing the need to identify inhibitors that are active in the natural biological environment, another study[224] employed a cell-based scintillation proximity assay (SPA) as the primary screening tool to identify compounds for targeting the B7-1: CD28 pathway. In this cell-based SPA assay,[224] B7-1 was presented in a multivalent fashion on the SPA beads (by capture using Ig domain) and CD28 was expressed on the CHO cell lines, while a distance-related energy transfer was monitored for discerning blockers and non-blockers of the target interaction. Screening of a ligand library of 4000 compounds in this cell-based assay resulted in one compound, named here as ligand 1 (Fig. 1.6), which inhibited 61% of the B7-1: CD28 interaction at a 30 μM concentration.[224] Based on this initial hit, 150 analogs were generated and re-screened using the SPA assay, which resulted in at least four compounds (named as ligand 2 – ligand 5 in Fig. 1.6), which showed improved activity in the SPA assay. All these compounds were very similar to the original hit (*i.e.*, ligand 1) with very small modifications. In particular, these compounds possessed a p-benzoic acid in the place of the phenol group in ligand 1, which highlights the benefit of having a carboxyl group towards the activity. For instance, replacing the hydroxyl group in the *para* position of the phenyl ring to a carboxyl group in ligand 2 and ligand 3 has improved their activity to nearly 100% in the cell-based assay. Having an extra fluorine atom in the fused six-membered ring in ligand 3 provided it a slight advantage over ligand 2 in terms of activity. The ability of these compounds to inhibit B7-1: CD28 was also assessed using a cell-free homogenous time-resolved fluorescence (HTRF) assay and the surface plasmon resonance (SPR) assay. Although both ligand 2 and ligand 3 exhibited almost 3 to 5-fold lower IC_{50} values than ligand 1 in HTRF assay, ligand 3 showed the best affinity (~10-fold higher affinity compared to ligand1) in the SPR assay. This was mainly because of a much slower dissociation rate seen in SPR for ligand 3 when compared to all the other tested compounds. Thus, having a fluorine atom on the fused ring, in addition to the p-benzoic acid group on the other end of the molecule, improved the interactions between ligand 3 and the protein. Thus, this study reported low molecular weight compounds that displayed specific and highly potent activity towards the inhibition of B7-1: CD28 pathway.

Another anti-B7-1 small molecule discovery effort[225] resulted in successful translation to clinical trials.[226-229] This work[225] was a follow-up on the compounds reported previously as potent inhibitors of B7-1: CD28 interactions in the cell-based SPA assay.[224] The authors initially reaffirmed the activity of some of the previously reported compounds[224] using a B7-1: CD28 time resolved-FRET (TR-FRET) assay.[225]

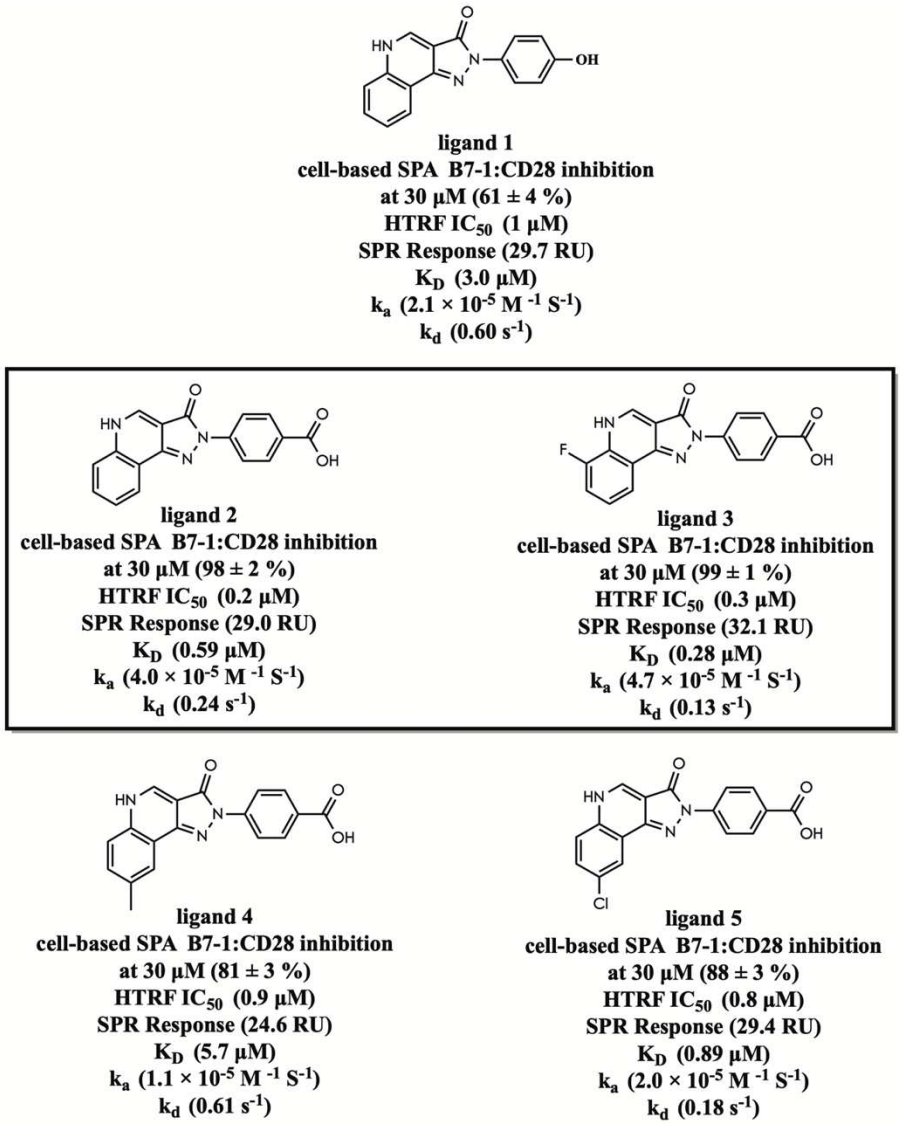

Figure 1. 6 The 2D structures of some of the most active small-molecule inhibitors of human B7-1 reported by Uvebrant *et al*.

All the structures were generated by ChemDraw Prime version 16.0.1.4 (61). The activity data from different assays, including the cell-based SPA assay, HTRF assay, and SPR experiments, are provided for each of the compounds. The topmost compounds are highlighted with a box. HTRF, homogenous time-resolved fluorescence; SPR, surface plasmon resonance. K_D: SPR equilibrium dissociation constant, K_a: cellular assay on-rate, K_d: cellular assay off-rate

This led to the synthesis and *in vitro* screening of several derivatives that eventually resulted in a number of potent small molecules (Fig. 1.7) with nanomolar range activities towards the inhibition of B7-1: CD28 pathway. For example, the best compound from this study (inhibitor 5 in Fig. 1.7) exhibited an EC_{50} value of 1.3 nM in the TR-FRET assay, and its K_D value was also estimated as 1.3 nM by the B7-1: CD28 SPR experiments.

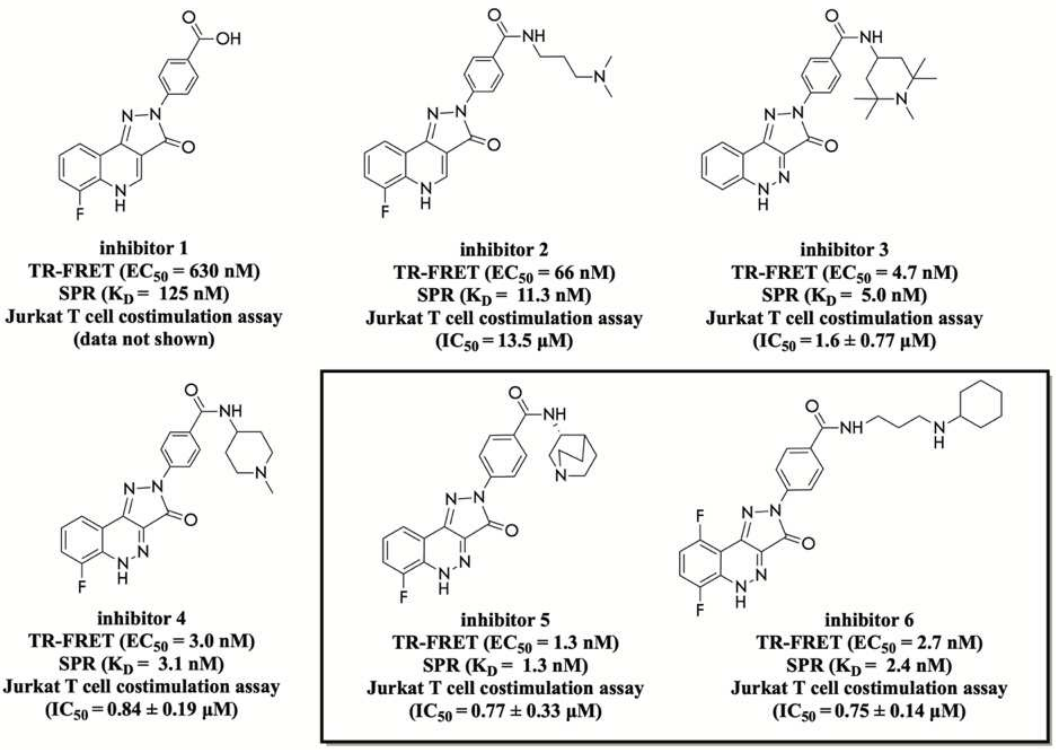

Figure 1. 7 The 2D structures and activity data of some of the most promising compounds developed by Huxley *et al*.

The activity data from different assays, including TR-FRET, SPR and Jurkat T-cell costimulation assay, are provided for each of the compounds. The topmost compounds are highlighted with a box. All the structures were generated by ChemDraw Prime version 16.0.1.4 (61). SPR, surface plasmon resonance; TR-FRET, time resolved-FRET

When tested in the cell-based co-stimulation assays, most of these compounds were confirmed to target the B7-1: CD28 interactions and inhibit the release of proinflammatory cytokines such as IL-2 and IFN-γ, which are downstream signals triggered by the costimulatory signal. However, it should be noted that these compounds were also found to inhibit the B7-1: CTLA-4 interactions, albeit with higher EC_{50} values. This suggests that the compounds are probably bound at a B7-1 site involved in the interactions with both receptors (*i.e.*, CD28 and CTLA-4). The implications from such non-specific targeting of both the CTLA-4 and CD28 pathways by small molecules within the tumor microenvironment or in the autoimmune conditions are still not clear. Further development of these compounds[227,230,231] resulted in the successful advancement of a lead compound named Rhudex into phase 1 clinical trials for the treatment of RA.[228,229]

Since there is no experimental structure for any of the reported compounds in complex with hB7-1, it is difficult to understand their binding modes through which they disrupt the

interactions of B7-1 with its receptors. However, it is possible to hypothesize the binding modes based on any structural consensus that can be seen amongst the reported compounds. In the case of anti-B7-1 compounds, it is interesting to note that all the optimized small molecules resulted from the major drug discovery efforts summarized above[217,219,224,225] exhibit high levels of structural and pharmacophore similarities (Fig. 1.8). Firstly, all these compounds have a core moiety that is made of three fused rings, although the type of rings in different scaffolds vary such as 5:6:5 (as in compound 1 and its analogs), 6:7:6 (as in compound 2), and 5:6:6 (as in ligand 5 and inhibitor 5, for example).

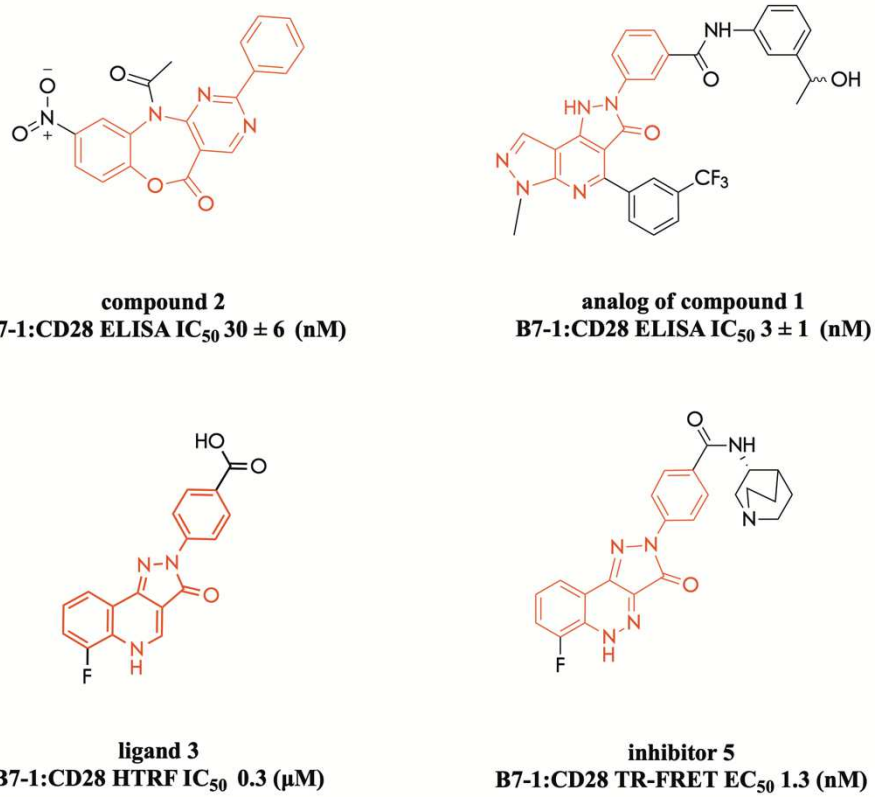

Figure 1. 8 The 2D structures, along with the activity data, of the most optimized compounds from the previous drug discovery efforts for B7-1 target are compared.

The common structural and pharmacophore features among all the structures are shown in red. It can be seen that there is a clear consensus in the structural/pharmacophore properties of the different scaffolds of anti-B7-1 small molecules reported till data, suggesting that they probably target the same site on B7-1. All the structures were generated by ChemDraw Prime version 16.0.1.4 (61) [Color figure can be viewed at wileyonlinelibrary.com]

In addition, at least two of the three fused rings in each case are heterocyclic and include one NH atom as part of a ring as well as a carbonyl moiety. Apart from these, all other compounds have a

phenyl ring on the fused ring. Considering all these similarities amongst different scaffolds of compounds, it could be hypothesized that, in each case, the fused rings are probably placed in a pocket in B7-1, where the NH and carbonyl moieties form hydrogen bonds to stabilize the placement of the fused ring. They could probably bind in an orientation such that the phenyl ring, which binds to the three fused rings in the molecules is projected outwards to disrupt the B7-1 interactions with the receptors. Indeed, this hypothesis is supported by the fact that the structures that have larger substitutions on the *meta* position of the phenyl ring, which binds to the three fused rings exhibited improved activities in the *in vitro* assays. However, either experimental validation or molecular modeling efforts are required to clarify this hypothesis for the binding modes of the most promising anti-B7-1 small molecules.

In terms of inhibition mechanisms, the motivation in most of the drug discovery efforts was to identify a potent small molecule that could bind to the B7-1 surface and directly interfere with its interactions with CD28 or CTLA-4 such that the chain of cytokines (*e.g.*, IL-2 and IFN-γ) associated with T-cell activation can be modulated. This mechanism of action is similar to that exhibited by most of the mAbs targeting immune checkpoints. However, the possibilities of alternate molecular mechanisms cannot be ruled out. For example, it was recently described that a selected class of low molecular weight small molecules bind specifically to the surface of PD-L1 (another important negative immune checkpoint ligand) and induce a non-native dimerization between two PD-L1 monomers.[232] Interestingly, these small molecules induce dimerization on the receptor-binding faces of two PD-L1 monomers such that it becomes merely impossible for them to interact with PD-1 and trigger T-cell inhibitory signal similar to the one generated by B7-1: CTLA-4 pathway.[232] Whether the small molecules discussed here induce PD-L1-like dimerization in B7-1 is still an open question. Thus, revealing the binding modes for the best set of current small molecules against B7-1 will be an important milestone to achieve on the track toward rationally designing a B7-1 inhibitor that can target either pathway, but not both.

1.7 Challenges Facing the Design of Potent Small-Molecule Inhibitors of B7-1

Current modalities targeting hCTLA-4 and hCD28 are still reliant on mAbs and not much progress has been done with respect to small molecules. A major impediment in the development of small-molecule inhibitors of B7-1 is to design compounds that can selectively block the interactions of B7-1 with either receptor. Given the opposite immunological roles of CD28 and

CTLA-4 pathways, non-specifically blocking both of them may not provide the desired therapeutic benefits. The blockade of B7-1: CD28 interaction impedes the costimulatory signal, leading to suppression of T-cells. A compound that can specifically target this costimulatory signal will be suitable for the treatment of autoimmune diseases, where silencing the adaptive self-reactive T-cells is desirable.[233] Further, in the conditions of autoimmune diseases, it is important to not only block the co-stimulatory signal but also activate the co-inhibitory signals from the B7-1: CTLA-4 pathway so as to control the immune flare-ups. In contrast to autoimmune diseases, cancer immunotherapy aims to facilitate the up regulation of co-stimulatory signals. In the tumor microenvironment, the inhibitory signals (from the B7-1: CTLA-4 pathway for example) are dominant, resulting in the suppression of anti-cancer immune responses and evasion by cancer cells. Therefore, an anti-cancer B7-1 inhibitor is required to particularly target the inhibitory B7-1: CTLA-4 association and trigger the co-stimulation by B7-1. Almost all the currently disclosed small-molecule B7-1 inhibitors target both the B7-1: CD28 and the B7-1: CTLA-4 pathways that physiologically leads to a state of anergy. The high levels of structural homology between the B7-1: CD28 and the B7-1: CTLA-4 complexes render a significant challenge. Thus, in depth understanding the molecular level similarities and differences between these two oppositely functioning immune checkpoint complexes may be required to design specific compounds. However, the three-dimensional structure of the B7-1: CD28 complex has not yet been resolved experimentally. Lately, this gap has been partly filled though the construction of molecular models of B7-1: CD28 complex, which helped to highlight some hotspots that discern the binding modes of the B7-1: CTLA-4 and B7-1: CD28 complexes.[167] Such molecular level insights are vital for the rational design of inhibitors that can specifically target either of these two pathways.

1.8 Conclusion

Given its importance in T-cell modulation via the CTLA-4 and CD28 axes, B7-1 has emerged as an important checkpoint target for therapeutic intervention for (predominantly) autoimmune disorders and (lately) cancers. There have been significant efforts to develop specific anti-B7-1 inhibitors, ranging from mAbs to fusion proteins to small-molecule antagonists. In this chapter, I have summarized the immunological roles of B7-1, its structures and interactions with the CD28 and CTLA-4 receptors as well as currently available therapeutic proteins and mAbs and the previous efforts toward developing small-molecule anti-B7-1 compounds. Recent studies

reported different small molecule scaffolds with nanomolar range activity against the B7-1: CD28 interaction. Unsurprisingly, most of them also disrupt the B7-1: CTLA-4 pathway thereby implicating the expected outcome. I have highlighted the interesting structure and pharmacophore similarities amongst these different small molecule scaffolds and hypothesized their probable binding modes within B7-1. Experimental validation to confirm the binding modes of these reported small molecules against B7-1 will be useful to develop more potent and more specific small molecule drugs. Ultimately, achieving this goal will provide a new tool to modulate an important immunotherapeutic target for the treatment of autoimmune diseases and cancers.

RATIONALE, HYPOTHESIS AND OBJECTIVES

RATIONALE

Human B7-1 is an important costimulatory protein from the B7 family and is involved in T-cell regulation. B7-1 is mainly expressed on the surface of activated antigen-presenting cells and regulates immune responses through its interaction with other key immune checkpoint proteins, namely CD28, CTLA-4, and PD-L1. When the B7-1/CD28 costimulatory pathway is blocked, the activation of T-cells is inhibited, leading to the possibility of alleviating autoimmune diseases. However, when the B7-1/CTLA-4 or B7-1/PD-L1 pathways are blocked, T-cells' activity to fight against cancers and chronic infections will be restored. Given its important roles in regulating T-cell activity, several small molecules have been discovered as B7-1 modulators. However, the binding sites and the mode(s) of action of these molecules are still to be fully characterized. Understanding how these molecules interact with hB7-1 may help in rationally designing more selective and more potent hB7-1 modulators. Hence, this thesis aimed at understanding the interactions of hB7-1 and two human B7-1 small-molecule inhibitors in detail.

HYPOTHESIS

I hypothesize that hB7-1 small-molecule inhibitors bind to the IgV domain of hB7-1, where also the binding domains for CTLA-4 and possibly CD28 are located. I also hypothesize that the binding site(s) for the small-molecule compounds in B7-1 overlap with the binding site(s) of CTLA-4 and probably CD28 in B7-1.

OBJECTIVES

To validate the hypotheses, I established the following aims for this thesis.

1) To build a model of human B7-1 with the C-terminal missing structures and carbohydrates included.
2) To study the probable interactions between human B7-1 and its small-molecule inhibitors.
3) To express and purify the extracellular domain of human B7-1 using the bacterial expression system.
4) To confirm the binding activity of the recombinant human B7-1.

CHAPTER 2: UNDERSTANDING THE MODE OF ACTION OF B7-1 INHIBITORS: A COMPUTATIONAL STUDY[b]

2.1: Introduction

T-cells play a central role in mediating immune responses. They combat pathogens and cancer cells[234] and maintain the immune responses against infections while preventing the immune system from attacking self-tissues (*i.e.* autoimmunity).[235] The activation of the naïve T-cells involves the coordination among plenty of proteins on the surfaces of both T-cells and antigen-presenting cells (APCs) (see Table 1.1 in Chapter 1). In this context, three distinct signals are required for T-cell activation. The first signal is triggered when T-cell receptors (TCRs) recognize the antigen fragments presented by the major histocompatibility complex (MHC) on the APCs. The co-receptors CD8 and CD4 expressed on T-cells bind to MHC I and MHC II, respectively to stabilize the complex structure.[236] The engagement of the antigen-specific interaction alone is necessary but insufficient for a complete T-cell activation and the absence of a second signal can lead to T-cell anergy (lack of reaction).[237] Therefore, the second signal, which is also known as the costimulatory signal is required to further activate T-cells.[237] In some cases, the cytokine-based third signal was proven to act directly on naïve T-cells[8] (*e.g.* interleukin (IL)-12, IL-1, interferons (IFN) α/β) or act indirectly on the APCs[238,239] (*e.g.* IL-4, IFN γ) to influence the expression of costimulatory proteins, thus providing extra stimulation towards an optimal T-cell response.

The growing number of T-cell related co-signaling molecules and the cross-linking between them (see Table 1.1 in Chapter 1) add more complexity to fully understand the processes behind T-cell response and activation. Among these co-signaling molecules, are the CD80 (B7-1) and CD86 (B7-2) ligands, which represent well-defined closely related players in the processes of T-cell modulation. Human B7-1 and human B7-2 are two homologous transmembrane glycoproteins from the immunoglobulin superfamily (IgSF), which share the common receptors CD28 and CTLA-4 and have high structural similarity (see Fig. 2.1).[12,14,17,240,241] Both of them consist of an extracellular Ig variable (IgV) like domain and an extracellular Ig constant (IgC) like domain. The two proteins can bind to the T-cell costimulatory receptor CD28 to provide the second signal required for T-cell activation. After T-cell activation, the coinhibitory T-cell receptor CTLA-4 is transported to the cell surface from the intracellular vesicles.[242] CTLA-4 has higher

[b]A version of this chapter will be submitted to the Journal of Molecular Graphics and Modelling.

binding affinities to B7-1 and B7-2, compared to that for CD28, which overcomes CD28 binding to the B7-1/2 proteins. The binding between B7-1/2 and CTLA-4 suppresses T-cell activation.[116,243] The coordinated and exchanged interactions among B7/CD28/CTLA-4 proteins maintain the balance between T-cell activation and inhibition, therefore, controlling T-cell homeostasis. Despite sharing highly structural similarity, human B7-1 and human B7-2 have a limited sequence identity (26 %)[17] and other differences. For instance, hB7-2 is constitutively expressed on the APCs as monomers, favoring to bind to CD28 at the immunological synapse (IS), thus, initiating T-cell activation.[244,245] In contrast, hB7-1 is predominantly expressed as homodimers on the APCs under induction, which helps in recruiting CTLA-4 to the IS, therefore, playing more roles in established T-cell responses, compared to hB7-2.[244,245]

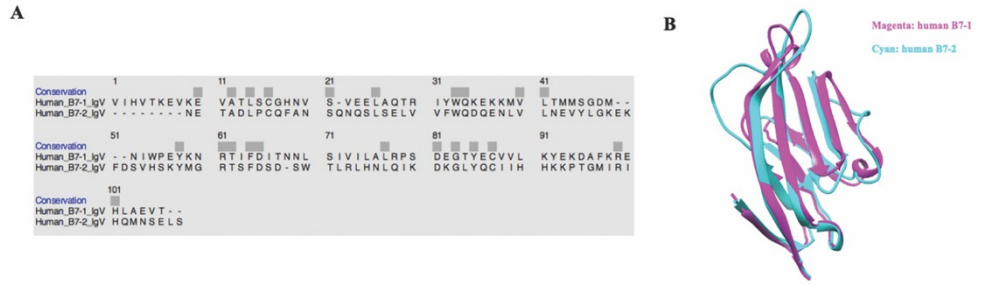

Figure 2. 1 Sequence and structure alignments of the IgV domains of human B7-1 and human B7-2.

A, Sequence alignment was performed by Clustal Omega. Gaps are shown as dash lines, conserved residues in each column are highlighted by gray bars. B, Sequence alignment was performed by Chimera. The structure of human B7-1 (residues 1 to 106, PDB ID: 1DR9) and human B7-2 (residues 0 to 109, PDB ID: 1NCN) are magenta and blue, respectively.

Given their important roles in modulating T cell homeostasis, over the last two decades many researchers were focused on designing modulators for B7-1 and B7-2. For example, the FDA approved two monoclonal antibodies (mAbs) targeting both B7-1 and B7-2, namely abatacept and belatacept for the treatment of rheumatoid arthritis, psoriatic arthritis, and renal transplant rejection.[171,246] As discussed above, B7-1/2 are not only important targets for the treatment of autoimmune diseases but also show great potential as targets for the treatment of cancers.[86,247] In addition to mAbs, efforts to design small-molecule inhibitors of hB7-1 have been reported in the last two decades, which was summarized in our previous work.[248] However, up to now, no literature clearly identified the binding sites or the mode(s) of action of these inhibitors. One attempt to answer that was done by Erbe *et al*.,[249] where they studied the binding of two hB7-1

small-molecule inhibitors (see Chapter 1 Fig. 1.4 A) against different fusing protein constructs of B7-1 and discovered that only the constructs involving IgV domain can bind to both small-molecule inhibitors. This suggested that the binding locations for these two compounds are located in the IgV domain of B7-1, with no major roles for the other parts of the protein to interact with the compounds.

In addition, one of the compounds (named as compound 1 in their study), which was identified through high throughput screening, was used as a parent compound for multiple chemical modifications, accelerating the development of more potent B7-1 small-molecule inhibitors.[219,224,250,251] In order to identify the specific binding site within the IgV domain of hB7-1, Erbe's lab performed mutagenesis assays and concluded that residues Asp46, Met47, Asn48, Ile49, Trp50 might form a direct interaction with both compounds, as the two compounds showed either a loss or a decreased binding to the mutated versions of hB7-1.[249] However, there is a possibility that the mutation of these residues does not directly relate to the binding of the compounds, where it only leads to a conformational change in the hB7-1, thus preventing the binding of these compounds to the protein. In this context, the mutational studies presented by Erbe's lab represent an excellent starting point for a comprehensive modelling study to investigate the interaction of hB7-1 inhibitors with the protein. Some of the current hB7-1 small-molecule inhibitors, bind to hB7-1 with high specificity and nanomolar affinity and were proven to inhibit cytokine (*e.g.* IL-2) release at a sub-micromolar dose in an *in vitro* T-cell costimulation assay.[227,250] Here I focused on two hB7-1 inhibitors (Fig. 2.2 A and B), namely inhibitor 1 and inhibitor 2, which were proved to have good performance in the IL-2 ELISA assays[227] and easier to be synthesized. As for the negative control, I used a human programmed death ligand 1 (PD-L1) small-molecule inhibitor (Fig. 2.2 C), namely BMS-103[252] (renamed as inhibitor 3 in this thesis). The SPR experiments were performed by our group and showed that inhibitors 1, 2, but not inhibitor 3, bind to hB7-1. (see Appendix A)

The current study aims to identify the binding sites of inhibitors 1 and 2 within hB7-1 and to understand their mode(s) of action. To answer this research question, I employed several state-of-the-art computational tools (Fig. 2.3). I first used molecular dynamics (MD) simulations to sample the different protein conformers for the non-bound B7-1 monomer and dimer proteins. Then I used root mean square deviation (RMSD)-based clustering to filter and select the dominant B7-1 conformations from these MD simulations for subsequent molecular docking studies.

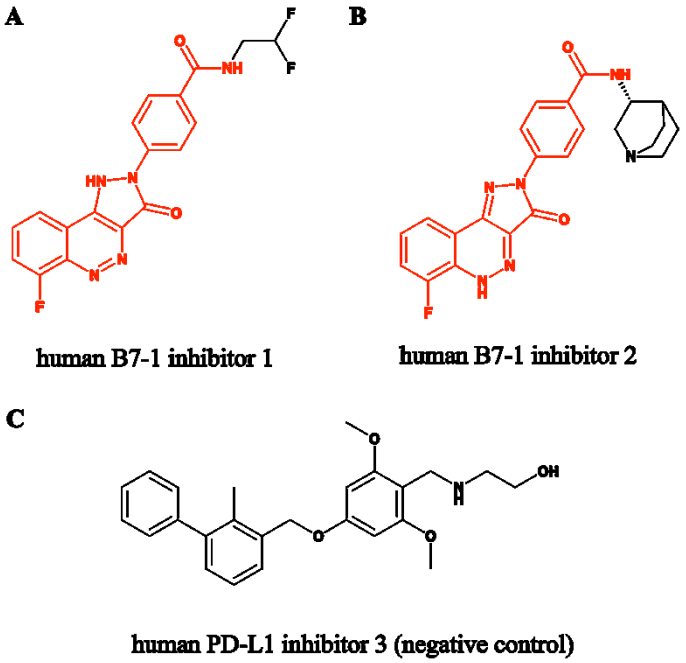

Figure 2. 2 Structures of two human B7-1 small-molecule inhibitors (A and B) and a PD-L1 small-molecule inhibitor (C) under studies in this work.

Two human B7-1 compounds share the same core structure as colored by red.

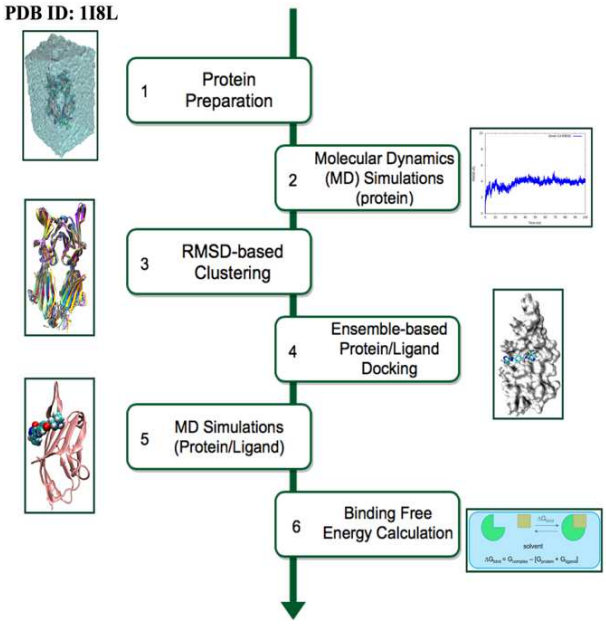

Figure 2. 3 Diagram of workflow in this study.

Following molecular docking, a few docked poses were selected for the subsequent studies. Then MD simulations of the protein/ligand complexes were used to refine the structures of the

complexes. The equilibrated trajectories from the MD simulations were then used for hydrogen bond (H-bond) analysis, molecular mechanics-generalized born surface area (MM-GBSA)[253] binding free energy calculations and energy decompositions to estimate the ligand binding affinities and further confirm the identification of the binding sites and mode(s) of action of the small-molecule inhibitors.

2.2 Methods

2.2.1 System preparation for MD simulations

The structures of the 9 residues at the C-termini ($T^{200}KQEHFPDN^{208}$) were missing from the resolved crystal structures for both hB7-1 monomer (PDB ID: 1DR9) and dimer (PDB ID: 1I8L). The missing structure was predicted as a loop using PSIPRED 4.0 package (http://bioinf.cs.ucl.ac.uk/psipred/) with high confidence in the prediction.[254] MODELLER[255] is a homology modelling tool to predict the protein three-dimensional (3D) structures. In this study, I used the high precision loop modelling protocol DOPE-HR as implemented in MODELLER to construct the missing loop. MODELLER was launched through the UCSF Chimera graphical interface, version 1.13.1.[256] Ranking of the models was evaluated using the zDOPE score and the top-ranked loop model was selected as the final loop structure. The protonation states of all amino acids were predicted using the PDB2PQR server version 2.1.1 (http://nbcr-222.ucsd.edu/pdb2pqr_2.1.1/).[257] It is important to mention that human B7-1 is a glycoprotein, which includes 3 glycosylation sites on the IgV domain and 5 glycosylation sites on the IgC domain of each monomer. A major goal of the current study is to identify all possible binding sites for the B7-1 small-molecule inhibitors, it was important to include the carbohydrates at the glycosylation sites such that I can weed out binding sites that would have any conflict with the glycosylation sites, as these sites would not be accessible for small molecules. To implement that, I included one monosaccharide beta-D-*N*-acetylglucosamine (β-D-GlcNAc) at each glycosylation site using the Glycan Modeller tool of CHARMM GUI (http://www.charmm gui.org).[258] Each β-D-GlcNAc formed a N-linked glycosylic bond with the Asparagine amino acid. The monomer and dimer systems were further solvated in 16 Å TIP3P water boxes and were neutralized in a 150 mM NaCl counter ions concentration. The ff14SB, GLYCAM_06j-1, TIP3P force fields were used to parameterize the systems for MD simulations. The glycosylic bonds and disulfide bonds were

generated through tleap (AMBER tool).[259] The NAMD package[260] (version namd-multicore/2.12) on the Cedar supercomputer was employed to run the MD simulations.

2.2.2 MD simulation protocol

In this project, MD simulations were initially performed on the non-bounded protein structures (to capture the low energy protein configurations) as well as on protein/ligand complexes (to refine the docked complex structures). Before production simulations, all systems were minimized to bring them to the low energy configurations. The minimization phase involved 20,000 iterations. During the minimization, a strong constraint of 50 kcal/mol was placed on the proteins' backbone heavy atoms. This was followed by heating the systems for 500 ps, which gradually increased their temperature from 0 K to 310 K in a stepwise manner. During the heating process, the constraints on the backbone heavy atoms were reduced to 5 kcal/mol. Then a three-stage equilibration phase was performed on each system. The constraining forces were 5 kcal/mol and were then reduced to 1 kcal/mol and then to no constraints. Each equilibration phase involved 5 ns NPT simulation time. After equilibration, up to 200 ns productions were performed using the NPT for each system.

The MD simulations were performed under periodic boundary conditions (PBC) with a time step of 2 fs. The constant temperature (310 K) and constant pressure (1atm) were achieved using the Langevin dynamics temperature control and Langevin piston pressure control. The calculations of the bonded interactions, short-range nonbonded interactions, and full electrostatics evaluation were performed every two timesteps, every timestep, and every two timesteps, respectively. A cut-off of 14 Å was employed for van der Waals (VDW) interactions and electrostatic interactions. A smooth truncation of the VDW interactions and the electrostatic interactions starts at 12 Å. The long-range electrostatic interactions were computed using the particle mesh Ewald (PME) method. The simulation snapshots were extracted from the trajectories every 2 ps.

In order to analyze and compare the stability and flexibility of the different systems, the RMSD and the root mean square fluctuation (RMSF) of the equilibrated trajectories were computed using CPPTRAJ (AMBER tool).[261] The hydrogen bond (H-bond) interactions were also analyzed using CPPTRAJ with a distance cut-off of 3 Å and an angle cut-off of 135 º for each frame of the equilibrated production trajectories.[261]

2.2.3 Druggable binding site predictions

In the current study, both the molecular operating environment (MOE)-Site Finder and the FTSite were utilized to predict the druggable binding sites.[262,263] MOE's Site Finder generates and filters alpha spheres to represent the active sites. Multiple clusters of the alpha spheres were generated and ranked according to their propensity for ligand binding (PLB) score. Excluding the misleading clusters (*e.g.* a site near the linker of the two Ig domains or a site at the C-terminal loops), the cluster, which has the best PLB score was selected. Predicting the probable binding sites on the three protein representatives separately. Comparing the alpha sphere clusters generated from these three protein conformers, the overlapped residues were defined as the first predicted druggable binding site (namely the MOE predicted druggable binding site).

FTSite is a free web server suitable for protein systems with less than 1100 residues to predict the druggable binding sites. FTSite is based on the observation that protein binding sites prone to bind small-molecule compounds.[262] Since the crystal structure of hB7-1 and CTLA-4 protein complex have been resolved, the identified hot spots could be utilized to guide the prediction of hB7-1 small-molecule compound binding sites.[264] Different from most of the energetic methods, FTSite uses 16 different small-molecule probes to sample the protein surface. The places with overlapping low energy clusters of small-molecule probes and have the most non-bond interactions are defined as the druggable ligand binding sites.[262] As discussed earlier, Erbe *et al.*[249] discovered that the mutation of five residues led to a loss or a reduction of the binding between two hB7-1 small-molecule compounds and hB7-1. The residues identified from the mutagenesis assay together with the FTSite identified residues were combined as the second predicted druggable binding site (namely the combined druggable binding site).

2.2.4 Molecular docking simulations

Two hB7-1 small-molecule inhibitors, namely inhibitors 1 and 2 in this study were selected from the same patent.[227] A hPD-L1 small-molecule inhibitor, namely inhibitor 3 in this study was used as a negative control (Fig. 2.2 C). The two hB7-1 small-molecule inhibitors shared the same scaffold. All the original structures of these compounds were obtained from the PubChem database (https://pubchem.ncbi.nlm.nih.gov).[265] Following that, all three compounds were further prepared using the wash utility of the MOE package (version 2019.0102).[263] These residues forming the

predicted druggable binding sites were selected through the Dock panel of MOE. The three compounds were then docked into the three protein conformers separately. The default Triangle Matcher placement method was used to superpose ligand triplets on receptor alpha sphere triplets to generate the initial ligand poses. The default London dG scoring function was used for pose scoring. Then the induced-fit refinement method and the GBVI/WSA dG scoring method were employed for the aim of initial poses refinement. A thousand docking poses were generated for each protein/ligand complex, and 50 poses were obtained after refinement. The docking pose with the best docking score was then selected as a reference. Other docking poses were superposed upon the reference pose to compute their RMSD relative to the reference. The RMSD cut-off of 0.5 Å was used to group and select the representative docking poses. Within each group, the docking pose with the best docking energy was selected as a representative of that group. The RMSD-based filtering may ignore some predicted binding poses. So, following that, all the docking poses were manually browsed and the RMSD clustering method ignored binding poses with relative high docking scores and unique mode(s) of action were added to the docking poses for MD simulations. Comparing these poses, the duplicate poses were removed from the subsequent studies. The detailed binding pose filtering method is shown in Figure 2.4.

2.2.5 Preparation of small-molecule compounds for MD simulations

In this study, the antechamber (AMBER tool) was employed to assign the atom types and calculate the atomic point charges of the compounds by using the AM1-BCC charge method. The general AMBER force field (GAFF) contains parameters for almost all the pharmaceutical molecules. Since the standard AMBER force field may not include all the force field parameters for the non-standard residues, an additional force file or the frcmod file can be generated using parmchk program. The protein/ligand complexes were solvated and ionized according to the same method as the non-bounded protein using tleap.

2.2.6 Binding free energy calculation and energy decomposition

After 15 ns from the MD simulations of the selected complexes, the binding free energy of these systems were computed using the MM-GBSA[253] method as implemented in AMBER 16[259] to further select the best complexes and confirm their binding sites and mode(s) of action of the

ligands. MM-GBSA combines the molecular mechanics' energy with the generalized born and surface area continuum solvation model.

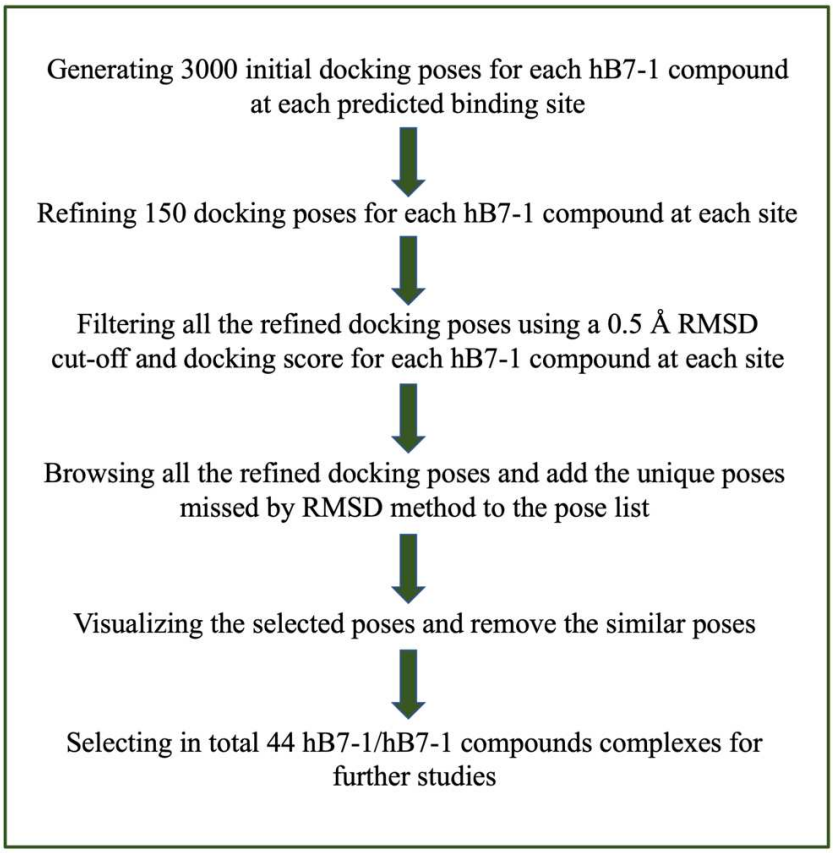

Figure 2. 4 Diagram of filtering docking poses.

The free energy of binding (ΔG_{bind}) is estimated from the free energies of the non-bounded protein receptor ($G_{receptor}$), non-bounded ligand (G_{ligand}) and the bounded protein/ligand complex ($G_{complex}$) as shown in equation (Eqn.) (1). Specifically, the ΔG_{bind} is the sum of the molecular mechanics' energy (ΔE_{MM}), the solvation free energy (ΔG_{solv}) and entropy contributions ($T\Delta S$) as shown in Eqn. (2). The ΔE_{MM} term is estimated from the bonded (bond length, angle and dihedral angle) and nonbounded (electrostatic and VDW) interactions in the gas phase. The ΔG_{solv} term is measured from the polar solvation free energy by using the GB model and the nonpolar solvation free energy by using the solvent-accessible surface area (SASA). For each chosen complex, the snapshots of every 10 ps extracted from the entire 15 ns production trajectories were used for the ΔG_{bind} calculation:

$$\Delta G_{bind} = G_{complex} - (G_{receptor} + G_{ligand}) \quad \text{Eqn. (1),}$$

$$\Delta G_{bind} = \Delta E_{MM} + \Delta G_{solv} - T\Delta S \quad \text{Eqn. (2).}$$

2.2.7 Visualizations and Analyses

Visualizations of the protein alone and protein/ligand complex were performed using visual molecular dynamics (VMD) software version 1.9.4a 12 and PyMOL (TM) 2.3.2 version.[266] Data analyses were plotted using Gnuplot version 5.2.2.

2.3 Results and Discussions

2.3.1 hB7-1 refinement using MD simulations

MD simulations dynamically simulate the motions of atoms. MD simulations relax the 3D structures of the protein and provide a dynamical picture on how the protein interacts with water, ions and bound molecules. It can also remove any unfavorable interactions among the different residues and transit the protein from energetically high conformations to low energy modes, mimicking physiological conditions. The following sections describe the outcomes of the MD simulations performed on the B7-1 protein in both monomer and dimer forms.

2.3.1.1 System preparation: pre-MD simulations

In this study, MODELLER[255] was used to add the missing C-terminal structure of both hB7-1 monomer and dimer. The sequence of this missing loop in the monomer is T^{200}KQEHFPDN^{208}. For the purpose of filtering the binding sites, each monosaccharide β-D-GlcNAc was added to each glycosylation site in B7-1. The systems were then prepared as discussed in the Methods section. A snapshot of the complete system encompassing a hB7-1 dimer system, water, NaCl ions (150 mM) and carbohydrates is shown as an example in Figure 2.5.

2.3.1.2 Analysis of the MD simulations of the unbound proteins

In this study, up to 200 ns MD simulations of both hB7-1 monomer and dimer were performed. The Cα backbone RMSD and Cα backbone RMSF analyses of these two systems were computed using the CPPTRAJ utility as implemented in the Amber software.[261] The data were plotted using gnuplot/5.2.2. The RMSD results (Fig. 2.6) show that the dimer system reached equilibrium and low-energy state after 40 ns. However, the monomer system is not stable. Comparing the RMSD results of the two systems, one can note that the dimer system is more stable than the monomer system.

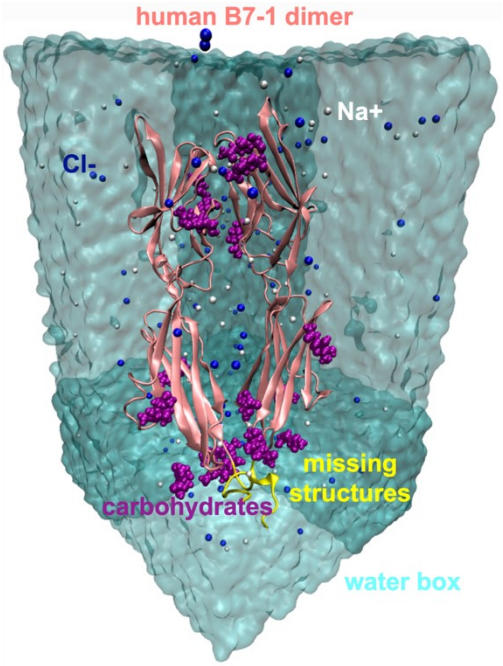

Figure 2. 5 The MD simulation system of the hB7-1 dimer.

The system consists of carbohydrates waters and ions (Na^+, Cl^-).

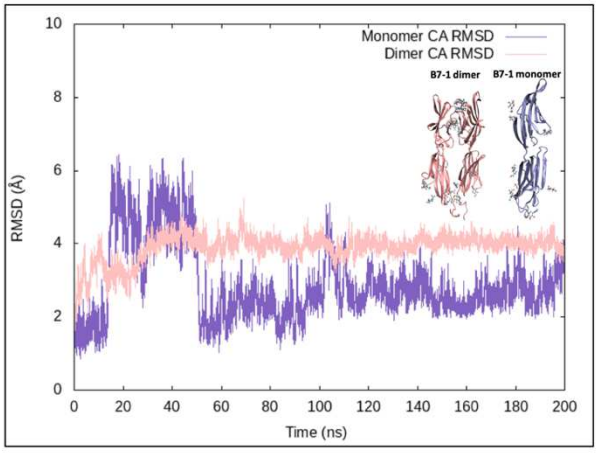

Figure 2. 6 MD trajectory root mean square deviation analysis (RMSD).

The Cα backbone RMSD analyses of hB7-1 monomer and dimer. The purple curve and the pink curve represent the hB7-1 monomer and dimer, respectively.

Although the average RMSD for the dimer system was fluctuating around 4 Å, the deviation in the dimer RMSD plot was much lesser compared to that of the monomer. Therefore, the MD simulations for both systems, suggest that B7-1 is more stable as a dimer and not as a monomer. This is an important outcome of the MD simulations and agrees with what has been reported in

the literature for B7-1, where it is well-documented that hB7-1 is predominantly expressed as a homodimer on the cell surface.[245] Based on this major finding, we executed the following studies using only the hB7-1 dimer system and ignored the monomer system. With this finding in hand, it was interesting to investigate which parts of B7-1 inducing this flexibility in the protein. To do that, we calculated the average RMSF for each residue in the dimer protein (Fig. 2.7). While most residues in the dimer trajectory were stable, the most flexible residues are within the loop structures (colored in yellow), especially in the C-terminal regions.

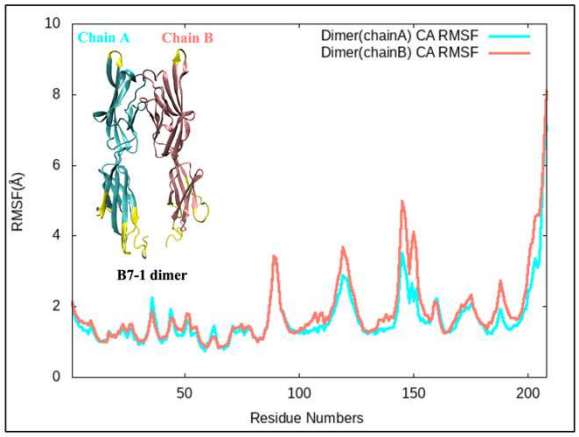

Figure 2. 7 MD trajectory root mean square fluctuation analysis (RMSF).

The Cα backbone RMSF analysis of hB7-1 dimer. The cyan curve and the coral curve represent chain A and chain B of the hB7-1 dimer, respectively.

2.3.2 Selection of B7-1 dominant conformations

With the increasing computational power, MD simulations on a nanosecond or even microsecond duration became common, the trajectories (atom coordinates path as a function of time) generated from such long MD simulations, therefore, include a huge amount of data. This data describes the evolution of dynamics for the simulated protein, which represents a wealth of structural knowledge. Working with every single conformation in these trajectories is practically impossible. Therefore, these huge trajectories must first be reduced into a manageable collection of dominant conformations to work with. In this way, clustering these trajectories is an efficient technique to group similar conformations from these trajectories and select a representative structure for each group. This can significantly reduce the number of protein conformations from thousands of snapshots to a handful of protein structures that represent the dominant dynamics visited by the protein during the MD simulations. Various clustering methods have been developed

to cluster MD trajectories, including top-down splitting algorithm and bottom-up merging algorithm and many others.[267] The major differences between these different algorithms are the way to define the distance between clusters and the selection of which clusters to combine.[267] In this thesis, we adopted the average-linked algorithm, which was proven to show an excellent performance for MD data, especially the number of clusters needed to analyze the data is not known in advance.[267] The average-linked algorithm is a bottom-up method, which starts with multiple clusters and proceeds by merging clusters until it reaches a cluster count that can optimally describe the variations observed in the data. The average-linked algorithm defines the distance between clusters by averaging all the distances between each pair of the compared clusters. For MD simulations, the clustering performance also depends on the reference atoms selected for the pairwise comparison as well as on the cluster count. In order to reduce the computational burden, only most of the IgV domain residues (except for the residues forming the loops) backbone atoms (exclude the hydrogens) or the heavy atoms were selected as the reference atoms for RMSD calculations (Fig. 2.8 A). We focused on the IgV domain mainly in the clustering because the IgV domain was shown by Erbe and his colleagues to be important for ligand binding. In addition, because of no interaction between the IgC domains of the dimer (as supported by the crystal structure,[264] PDB ID: 1I8L), they are relatively more flexible than the IgV domains. Including the IgC domain residues as the reference residues may lead to high RMSD value. This high RMSD value is not because of the real IgV domain conformational change, but the nature of the flexible IgC domains. Therefore excluding the IgC domain residues from the pairwise comparison may increase the accuracy of the clustering result and remove any noise that may emerge from the calculations, by focusing only on the important parts of the protein. In order to identify the optimal cluster count, we performed multiple clustering calculations with a range of cluster counts (from 5 to 95) using CPPTRAJ.[261] We then evaluated the quality of these calculations using different clustering metrics, including the Davies-Bouldin index (DBI) meteric[268] and the SSR (the sum of squares regression) /SST (the total sum of squares) ratio.[267] A minimum in the DBI graph and a plateau in the SSR/SST graph indicate a convergence towards the optimal cluster count. As shown in (Fig. 2.8 B), this DBI minimum was observed initially around a cluster count of 10, which was refined at a higher resolution of cluster counts to show an optimal clustering number of 9.

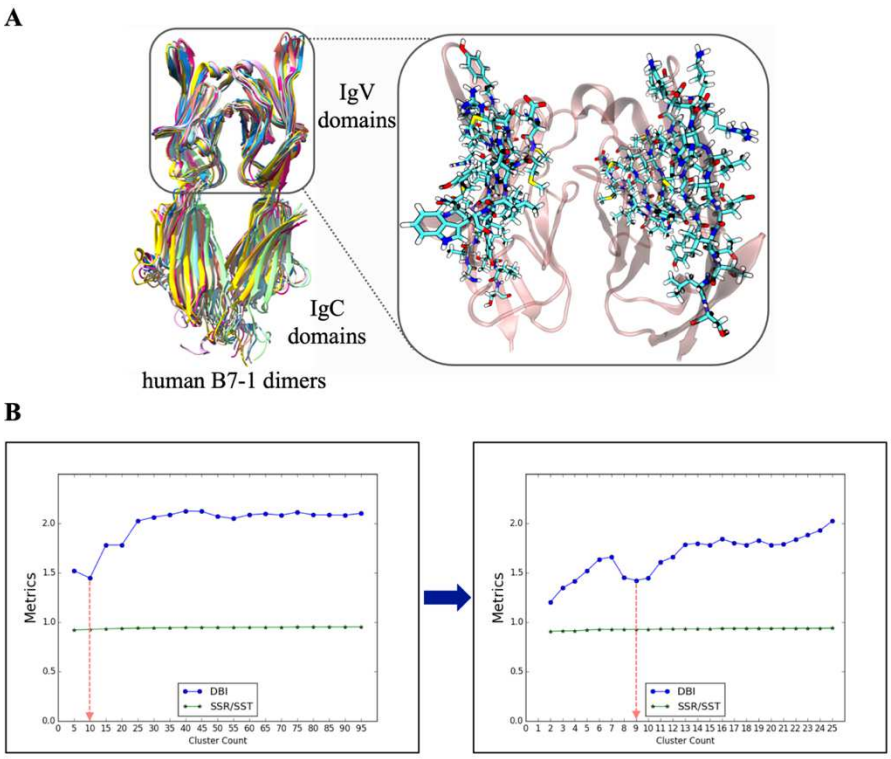

Figure 2. 8 Clustering analysis of the human B7-1 dimer conformations from the equilibrated MD simulation trajectories.

A, The human B7-1 IgV domain reference residues for clustering analysis. B, The selection of the optimal cluster count. An optimal clustering number is reached when a plateau in the SSR/SST ratio coincides with a local minimum in the DBI metric. Nine is regarded as the optimal clustering number.

Through clustering, the most similar protein configurations (in this case hB7-1 dimers) were grouped into the same group. In total, 16,000 protein conformations were extracted from the equilibrated MD trajectories at 10 ps intervals and were fitted to the first frame before any clustering calculation and finally grouped into 9 clusters (Fig. 2.8 B). As shown in Figure 2.9, among these 9 clusters, the first three clusters encompassed more than 95 % of all the protein conformations. The structures which have a minimal deviation from the other structures in the cluster and themselves during the trajectories were selected as the protein representatives. These protein conformers are regarded as the dominant protein conformations during the MD simulation. In total, three protein representatives forming a conformational ensemble were used for docking studies. For more details about clustering please visit a comprehensive review.[267]

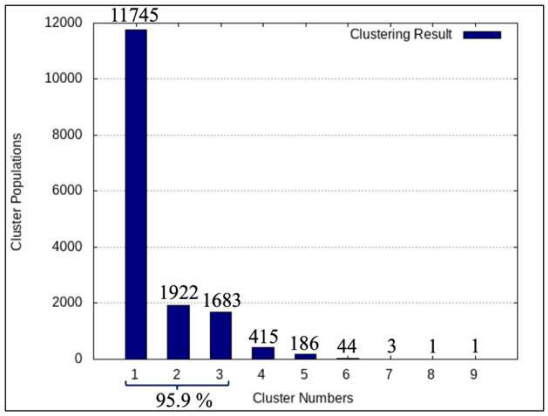

Figure 2. 9 The occurrences of each cluster.

Clusters 1 to 3 occupied more than 95 % of all the protein conformations through the MD simulation, were selected as the protein representatives for the following studies.

2.3.3 Druggable binding sites prediction

Identifying a suitable binding site within B7-1 is a prerequisite for any molecular docking studies. This binding site not only has to fit with the shape of the tested compounds but also has to complement their physiochemical properties (*e.g.* electrostatic potential, hydrogen bonds, *etc*.). In the recent decades, plenty of protein/ligand binding site prediction methods have been developed, including but not limited to geometry-based methods (*e.g.* MOE-Site Finder),[263] energy-based methods (*e.g.* FTSite),[262] sequence-based methods (*e.g.* ConCavity)[269] and the most recent machine learning-based methods (*e.g.* P2Rank)[270] as well as the combination of different methods (*e.g.* COACH).[271] In this work, I used the MOE-Site Finder and the FTSite to predict the binding sites of the tested small-molecule compounds (see Methods 2.2.3).

I focused on three protein conformations, representing the three dominant clusters as described above. By comparing the alpha sphere clusters generated from these three B7-1 structures, six conserved residues, including Lys34, Lys37, Glu52, Tyr53, Arg73, Ser75, located in the IgV domain of B7-1 were defined as the first binding site (see Fig. 2.10 A). Eight residues were identified using FTSite, which included ARG29, LIE30, TYR31, THR41, MET42, MET43, VAL83 and LEU85. As these FTSite predicted residues were close to the 5 residues identified by Erbe's mutational analysis, I decided to group them and construct the second binding site encompassing thirteen residues. These thirteen residues include ARG29, LIE30, TYR31, THR41, MET42, MET43, Asp46, Met47, Asn48, Ile49, Trp50, VAL83, and LEU85 (see Fig. 2.10 B). Both

binding sites were used as search space for the docking simulations to study the interactions of the three compounds (inhibitors 1,2 and 3) within B7-1, as described below.

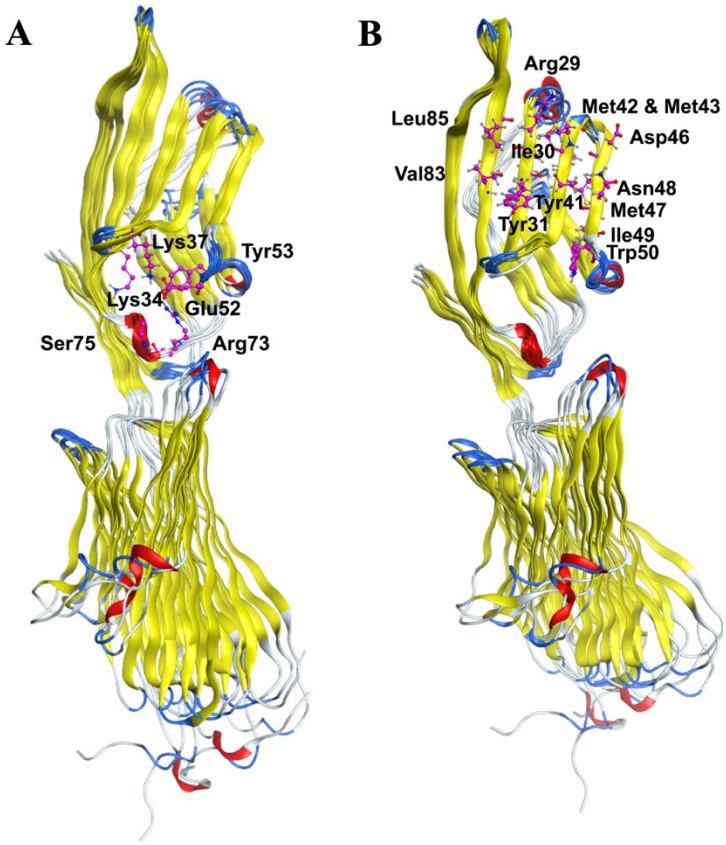

Figure 2. 10 Residues forming the MOE predicted binding site (A) and the combined binding site (B).

Three protein representatives were superposed on the binding site residues, which were shown as VDW representations by using MOE.

2.3.4 Molecular docking studies of hB7-1 and small-molecule compounds

Molecular docking is one of the most important tools of structure-based drug design, which not only predicts the most probable binding poses of the ligands through multiple sampling algorithms but also evaluates the binding affinities of the ligands through different scoring functions. MOE is a commercial docking software, which was proven to use robust sampling algorithms (*e.g.* the triangle matcher algorithm) and excellent scoring functions (*e.g.* the London dG function).[272] Therefore, in this study, MOE was employed to perform all the molecular docking studies. A common problem of various docking programs is the neglect of the flexibility of the

target receptors. In order to overcome this problem, I generated an ensemble including the three dominant protein conformers obtained from the clustering analysis as discussed above. In addition, the induced-fit refinement method was also used to further consider the sidechain flexibility of the binding site residues of the protein. Duplicate poses were removed after refinement.

Both identified binding sites (see above) were used to test the interactions of the compounds to B7-1. For the first binding site (identified by MOE), 10 out of 150 different binding poses of hB7-1/inhibitor 1 complexes and 10 out of 150 different binding poses of hB7-1/inhibitor 2 complexes were selected for further studies. For the second binding site (predicted by FTSite), 14 out of 150 different binding poses of hB7-1/inhibitor 1 complexes and 10 out of 150 different binding poses of hB7-1/inhibitor 2 complexes were selected for further studies.

2.3.4 hB7-1/compound complex refinement using MD simulations

With the help of the significantly increasing computer power, most of the docking programs can fulfill a sufficient sampling of all possible binding poses for a compound. However, the accurate scoring function to select the most probable binding pose is still challenging. The best docking score may not guarantee the best binding affinity of the ligand. One cannot only rely on the docking score without other considerations. Because, the protein/ligand interaction is a dynamic process, in some cases, the compound may leave the predicted binding site after a long MD simulation, indicating a less stable binding. Furthermore, the orientation of the predicted complex may not be in a relaxed low energy state, due to unfavorable interactions that may not be observed during the docking simulations. Therefore, a post-processing of the docked structures using MD simulations is essential to refine the obtained protein/ligand complexes to help the systems reach their lowest energy states, leading to more realistic and physiologically relevant stable complexes.

In total, forty-four docked complexes were used as starting points for 15 ns MD simulations. The preparation of the bound protein-ligand systems is described in the Methods section (see above). The RMSDs of the ligands (exclude the hydrogen atoms) within the entire 15 ns production runs were calculated using CPPTRAJ[261] and plotted using Gnuplot version 5.2.2 (see Figure 2.11 to Figure 2.14). VMD[266] was used to monitor the movement of these complexes during the MD simulations. The binding free energies of these complexes were computed using the MM-GBSA method by the CPPTRAJ program (see Figure 2.11 to Figure 2.14).[261] For each complex, the

snapshots at every 10 ps were extracted from the entire 15 ns trajectories (1,500 frames). Three parameters were used to analyze and rank the different poses, namely the ligands' RMSDs, the dynamics of the bound complexes and the binding free energies between B7-1 and each ligand. Only complexes that show stable RMSDs and less dynamicity during the simulations as well as acceptable binding affinities were considered as the optimal protein/ligand conformations and were qualified for further analyses.

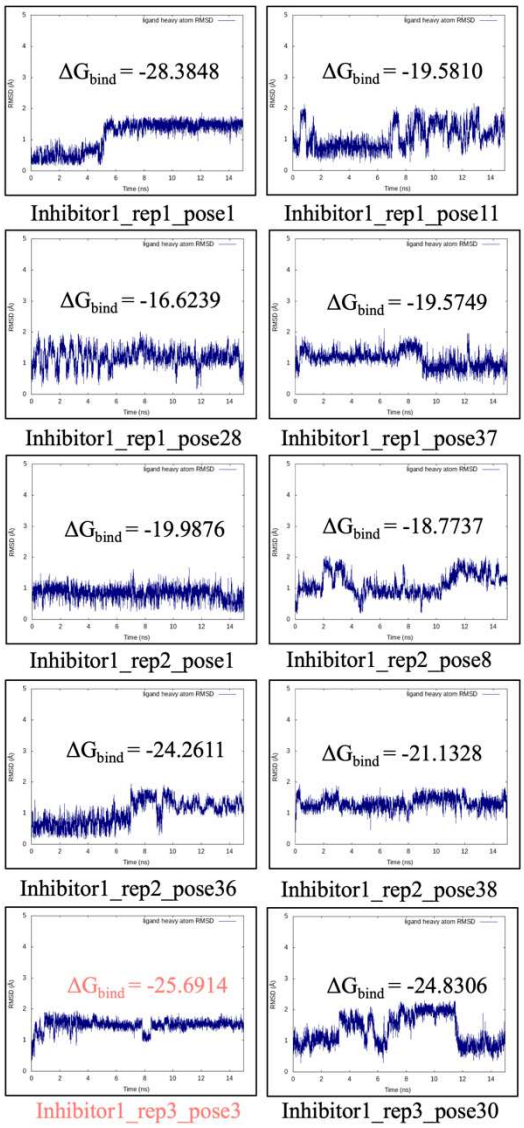

Figure 2. 11 Ligand heavy atom RMSD analyses and binding free energies (kcal/mol) of the human B7-1/inhibitor 1 complexes in the MOE predicted binding sites.

The binding free energy of each system was computed using the MM-GBSA method. The most stable complex is colored in pink.

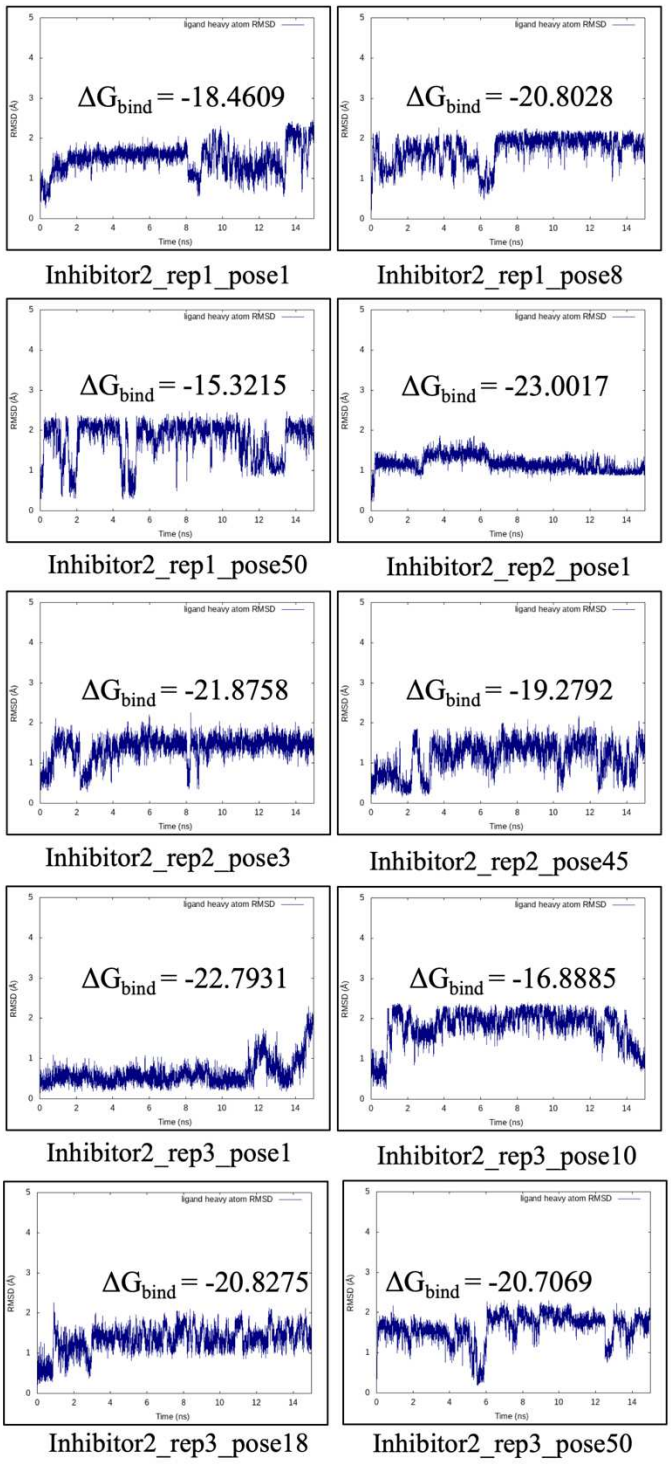

Figure 2. 12 Ligand heavy atom RMSD analyses and binding free energies (kcal/mol) of the human B7-1/inhibitor 2 complexes in the MOE predicted binding sites.

The binding free energy of each system was computed using the MM-GBSA method.

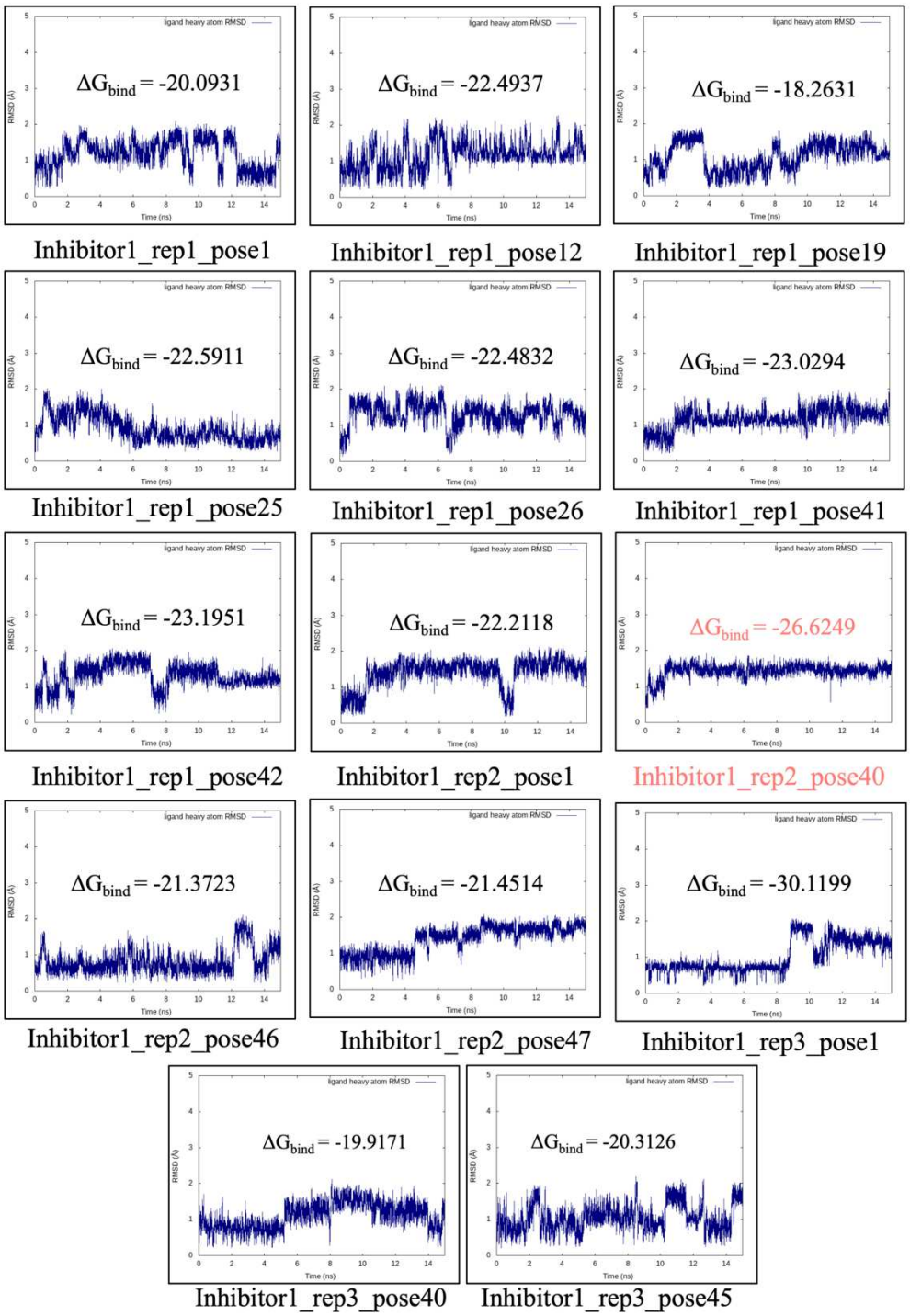

Figure 2. 13 Ligand heavy atom RMSD analyses and binding free energies (kcal/mol) of the human B7-1/inhibitor 1 complexes in the combined binding sites.

The binding free energy of each system was computed using the MM-GBSA method. The most stable complex is colored in pink.

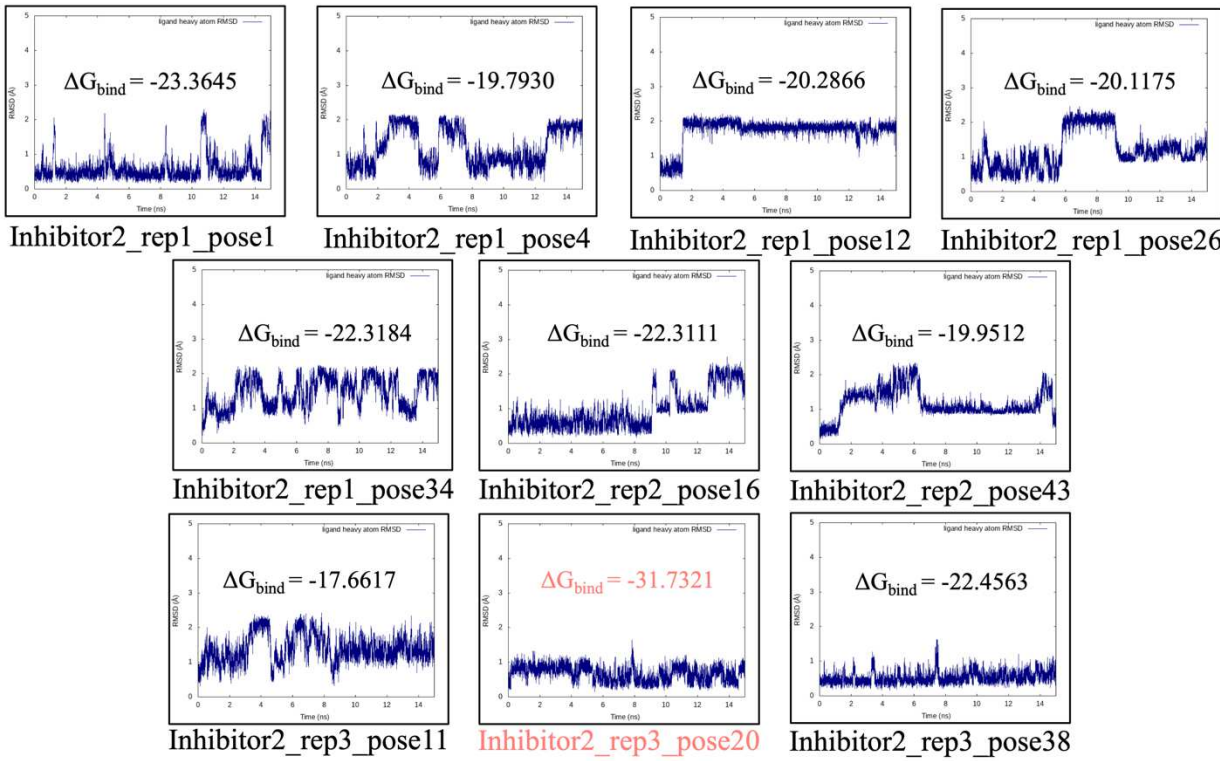

Figure 2. 14 Ligand heavy atom RMSD analyses and binding free energies (kcal/mol) of the human B7-1/inhibitor 2 complexes in the combined binding sites.

The binding free energy of each system was computed using the MM-GBSA method. The most stable complex is colored in pink.

The complexes, which have the binding free energies lower than – 25 kcal/mol were visualized using VMD.[266] Some of the systems were stable at the beginning, however, they showed large flexibilities at the end of the simulations. In some systems, the ligands even moved out of the binding sites. These observations highlight the importance of using MD simulations to further analyze the docking results, as most of these parameters would not be shown during the docking simulations. Comparing all systems, inhibitor 1-protein conformer 2-pose 40 (namely inhibitor 1 binding pose 2) and the inhibitor 2-protein conformer 2-pose 20 (namely inhibitor 2 binding pose) within the combined binding site were identified as the most stable binding poses. Interestingly, MOE predicted a similar binding site, but different ligand orientation for inhibitor 1 (inhibitor 1-protein conformer 3-pose 3, namely inhibitor 1 binding pose 1). This binding site locates in the overlapping area of MOE-Site Finder predicted binding site search space and the combined binding site search space. In the abovementioned three complexes, the ligands are stable as

supported by the three parameters I used to filter the complexes as described above. Two different binding site prediction methods identified the same or at least a very similar binding site confirming the accuracy of the results.

To validate the models, I further investigated the interaction between inhibitor 3 (a PD-L1 small-molecule inhibitor) and hB7-1. To do that, I used the same docking procedure I adopted for inhibitors 1 and 2. After testing inhibitor 3 in the two predicted binding sites of B7-1, I manually selected one complex in each site. In the first complex (see Figure 2.15 A), inhibitor 3 was shown to bind at a similar site to the one I observed for the optimal conformation of inhibitor 1 as supported by the residues within 5 Å of these two ligands (inhibitor 1 and inhibitor 3) were almost the same. In the second complex (see Figure 2.15 B), inhibitor 3 was shown to bind at a similar site as inhibitor 2. The 15 ns-length MD simulations of the hB7-1/inhibitor 3 complexes were performed and the ligand heavy atom RMSDs were computed (as shown in Figure 2.15). Results from this calculation show that the hB7-1/inhibitor 3 complex is very flexible with a maximum deviation of 3 Å within the inhibitor 1 binding site and less flexible within the inhibitor 2 binding site. Then the binding free energies of inhibitor 3 within these two complexes were computed according to the same method. The binding free energies are smaller than that of the inhibitor 1/protein and inhibitor 2/protein complexes. Visualizing the dynamics of the hB7-1/inhibitor 3 complexes using VMD also confirms the large fluctuations of inhibitor 3. Taken together, these findings suggest that inhibitor 3 may not bind to hB7-1 in the predicted inhibitor 1 and inhibitor 2 binding sites.

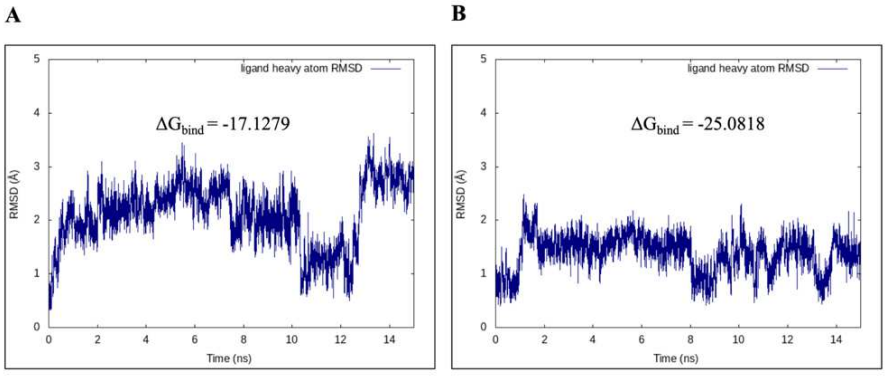

Figure 2. 15 Ligand heavy atom RMSD analysis of the human B7-1/inhibitor 3 complexes.

A, Inhibitor 3 binds to a similar binding site of inhibitor 1 in hB7-1. B, Inhibitor 3 binds to a similar binding site of inhibitor 2 in hB7-1. The residues within 5 Å of the compounds in the first frames of the MD trajectories are almost the same.

To confirm the stabilities of the final three protein/compound systems, I expanded the MD simulations to in total of 25 ns. The heavy atom RMSDs of the ligands are shown in Figure 2.16. These results indicate that all of the three systems are stable after expanding the MD simulations, this further confirms the accuracy of the results.

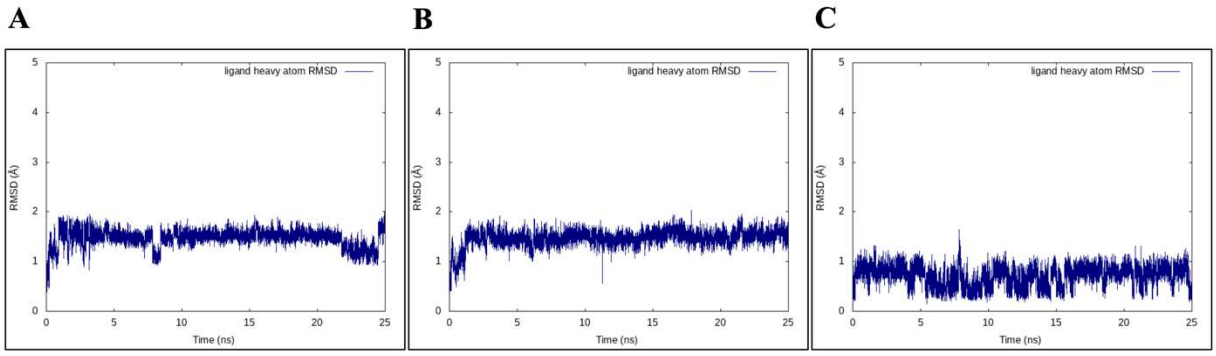

Figure 2. 16 Ligand heavy atom RMSD analysis during the 25 ns MD trajectories of the final three protein/compound complexes.

A, Inhibitor 1 binds with hB7-1 in the first predicted orientation. B, Inhibitor 1 binds with hB7-1 in the second predicted orientation. C, Inhibitor 2 binds with hB7-1 in the predicted orientation.

2.3.5 Analysis of complex interactions

As discussed above, I obtained two different orientations for inhibitor 1 within the same binding location. The two orientations seem to exhibit similar binding affinities to B7-1. It is important to understand which of the observed orientations for inhibitor1 is more favorable and also to gain more structural insights into the differences between these two modes of interactions. Furthermore, comparing that to the mode of binding of inhibitor 2 may explain the differences in binding affinity between the two compounds. For that, I analyzed the H-bond networks surrounding each compound in their bound conformations. I also performed a per-residue total energy decomposition of the three complexes (two complexes for inhibitor 1 and one complex for inhibitor 2). H-bonds were defined by a distance cut-off of 3 Å and an angle cut-off of 135 º for each frame of the MD trajectories. In addition, some residues forming weak H-bonds with occupancy less than 5 % were not considered and are not shown here. Moreover, any residue showing a binding free energy contribution higher than -1 kcal/mol was not considered for further analysis and is not discussed below.

2.3.5.1 H-bond analyses

A CPPTRAJ script was used to analyze and compare the H-bond interactions of the three protein/ligand complexes. As discussed above, Inhibitor 1 showed two different modes of binding within the same site. In the first binding orientation (see Figure 2.17), the ring structures of inhibitor 1 are pointing to the right. The Asp55 residue is forming the strongest H-bond (~ 55 % occupancy) with the inhibitor 1, with an average distance of 2.8 Å and an average angle of 158 º. A weaker H-bond (~ 7 % occupancy) is also formed between the Glu160 and inhibitor 1, with an average distance of 2.9 Å and an average angle of 147 º.

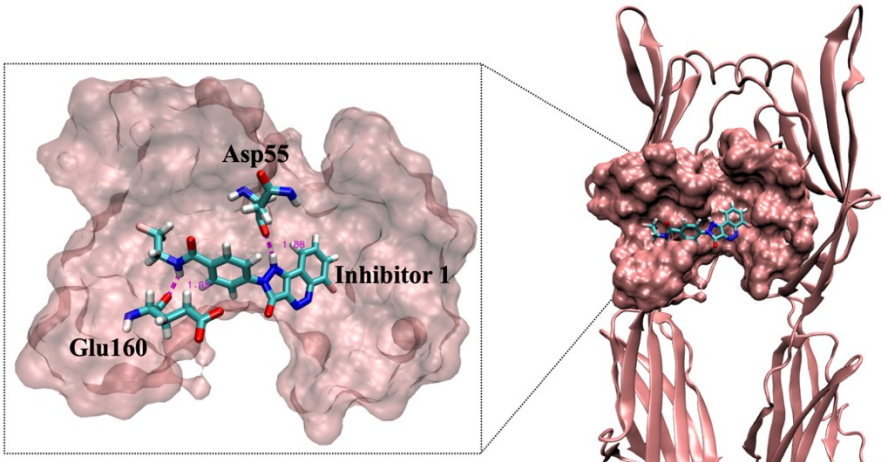

Acceptor	Donor H	Donor	Occupancy
ASP55@O	L@H1	L@N7	55.29 %
GLU160@O	L@H9	L@N10	6.79 %

Figure 2. 17 H-bonds analysis of hB7-1/inhibitor 1 in the first identified binding pose.

The protein atoms within 10 Å of the ligand are shown as surface representation. H-bond interactions of the last frame of the 15 ns MD trajectories were shown as an example using purple dashed lines with bond length labeled. H-bonds, which have less than 5 % occupancy were ignored.

In the second binding orientation (see Figure 2.18), the ring structures of inhibitor 1 are pointing to the left and Arg56 is forming the strongest H-bond (~16 % occupancy) with the ligand with an average distance of 2.9 Å and an average angle of 147 º. Asp55 is forming a weaker H-bond (~ 11 % occupancy) with the ligand with an average distance of 2.9 Å and an average angle of 158 º. In addition, a H-bond is formed between the Arg73 and the inhibitor (~ 8 % occupancy) with an average distance of 2.9 Å and an average angle of 146 º. Comparing the two different orientations of inhibitor 1, one can observe that Asp55 of hB7-1 is always located near the middle

of the ligand, therefore, playing a key role in the H-bond interactions. With the multiple ring structures point to the right, this allows the formation of a H-bond with Glu160. However, when the multiple ring structures of inhibitor 1 pointing to the left, allows the formation of H-bonds with two Arg residues (namely Arg56 and Arg73). Comparing the total H-bond occupancy in both cases, it is clear that in the first orientation, inhibitor 1 can almost double the number of H-bond interactions.

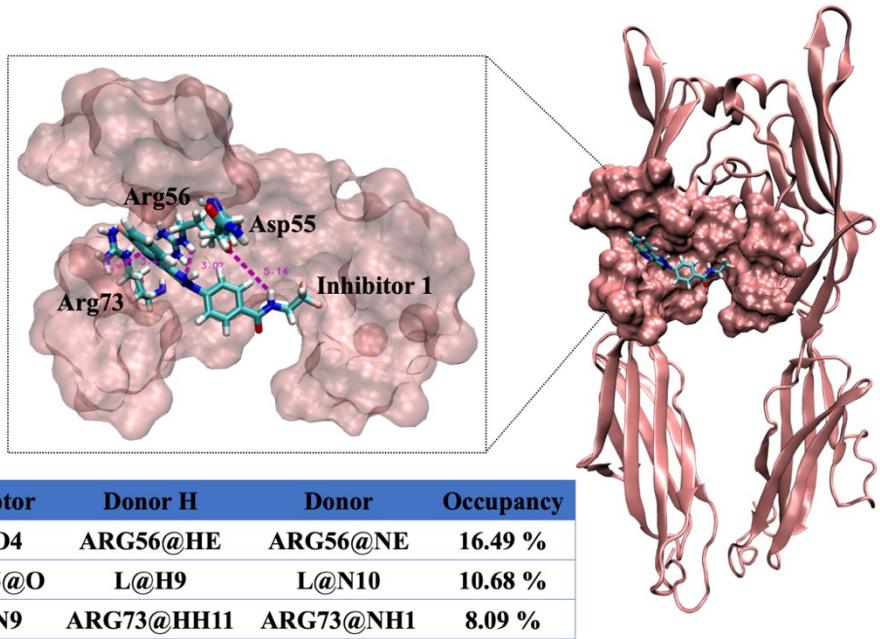

Acceptor	Donor H	Donor	Occupancy
L@O4	ARG56@HE	ARG56@NE	16.49 %
ASP55@O	L@H9	L@N10	10.68 %
L@N9	ARG73@HH11	ARG73@NH1	8.09 %

Figure 2. 18 H-bonds analysis of hB7-1/inhibitor 1 in the second identified binding pose.

The protein atoms within 10 Å of the ligand are shown as surface representation. H-bond interactions of the last frame of the 15 ns MD trajectories were shown as an example using purple dashed lines with bond length labeled. H-bonds, which have less than 5 % occupancy were ignored.

For inhibitor 2, the data demonstrates that it binds to a completely different binding site, compared to inhibitor 1 (see Figure 2.19). In this site, inhibitor 2 occupies the β sheets of the IgV domain, where Arg29 is forming two H-bonds with the same oxygen atom of inhibitor 2. One of these H-bonds is much stronger (~ 65 % occupancy) than the other one (~ 8 % occupancy). In addition, Asn48 is forming another relatively strong H-bond with the ligand (~ 22 % occupancy). In all the three complexes, inhibitor 2 formed stronger H-bond networks with the protein than the inhibitor 1. As shown in Figure 2.15 to 2.17, the residues of the protein are all forming H-bonds

with the two ligands on both sides, in this way they are stabilizing the ligand in the shallow surface of the B7-1 structure.

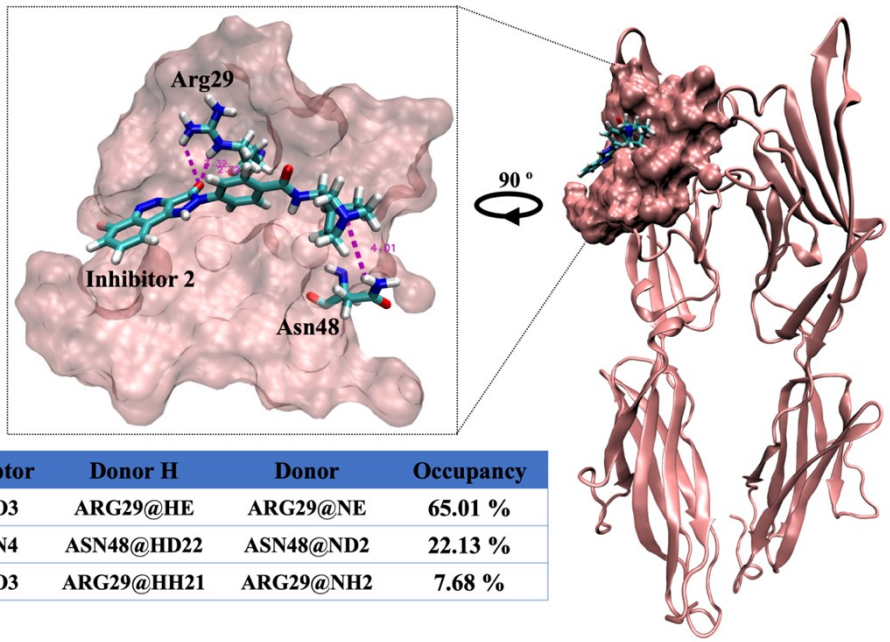

Acceptor	Donor H	Donor	Occupancy
L@O3	ARG29@HE	ARG29@NE	65.01 %
L@N4	ASN48@HD22	ASN48@ND2	22.13 %
L@O3	ARG29@HH21	ARG29@NH2	7.68 %

Figure 2. 19 H-bonds analysis of hB7-1/inhibitor 2 in the identified binding site.

The protein atoms within 10 Å of the ligand are shown as surface representation. H-bond interactions of the last frame of the 15 ns MD trajectories were shown as an example using purple dashed lines with bond length labeled. H-bonds, which have less than 5 % occupancy were ignored.

2.3.5.2 Binding free energy decompositions

The binding free energy decomposition can divide the total binding free energy into electrostatic energy, VDW energy, polar and non-polar solvation energy. Through binding free energy decomposition, one can identify the key residues forming protein/compound interaction and how each residue contributes to the total binding free energy. Furthermore, the results of the binding free energy decomposition can be further utilized to confirm the findings obtained from the H-bond analyses. Based on the energy decomposition, in the first binding orientation of inhibitor 1, I identified three key residues, namely Arg56, Leu70, and Arg73, which showed to contribute most of the total binding free energy. Among them, the VDW interaction of Arg56 (~ -3.0 kcal/mol) seems to dominate its contribution to the binding interactions with inhibitor 1. Asp55 contributes about -2.6 kcal/mol mainly through its electrostatic interaction with inhibitor 1, while

Glu160 contributes relatively less electrostatic energy (~ -0.4 kcal/mol), which supports the H-bond analyses. In the second binding orientation of inhibitor 1, Arg56 and Arg73 were identified as the key residues to interact with the ligand, mainly through electrostatic energies (~ -6.0 kcal/mol for each interaction), which also supports out H-bond analyses. Arg56 also contributes about -3.1 kcal/mol of the total electrostatic energy. In addition, Leu70 and Lys222 also contribute to the total binding free energy in a lower degree (lower than -1.0 kcal/mol).

Inhibitor 2 binds to the shallow protein surface mainly through the following residues: Arg29, Tyr31, Met42, Met43, Asn48. Among them, Arg29 and Asn48 interact with the ligand mainly through electrostatic interactions, which confirms the H-bond analyses. Especially, Arg29 is forming two H-bonds with the same oxygen of the ligand and contributing about -7.7 kcal/mol to the total binding free energy through electrostatic interactions alone. On the contrary, the VDW energies of residues Tyr31, Met42 and Met43 dominating their interactions with the ligand. Comparing with the discovery of Erbe's lab, both of us found that residue Asn48 might be important for the ligands binding. Since the specific binding between Asn48 and compound 1 (see Fig. 1.4A) in their research was not revealed, I could not compare with the identifications in this thesis. However, from the results, Asn48 binds to a unique chemical group with inhibitor 2 (see Fig. 2.2B, Fig. 2.19), which is not in compound 1. The inhibitor 2 predicted binding site identified by the research may partially overlap with the hB7-1/hCTLA-4 protein/protein binding surface as supported by both hB7-1 residues Tyr31 and Met43 were involved in the complex (protein/protein or protein/compound) formation. Besides, Arg29 on hB7-1, which was proved to dominate the H-bond interactions with inhibitor 2 in the studies was previously proved also forming a H-bond with Glu33 of hCTLA-4. As for the inhibitor 1 binding site, based on the current knowledge, it's far away from the hCTLA-4 binding site.

2.4 Conclusions

Human B7-1 is one of the vital costimulatory proteins for T-cell modulation and is regarded as a crucial target for the treatment of autoimmune diseases and, possibly cancers. In this project, I aimed to explore the interactions of human B7-1 with two human B7-1 small-molecule inhibitors, namely inhibitor 1 and 2. To validate the modelling, a human PD-L1 small-molecule inhibitor was used as negative control. To resolve this research question, I used a workflow involving binding site identification tools, MD simulations, RMSD-based clustering, ensemble-based docking

studies, hydrogen bond analysis and binding free energy calculations. Three parameters, including the ligand RMSD, the protein/ligand dynamicity and the binding affinities of the ligands were employed to filter the most favorable complex configuration. H-bond interaction analysis and decomposition of the binding free energy allowed us to identify the key residues stabilizing the protein/ligand interactions. The findings suggest that both inhibitors 1 and 2 can bind to B7-1, while the PD-L1 compound doesn't bind to B7-1 in the identified binding sites of these B7-1 inhibitors. The data show that inhibitor 1 binds to B7-1 in two different modes of binding. In the second binding pose, the stronger electrostatic contributions were identified compared to that of the first binding pose, which although has almost double of H-bond occupancy. Therefore, with the current knowledge, it's hard to estimate which orientation of inhibitor 1 is better. A stronger interaction was identified between the protein and inhibitor 2 as a result of stronger VDW and electrostatic contributions. The inhibitor 2 may interact with hB7-1 through a site partially overlapped with the hCTLA-4 binding site. The results reveal the interactions between hB7-1 and two hB7-1 inhibitors in detail. These findings can help the rational design of more potent hB7-1 small-molecule inhibitors.

CHAPTER 3: EXPRESSION AND PURIFICATION OF HUMAN B7-1[c]

3.1: Introduction

B7 family is a group of structurally related immune checkpoint proteins, which is associated with immune response regulation.[273] The B7 family consists of 10 members, namely, B7-1 (CD80), B7-2 (CD86), B7-DC (CD273, PD-L2), B7-H1(CD274, PD-L1), B7-H2 (CD275, ICOSL), B7-H3 (CD276), B7-H4 (VTCN1, B7x), B7-H5 (VISTA, PD-1H), B7-H6 (NCR3LG1), B7-H7 (HHLA2).[273,274] Among them, human B7-1 (hB7-1) is the most characterized member. B7-1 is a peripheral transmembrane glycoprotein mainly expressed on the activated antigen-presenting cells (APCs).[275] hB7-1 regulates immune response through delivering the costimulatory signal (when interacting with human CD28) and coinhibitory signals (when interacting with human CTLA-4 or human PD-L1).[15,44,67] In simple terms, the blockade of the hB7-1/hCD28 costimulatory pathway, inhibits the activation of T cells, leading to the possibility of alleviating autoimmune diseases. When the hB7-1/hCTLA-4 or hB7-1/hPD-L1 pathways are blocked, T cells' activity to fight cancers and chronic infections will be restored.

The first crystal structure of the extracellular domain of human B7-1 was resolved using X-ray diffraction to 3 Å resolution in 2000.[14] A mature hB7-1 consists of 208 amino acids in the extracellular domain, including a membrane-distal immunoglobulin variable (IgV) like domain and a membrane-proximal immunoglobulin constant (IgC) like domain. The following year, the crystal structure of the extracellular domains of the hB7-1/hCTLA-4 complex was also resolved using X-ray diffraction to 3 Å resolution.[58] The discovery of these crystal structures forming milestones in the study of hB7-1. These identifications revealed the important structural information of hB7-1 and clear insights on its interaction with CTLA-4, as well as promoted the structure-based drug design greatly. Indeed, since then some researchers focused on developing hB7-1 modulators ranging from fusion proteins, monoclonal antibodies (mAbs) to small molecules.[170,171,179,217,219,224,225] For example, abatacept and belatacept (two fusion proteins that target hB7-1/2) were approved by the United States Food and Drug Administration (FDA) for the treatment of autoimmune diseases and renal transplant rejection, respectively.[170,171] The development of small-molecule inhibitors was lagging. The crystal structure of the hB7-1/hCD28 complex is still unsolved, which impedes the understanding of the subtle differences of the binding between hB7-1/hCD28 and hB7-1/hCTLA-4 complexes. Based on my knowledge, currently, all

[c]A version of this chapter will be submitted to the Journal of Membrane Biology.

the identified hB7-1 small-molecule inhibitors block both hB7-1/hCD28 and hB7-1/hCTLA-4 pathways.[217,224,225] In this chapter, I aim to express and purify the entire extracellular domain (the ectodomain) of hB7-1, the details for which were not completely available in the published literature. This study will help us overcome the first main hurdle towards decoding the interactions between hB7-1 and its small-molecule inhibitors and understand their modes of binding to hB7-1. In the long run, this can help with understanding the selectivity of different small-molecule inhibitors towards hB7-1/hCD28 and hB7-1/hCTLA-4 pathways.

The deep understanding of molecular biology together with the rapid progress of genetic engineering have improved the possibility of expressing and purifying recombinant membrane protein with high quality.[276] hB7-1 was previously expressed in the insect cell (Bac-GPI-B7-1),[277] the mammalian cell (mutant Chinese hamster ovary cell line-Lec3.2.8.1),[14] and the bacterial cell (*Escherichia coli,* (*E. coli*)).[278,279] These groups expressed hB7-1 with different constructs, each protocol is specific for their system. Although the expression of apo-hB7-1 in mammalian cells has been used for X-ray crystal structure determination, the bacterial expression system remains a reliable method. Protein expression in eukaryotic expression systems is able to induce the post-translational modification (PTM) (*e.g.* glycosylation and phosphorylation), which is often important for protein folding and protein function.[280] However, the lengthy-expression period, high cost, and relatively low yield remain a problem. Hence, protein expression in bacterial systems is faster, economic, and usually has a higher yield – an important aspect for functional and structural studies. The main drawback when expressing the protein in the prokaryotic system is that they have different folding properties/chaperones[281] and also cannot perform the PTM that typically take place in eukaryotic cells.[282] Based on the 2 hB7-1 related crystal structures,[14,58] none of the glycosylation sites are involved in the dimer interface and receptor/ligand interface. Dr. Tykocinski's team generated non-glycosylated hB7-1 through both *N*-glycosylation inhibitor tunicamycin and bacterial expression system and confirmed that *N*-glycosylation of hB7-1 is not required for the interactions with its receptors CD28 and CTLA-4.[278] Since the *N*-glycosylation doesn't dramatically affect the receptor-binding ability of hB7-1, I decided to express the extracellular domain of hB7-1 in a bacterial system.

Protein expression in the bacterium *E. coli* is a frequently used approach to produce recombinant proteins. This is mainly due to its fast growth, fast plasmid transformation, and inexpensive cost.[283] The BL21(DE3) is one of the widely used strains for protein expression under

the control of the lacUV5 promoter for T7 RNA polymerase.[284] A hexahistidine (6 × His) tag is attached to the C-termini of the protein for the purification purpose. A Tobacco Etch Virus (TEV) protease, which is commonly used for the cleavage of fusion proteins and tags was inserted between the protein gene and the 6 × His tag. Expressing a eukaryotic protein in a bacterial system is challenging. The overexpression of a recombinant protein in *E. coli*, especially for a eukaryotic protein, which lacks the PTM and the eukaryotic chaperons to assist protein folding and stabilize the protein, can lead to the protein aggregation.[283,285] The aggregated proteins are commonly referred to as the inclusion bodies (IBs). Forming IBs are always problematic in the field of protein expression. However, in some cases, the formation of IBs can be beneficial. IBs contain approximately 90% pure recombinant protein and the insoluble and misfolded proteins can be easily extracted through cell lysis.[286] The challenging part of expressing the recombinant protein from IBs is to refold the protein correctly. In this chapter, I established a protocol to generate the recombinant extracellular domain of hB7-1. The protein was expressed in the form of IBs, harvested and purified by denaturing the protein first and then refolding it *in vitro*. Immobilized metal affinity chromatography and size exclusion chromatography were used to further purify the recombinant protein. Here I provide the detailed steps for the expression and purification which required multiple rounds of optimizations to generate the pure hB7-1 protein suitable for drug-binding studies.

3.2: Methods

3.2.1: Construction of His-TEV-hB7-1[35-242]

The gene of the recombinant hB7-1 was synthesized and cloned into the pET21b plasmid (Bio Basic Canada Inc.). The plasmid contains the hB7-1 gene with a TEV protease cleavage site and a 6 × His tag in its C-terminus, as well as an ampicillin resistance gene and a T7 inducible promoter (Fig. 3.1). The 222 amino acid protein sequence was codon-optimized for better expression in *E. coli*, including but not limited to codon usage bias and average GC content.

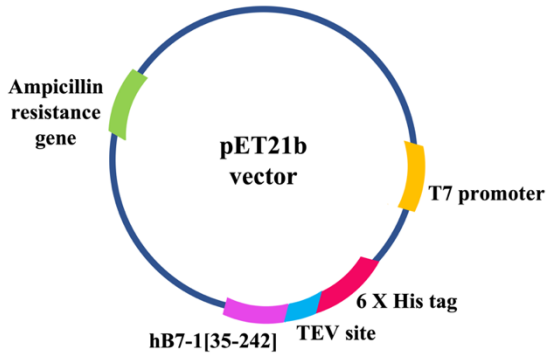

Figure 3. 1 Schematic diagram of the pET21b-hB7-1 construct.

The hB7-1 target gene with a TEV protease cleavage site and a poly-histidine tag was cloned into the pET21b vector downstream to the T7 inducible promoter. The pET21b vector carries the ampicillin resistance gene.

3.2.2: Transformation of recombinant B7-1 in BL21(DE3)

Subsequently, 50 µL of the competent BL21(DE3) cells, stored at -80 °C, were thawed on the ice. 2 µL of the plasmid (86 ng/mL) was added to the competent cells and incubated on the ice for 20 minutes. After heat shock at 42 °C for 1 min, the cells were cooled down on the ice for 2 min. 1 mL lysogeny broth (LB) was added into the cells and then incubated at 37 °C for 1h with shaking. The cells were then plated onto the LB agar (LBA) and ampicillin petri dish under sterile conditions. The plate was incubated at 37 °C overnight.

3.2.3: *E. coli* cell growth and cell lysis

After overnight incubation, one single colony was sterilely transformed into 100 mL LB and 100 µg/mL ampicillin, incubated at 37 °C overnight with agitation. The following day, 25 mL preculture was transformed into 1 L LB and 100 µg/mL ampicillin culture. Typically, 6 L of cell culture was carried out. The aforementioned cultures were incubated at 37 °C with shaking (200 rpm) until the optical density (OD) at 600 nm reached the exponential phase of the growth (OD_{600nm} of 0.7). The culture was induced by the addition of 1mM Isopropyl β-D-1-thiogalactopyranoside (IPTG), and simultaneously the temperature was remained at 37 °C for 3 hours with shaking (200 rpm) or reduced to 24 °C for 5 hours with shaking (200 rpm). Then the cell pellets were harvested at 800 × g for 20 min at 4 °C using the Avanti JLA8.1 rotor. The cell pellets were used for protein purification freshly or stored at -20 °C. After harvesting, the cell

pellets were resuspended using cell lysis buffer in the ratio of 1:10 (w/v). The cell lysis consists of 50 mM Tris-HCl pH 8.0, 200 mM NaCl, 5% glycerol and freshly dissolved EDTA-free protease inhibitor (Sigma Aldrich, USA). The cell slurry was then passed through the Emulsiflex-C3 homogenizer (ATA scientific, New South Wales, Australia) three cycles at 40 kpsi for cell lysis.

3.2.4: Isolation of inclusion body

Following cell lysis, 0.5% Triton X-100 was added to the cell lysate to further break the non-specific interactions between proteins. Then the cell lysate was harvested at 20, 000 × g for 20 min at 4 °C using the Beckman TI45 rotor. The supernatant was discarded and the pellets, which contain the IBs, the unbroken cells and the cell debris were collected. The pellets were washed by two centrifugation steps at 20, 000 × g for 20 min at 4 °C using the Beckman TI45 rotor. Before centrifugation, the pellets were resuspended with a buffer contains 50 mM Tris-HCl pH 8.0, 200 mM NaCl, 5% glycerol and 0.5% Triton X-100 and then homogenized. A final wash step was performed using the above buffer except for the 0.5% Triton X-100.

3.2.5: Denature of His-TEV-hB7-1[35-242] protein

As discussed earlier, IB contains high purity of the target protein but in an insoluble, unfolded or misfolded state, which needs to be denatured and refolded to recover the activity. Denaturation typically takes place with strong chaotropic agents such as urea or guanidium hydrochloride. Urea disrupts the hydrogen bonding network of water molecules, thus reduces the hydrophobic effects of the hydrophobic part of the protein, thereby solubilizes the hydrophobic part of the protein and denatures the protein. In this project, an unfolding buffer, which consists of 50 mM Tris-HCl pH 8.0, 200 mM NaCl and 8 M urea was used to denature the protein with stirring at 4 °C overnight.

3.2.6: Immobilized metal affinity chromatography purification of recombinant B7-1

Poly-histidine tag is one of the most commonly used tags and can bind to different immobilized ions, such as nickel, copper, and cobalt.[287] In this project, I performed the nickel nitrilotriacetic acid (Ni-NTA) immobilized metal affinity chromatography (IMAC) purification as the initial purification step. The denatured protein suspension was homogenized and harvested at 20,000 × g for 20 min at 4 °C using the Beckman TI45 rotor. The supernatant was combined with

nickel resin and mixed at 4 °C for 1.5 hours. The suspension, which contains the mixture of the protein and the resin was then passed through a gravity flow column and the flow-through was collected. Followed by a wash step (20 mM imidazole, until OD_{280nm} less than 0.1) and an elution step (500 mM imidazole, until OD_{280nm} less than 0.1), the protein fractions, which contain the protein of interest were collected for refolding. 3 mM β-mercaptoethanol (βME) was added to the protein fractions to reduce the nonnative disulfide bonds, thus alleviate the aggregation. The purity of His-TEV-hB7-1[35-242] in each fraction was assessed based on the sodium dodecyl sulfate polyacrylamide gel electrophoresis SDS-PAGE (Coomassie staining) result.

3.2.7: Refolding of His-TEV-hB7-1[35-242] protein

Prior to refolding, the denaturant needs to be removed. The dialysis buffer, which contains 5 M urea, 50 mM Tris-HCl (pH 8.0), 200 mM NaCl, 10% glycerol, 0.05% Tween-20, 150 mM glycine, 5 mM cystamine and 0.5 mM cysteamine was used to slowly remove the urea from the protein and thus refold the protein (the detail of the other dialysis systems see Table 3.1). The protein was dialyzed against 5 M urea, 4 M urea until 1 M urea. Each step maintains 1.5 hours with stirring at 4 °C. In the end, the protein was dialyzed against the same buffer except for no urea overnight at 4 °C. The purpose of the slow dialysis is to reduce the protein aggregations.

3.2.8: Size exclusion chromatography purification of recombinant B7-1

Size exclusion chromatography (SEC) was performed as the final step of protein purification. The refolded proteins were harvested for 10 min at 4 °C to remove the precipitants and then concentrated to increase the concentration. Then the concentrated proteins were loaded onto a Superdex 200 10/300GL column and run at 0.3 mL/min. The running buffer contains 50 mM Tris-HCl (pH 8.0), 200 mM NaCl, 5% glycerol. The elution of the target protein was then confirmed by SDS-PAGE followed by Coomassie staining. After SEC, all the fractions containing the target protein were pooled together and concentrated. The generated recombinant protein was either flash used or kept at - 80 °C.

3.2.9: SDS-PAGE and western blotting

SDS-PAGE and western blotting were performed to confirm the expression and the relative purity of the recombinant protein. The protein fractions were loaded to 16% SDS-PAGE gels and

the electrophoreses were performed under 180 volts. Then the separated proteins on the gels were blotted on the polyvinylidene fluoride (PVDF) membranes by transfer buffer (methanol 150 ml, Tris-base 4.35 g, glycine 2.18 g, SDS 0.28 g) using electrophoresis method for 1 hour at 100 volts. The membranes were blocked using blocking buffer (1 × TBS-(0.05%) Tween-20 (pH 7.6), 5% (w/v) dry milk) for 1 hour with shaking followed by overnight incubation at 4 °C. On the following day, the membranes were thoroughly washed using washing buffer (1 × TBS-(0.05%) Tween-20 (pH 7.6)). Further, the primary mouse anti-His tag antibody (1:460 dilution) was added to the membranes and incubated at room temperature for 1 hour with shaking. Next, the membranes were washed three times. Then the secondary rabbit anti-mouse IgG peroxidase antibody (1:5000 dilution) was added to the membranes and incubated at room temperature for 1 hour with shaking. Then the membranes were washed three times. The Amersham™ ECL™ western blotting detection reagents were mixed well to detect the reaction and the photos were recorded using the Odyssey® Fc imaging system.

3.2.10: Determination of protein concentration

Bicinchoninic acid (BCA) assay is one of the commonly used methods to determine protein concentration. In this project, the concentrations of the in-house proteins and the commercial protein were determined by microplate BCA assays using the Pierce™ BCA protein assay kit (Thermo Fisher Scientific, USA). BCA working reagent was prepared freshly according to the manufacturer's instruction. The BSA standard buffers (working range = 125 – 2000 µg/mL) were prepared using the SEC running buffer as the dilution buffer so that the BSA samples have the same buffer system as the in-house proteins. Add 10 µL of each BSA standard or protein sample (duplicate) into a microplate well. Then add 200 µL BCA working reagent to each well, mixed by shaking for 30 seconds and incubated at 37 °C for 30 minutes. The absorbance at 562nm (A_{562nm}) was measured by a microplate spectrophotometer. The average A_{562nm} values of the blank samples were subtracted from all the other samples. The average blank corrected BSA standard curve was plotted by A_{562nm} values against concentrations (µg/mL). The standard curve was then used to determine the unknown protein concentrations.

3.2.11: hB7-1/hCTLA-4 binding assay

His-tagged commercial hB7-1[35-242] (R & D systems, Minnesota, USA, Lot: DDIK0418051), His-tagged in-house hB7-1[35-242] and biotinylated Fc-tagged commercial hCTLA-4[37-162] were used for the binding assays. The binding assays were performed by coating commercial hB7-1 or in-house hB7-1 to the high binding surface 96-well microplates. Some wells were left without coating with hB7-1 were treated as backgrounds. The microplates were incubated at 4 ℃ overnight. The following day, all the wells were washed three times and then blocked with the blocking buffer for 1.5 hours at 37 ℃. Subsequently, the wells were thoroughly washed. The diluted biotinylated hCTLA-4 was added to the wells, leaving some wells as no-binding controls. Then repeat the washing step and blocking step (at 37 ℃ for 10 minutes). After the wells were washed three times, the diluted streptavidin horseradish peroxidase (HRP) (1:200) was added for the conjugation with the biotinylated hCTLA-4 at 37 ℃ for 1 hour. After washing, the 3,3′,5,5′-Tetramethylbenzidine (TMB) substrate was added to each well and incubated at 37 ℃ in dark. In the end, the stop solution was added to each well to terminate the reactions. The A_{450nm} was detected by the microplate spectrophotometer. The results were corrected by subtracting the averaged A_{450nm} value of the background. The results were analyzed by GraphPad Prism version 8.3.0 (328).

3.3: Results and discussions

Different parameters were optimized to improve the yield of the recombinantly expressed hB7-1, including the parameters in protein expression (such as induction agent concentration, induction time and temperature, and media) and protein purification (such as refolding conditions). The results of the major steps were also shown below.

3.3.1: Induction agent concentration optimization for the expression of recombinant B7-1

Some proteins are highly sensitive to the concentration of the inducer. For example, the recombinant cyclomaltodextrinase formed soluble or insoluble protein when induced with different concentrations of IPTG.[288] Inducing the recombinant protein with a higher concentration of the inducer speeds up the transcript process, thus facilitates IB (aggregated proteins) formation. I cultivated the bacterial culture at 37 °C until the OD_{600nm} reaches 0.7, then induced the culture at 37 °C with 0.01 mM IPTG, 0.1 mM IPTG, 1 mM IPTG for 1 hour and 5 hours. Figure 3.2 shows

the His-TEV-hB7-1[35-242]. At this temperature despite the concentration of the inducer IPTG, I observe very little recombinant protein. I decided to further analyze other conditions with the most commonly used concertation of 1 mM IPTG to induce the recombinant protein.

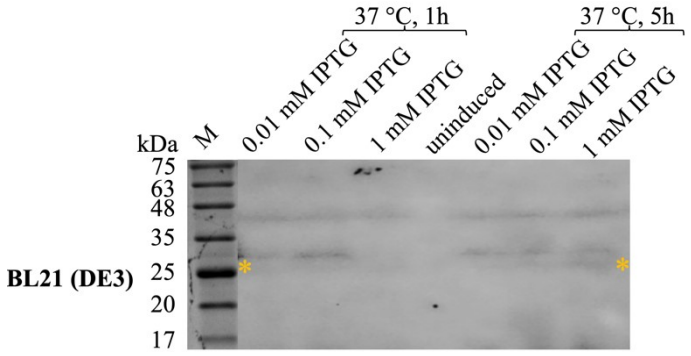

Figure 3. 2 Western blotting analysis of induction agent concentration optimization.

M represents the protein marker, h represents the hour. His-TEV-hB7-1[35-242] is 25.5 kDa and labeled by the asterisk (*).

3.3.2: Induction time and temperature optimization for the expression of recombinant B7-1

Normally, low temperature slows down the rate of transcription and translation, providing sufficient time for recombinant protein to fold correctly. To test this, I cultivated the overnight bacterial culture at 37 °C until the OD_{600nm} reaches 0.7, then subincubated the culture with 1 mM IPTG at 24 °C and 37 °C, respectively. The recombinant proteins forming insoluble IBs, they have a higher yield at a lower temperature, which is a common phenomenon due to the slowing down of the translation machinery.[289] I compared the different induction times at 24 °C (Fig. 3.3), including 1 hour, 3 hours, 5 hours, 8 hours, and 20 hours. Figure 3.3 and Figure 3.4 prove the optimal His-TEV-hB7-1[35-242] expression is performed at 24 °C induced by 1 mM IPTG for 5 hours in *E. coli* BL21 (DE3). Inducing the protein expression at 24 °C generated more protein compared to 37 °C (Fig. 3.4), however, whether the recombinant protein at this stage in the optimization was in the soluble or inclusion body fraction was unclear. Therefore, moving forward both the original expression method (induction with 1mM IPTG at 37 °C for 3 hours) and the optimized expression method (induction with 1 mM IPTG at 24 °C for 5 hours) were used to prepare the target protein.

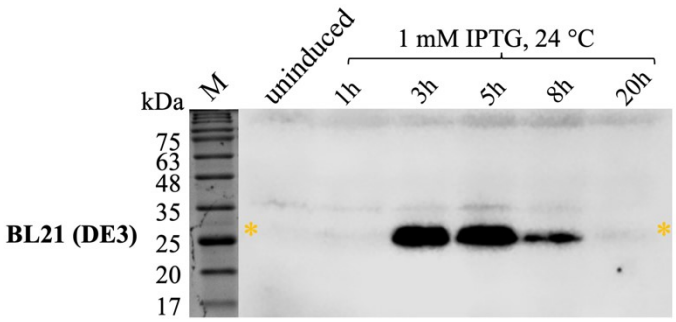

Figure 3. 3 Western blotting analysis of induction time optimization.

M represents the protein marker, h represents the hour. His-TEV-hB7-1[35-242] is 25.5 kDa and labeled by the asterisk (*).

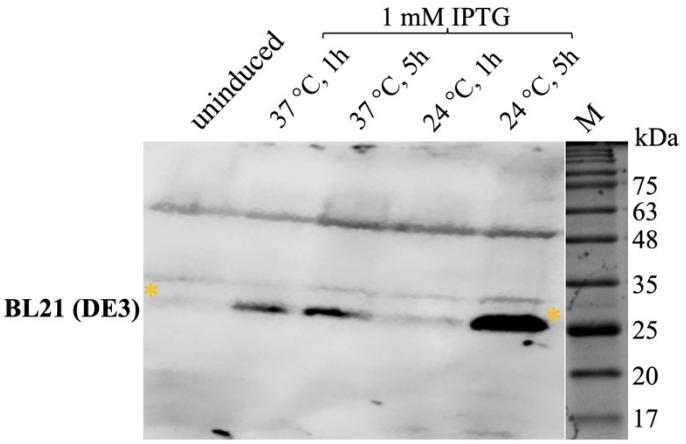

Figure 3. 4 Western blotting analysis of induction temperature optimization.

M represents the protein marker, h represents the hour. His-TEV-hB7-1[35-242] is 25.5 kDa and labeled by the asterisk (*).

3.3.3: IMAC purification of recombinant B7-1

Before the IMAC purification step, the IBs (aggregated proteins) were denatured by using 8 M urea with stirring at 4 °C overnight. As mentioned earlier, 6× His tag can bind to different immobilized metal ions, such as cobalt, zinc, and nickel. Among them, cobalt has the highest binding selectivity, which can efficiently reduce the non-specific binding. However, cobalt also has low binding capacity. Thus, in this project, I used Ni-NTA resin, which has both relatively high binding selectivity and binding capacity (https://www.thermofisher.com/order/catalog/product/88221#/88221). IMAC was performed for the protein expressed at both 37 °C and 24 °C simultaneously to identify the best expression

conditions to generate protein (Fig. 3.5). Upon my initial IMAC, His-TEV-hB7-1[35-242] proteins were found in the elution fractions, but some were also detected in the flow-through. To improve the purification, I then increased the incubation time of the target protein with the nickel resin. I proceeded with the purification by accessing the purity of the eluted protein fractions on SDS-PAGE (Fig. 3.5). The His-TEV-hB7-1[35-242] protein was identified as a single band of 25.5 kDa.

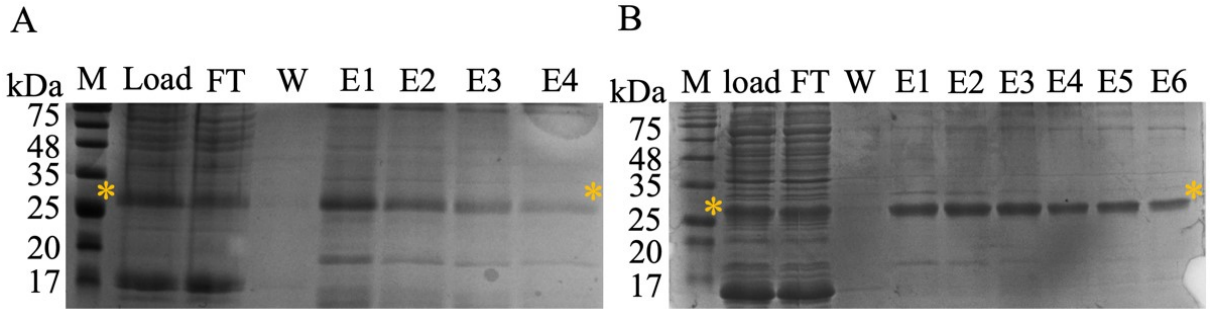

Figure 3. 5 16% SDS-PAGE gel for purification of recombinant B7-1 using Ni-NTA IMAC.

A, Induction of protein expression at 37 °C for 3 hours. B, Induction of protein expression at 24 °C for 5 hours. M represents the protein marker, load represents column load, FT represents flow through, W represents wash, the other lanes represent eluted protein fractions with the same imidazole concentration (500 mM). His-TEV-hB7-1[35-242] protein is 25.5 kDa and labeled by the asterisk (*).

3.3.4: Optimizing dialysis systems and SEC purification of recombinant B7-1

After IMAC purification, the His-TEV-hB7-1[35-242] was in the unfolded state, which needs to be refolded to the functional structure. In order to do that, the denaturant (urea) needs to be gradually removed. Dialysis is one commonly used method that allows removal of the denaturant thus allowing the refolding of the recombinant protein. One-step dialysis is fast but is prone to form a huge amount of protein aggregations. Stepwise dialysis is slow but alleviates the aggregation to some extent. Different types of chemical molecules have been added to the refolding buffer to reduce the non-covalent interactions between proteins, thus aiding in proper protein folding and reduction of aggregation subsequently leading to an increased yield of the recombinant protein.

In the unfolding buffer, urea was used as the denaturant to unfold the protein; glycerol and glycine were used as the protein stabilizer. There are four cysteine residues in the His-TEV-hB7-1[35-242] protein monomer. However, urea can neither break the existing disulfide bonds nor impede the formation of new disulfide bonds. Therefore a reducing agent is essential in Cys-

containing protein refolding. Reduced glutathione (GSH) works as a reducing agent to break the existing disulfide bonds, oxidized glutathione (GSSG) works as an oxidant to assist the formation of correct disulfide bonds.[290,291] Additionally, I also tried cystamine and cysteamine, which is cost-effective and had been used to successfully refold human programmed death receptor 1 (PD-1).[292] As discussed earlier, I also include βME, another commonly used reducing agent in the dialysis system to make sure the disulfide bonds fold properly. Different types of detergents were used to solubilize protein into the aqueous solutions, including Tween-20, Tween-80 and sodium lauryl sulfate (SLS).

The dialysis is a trial-and-error process, where I have explored the combinations of different chemical additives (Table 3.1) intending to obtain the high yield of refolded protein with intact biological activity. Thus the refolded proteins were further purified and analyzed by SEC (Table 3.1, Fig. 3.6). The peaks containing the refolded protein were highlighted by the blue circles, 2 mL protein samples were injected into the machine.

3.3.5 Characterization of purified recombinant B7-1

3.3.5.1 BCA assays

The commercially manufactured His-hB7-1[35-242] was obtained from the R & D systems, (Minnesota, USA, Lot: DDIK0418051). This protein was purified from human embryonic kidney (HEK) cell HEK293 using its 6 × His tag (with no TEV cleavage site). This protein was used as a control to compare with the recombinant His-TEV-hB7 expressed in the bacterium system. The biggest difference between the commercial protein and the in-house proteins is the PTM, especially the glycosylation. However, as mentioned earlier none of the glycosylated sites is involved in the receptor/ligand interface and these glycans are not required for CTLA-4 binding.[14,58,278] So the binding assays between the commercial protein and the in-house proteins are comparable.

Before the binding assay, protein concentration was measured in duplicates using BCA assays. The average concentrations of the His-TEV-hB7-1[35-242] protein sample 1 and sample 2 were 540 μg/mL and 196 μg/mL, respectively. The concentration of the commercial His-hB7-1[35-242] was 517 μg/mL.

Table 3. 1 Different refolding conditions and the SEC results for recombinant B7-1.

Dialysis Systems	Components	SEC traces
1	50mM Tris-HCl pH 8.0 300 mM NaCl 10% glycerol **0.05% Tween-80** **Glutathione (reduced) 1mM** **Glutathione (oxidized) 0.5 mM**	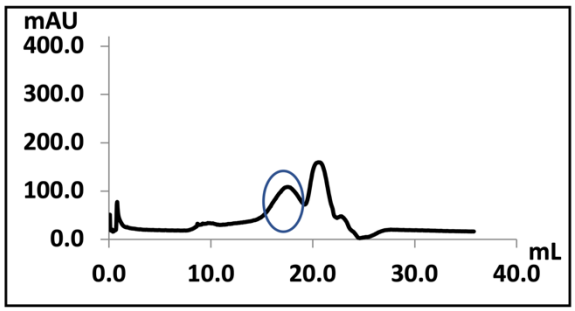
2	50mM Tris-HCl pH 8.0 300 mM NaCl 10% glycerol **150 mM glycine** **Glutathione (reduced) 1mM** **Glutathione (oxidized) 0.5 mM**	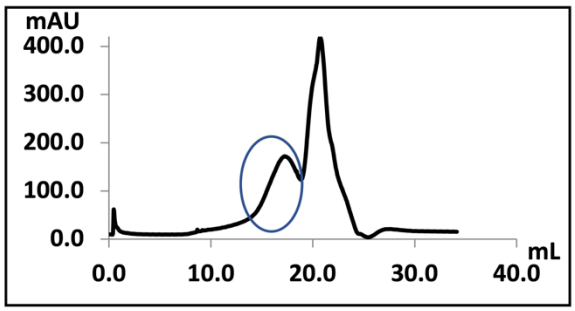
3	50mM Tris-HCl pH 8.0 300 mM NaCl 10% glycerol **0.05% SLS** **150mM glycine** **Cystamine 5mM** **Cysteamine 0.5 mM**	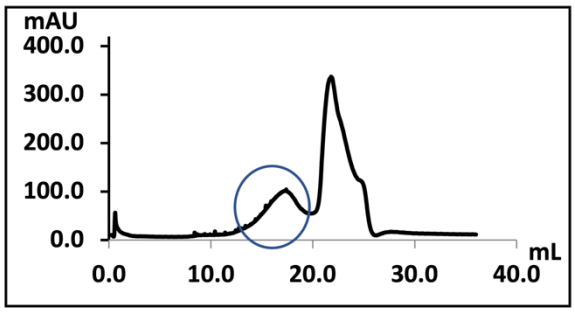
4	50mM Tris-HCl pH 8.0 300 mM NaCl 10% glycerol **0.05% Tween-20** **150mM glycine** **Cystamine 5mM** **Cysteamine 0.5 mM**	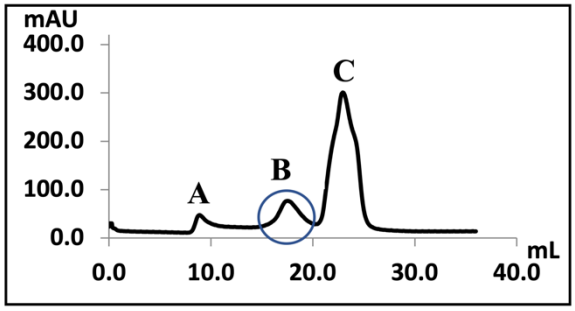

The parameters, which were changed in each refolding system are highlighted in bold. The peaks containing the refolded protein were highlighted by blue circles.

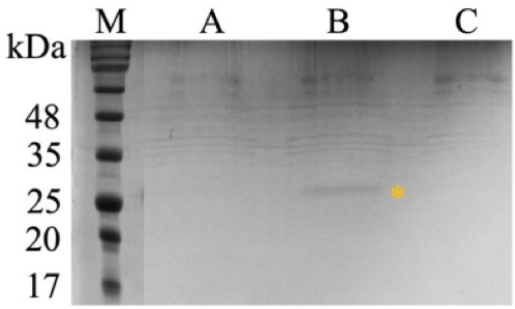

Figure 3. 6 Representative 16% SDS-PAGE gel for purification of recombinant B7-1 using SEC.

M represents the protein marker, load represents the protein sample before SEC, A represents the aggregation peak in row 4 of Table 3.1, B represents the concentrated recombinant hB7-1 peak in row 4 of Table 3.1, C represents the chemical peak in row 4 of Table A. His-TEV-hB7-1[35-242] protein is 25.5 kDa and labeled by the asterisk (*).

3.3.5.2 hB7-1/hCTLA-4 binding assays

The hB7-1/hCTLA-4 binding assays were performed to detect the binding activities of the recombinant hB7-1 to the hCTLA-4 and compare with the commercial hB7-1. There is no commercially available bacterial cell line expressed hB7-1 extracellular domain protein. In the beginning, I compared the binding ability of the two protein samples with the commercial protein. These two protein samples were prepared following the same protocol, except for the dialysis system. Table A row 2 and row 3 show the dialysis systems of the in-house protein sample 1 and sample 2. The same amount (0.1 μg/well) of the commercial and protein samples were coated to the plate to bind with different concentrations of the biotinylated hCTLA-4. Figure 3.7A shows that the commercial protein has stronger binding to hCTLTA-4, however, both in-house proteins have similar and weak binding to hCTLA-4, even when the concentration of hCTLA-4 increased. Based on the Two-way ANOVA followed by Turkey post-test, the hCTLA-4 binding activity between commercial hB7-1 and both the in-house proteins have a significant difference ($P < 0.0001$). However, the hCTLA-4 binding activity between the two in-house proteins doesn't have a significant difference. Then I assumed it could be the amount of the coated in-house protein is low. Thus compared the in-house protein sample 1, which has higher protein concentration, with the commercial protein. I increased the coating amount of the in-house protein: 0.1 μg/well, 0.5 μg/well and 1.0 μg/well. The results can be seen in Figure 3.7B. Two-way ANOVA result shows

there is no significant difference of the hCTLA-4 binding activity between the different doses of the in-house hB7-1.

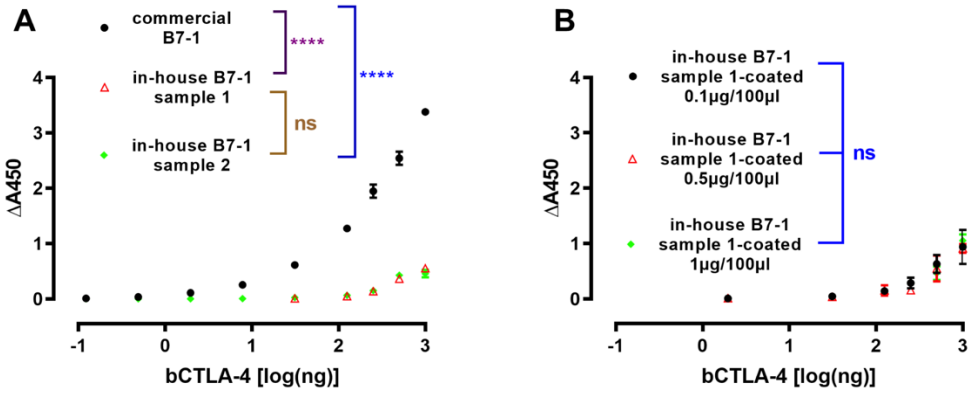

Figure 3. 7 Comparison of the binding activity of commercial and recombinant hB7-1 against hCTLA-4.

A, Comparison of different recombinant proteins. B, Comparison of the same recombinant protein using different concentrations. **** represents significant difference ($P < 0.0001$), ns represents no significant difference.

The limited hCTLA-4 binding activity of the recombinant proteins could be because the majority of the recombinant protein is misfolded or partially folded. As previously discussed, the PTM, to be specific the glycosylation doesn't influence the ligand binding.[14,58,278] Based on the comparison of the hCTLA-4 binding activity between the bacterial system and mammalian system prepared recombinant proteins, I infer that it could be the lack of chaperones that leads to the misfolding and limited activity of the recombinant protein.[293]

3.4: Conclusions and Future Directions

In this project, I tried to optimize parameters mainly for protein expression and protein refolding of B7-1 expressed in *E. coli*. I recombinantly expressed and purified the extracellular domain of hB7-1. I identified that the addition of 150 mM glycine, glutathione (reduced) 1mM, glutathione (oxidized) 0.5 mM in the refolding buffer could improve the yield of refolded protein a little bit. However, the comparison of binding activities of the refolded hB7-1 with that expressed and purified from mammalian cell lines (commercial hB7-1) indicated that the later has significantly higher activity.

Given the low expression and low affinity for CTLA4, in the future, I will focus on expressing the hB7-1 in the mammalian cell line. This will provide well folded and biologically

active protein to perform interaction studies with hCTLA-4. This protein will then be complexed with small molecule inhibitors, which have been predicted to bind using computational methods. would be used for further structural analysis. Additionally, site-directed mutagenesis will be performed to understand the significance of crucial residues predicted using computational studies.

CHAPTER 4: GENERAL DISCUSSION

Human B7-1 is the first and the most characterized costimulatory protein from the B7 family, which is an important target for the treatment of autoimmune diseases and possibly cancers.[86,171,246,247] The expression of hB7-1 was mainly detected on various lymphocytes, including B cells, T cells, macrophages, dendritic cells, *etc*.[113] In addition to positively regulates the T-cell activation through a T-cell receptor CD28, hB7-1 also negatively mediates the T-cell responses through a CD28 homolog CTLA-4 or another B7-1 family member PD-L1.[15,44,67] By this way, hB7-1 plays a crucial role in maintaining T-cell homeostasis.

Except for the molecular cloning of the gene encoding B7,[13] the discovery of the hB7-1 binding partners and their corresponding biological functions,[15,44,67] the reports of the hB7-1 related crystal structures are undoubtedly also significant for the studies of hB7-1.[14,58] To date, two hB7-1 related crystal structures were determined. The first crystal structure determined the extracellular domain of hB7-1 using X-ray diffraction to 3 Å resolution in 2000.[14] The second crystal structure of the extracellular domains of the hB7-1/hCTLA-4 complex was also resolved using X-ray diffraction to 3 Å resolution in the following year.[58] These findings provided crucial structure information of hB7-1 as well as revealed the hot spots of hB7-1/hCTLA-4 protein/protein interaction. Therefore, facilitating the structure-based drug design. So far, two mAbs were proved by the FDA mainly for the treatment of autoimmune diseases.[246,294] Witnessed the clinical efficacy of targeting hB7-1, many researchers devoted to the development of other hB7-1 modulators, including mAbs, fusion proteins, and small-molecule inhibitors, which were summarized in our previous work.[248] As discussed above, hB7-1 interfere with both CD28 and CTLA-4 pathways, the developed hB7-1 small-molecule inhibitors were proven to block both pathways.[249,250] The crystal structure of the hB7-1/hCD28 complex is currently unresolved, it will help people understand the subtle differences between the hB7-1/hCD28 and hB7-1/hCTLA-4 interactions, thus, develop pathway-specific modulators.

Besides, most of the published studies focus on the development of hB7-1 modulators through high-throughput screening methods and chemical structure modifications of the lead compounds. This requires plenty of work and a huge amount of time. Even though different groups identified hB7-1 small-molecule inhibitors with high specificity and nanomolar affinity, a clear explanation about how these compounds interact with hB7-1 is still a gap in this field of

research.[249,250,295] The identity of the hot spots for hB7-1/small-molecule compounds binding will provide clues to develop hB7-1 modulators in a more meaningful and efficient way. Therefore, in this thesis, I aim to understand the binding sites and mode(s) of action of two hB7-1 small-molecule compounds (pre-checked using SPR assay) as discussed in Chapter 2. One hPD-L1 small-molecule compound (pre-checked using SPR assay) was utilized as the negative control. Then it is of utmost importance to confirm the identities of the modelling working on the experimental level. The preliminary results were described in Chapter 3.

To understand the interactions of the protein/compound complexes, I employed multiple advanced modelling techniques, protein preparation skills, and basic pharmaceutical analysis assay and physicochemical experiments. This thesis was presented according to the following order. Chapter 1 provided a comprehensive background of human B7-1, including the detailed structure information, the important B7/CD28/CTLA-4 interactions, the therapeutic roles of hB7-1, the current reported hB7-1 modulators, and the challenges of developing hB7-1 small-molecule inhibitors. Followed Chapter 1, the research aims of this thesis were described. Chapter 2 presented all of the modelling work, containing constructing hB7-1 dimer in the physiological state, binding sites prediction, the investigation of the protein/compound interactions. Then, Chapter 3 described all of the experimental progress, ranging from the details of the preparation of hB7-1 extracellular domain employing the bacteria system to the preliminary binding studies. Appendix A provided the protocol and results of the SPR assays.

In Chapter 2, two structural models, namely the human B7-1 monomer and dimer were constructed. It is worth mentioning that, the systems contain the C-terminal missing structures and the carbohydrates. These two models were then refined through 200 ns MD simulations. Such long MD simulations allowed the relaxation of the protein structures and the removal of the unfavorable interactions between residues. Thus, achieving the transition of the high energy state to the low energy state. In addition, the long MD simulations collected the representatives of the protein conformations into a conformational ensemble through RMSD-based clustering, which is required for more accurate molecular docking studies. Analyzing and comparing the MD trajectories of both the monomer and dimer systems allowed us to select the most stable system is the dimer. This was supported by the identity that the majority of hB7-1 expressed as homodimers on the cell surface.[245] The assembling of the protein/compound complexes were required to perform the molecular docking studies and to understand their interactions. Based on the knowledge, there is

no hB7-1/small-molecule compound model available. Only the hB7-1/hCTLA-4 protein/protein crystal structure was resolved in a 2:2 stoichiometry.[58] However, hB7-1 and hCTLA-4 forming such a dimer-dimer complex is because their especially complementary shape, this may not be the case of the hB7-1/compound complex. Therefore, I assembled the hB7-1/ small-molecule compound in a 2:1 stoichiometry and performed the following studies. In the future, different stoichiometries of the complex can be tested. Since currently, there is no literature reported on the detailed protein/compound binding site, I need to predict the binding sites before docking studies. MOE-Site Finder and FTSite relied on geometry-based and energy-based methods, respectively to identify the probable binding sites.[262] I have two reasons to use two different binding sites prediction methods. The first reason is that different binding site prediction methods may provide more possible predicted sites for the docking studies. Secondly, if the two binding site prediction methods identified the same or at least similar predicted sites, this can confirm the accuracy of the binding site prediction results. To investigate the interactions of hB7-1 and these compounds, the three compounds were docked into the two predicted binding sites. I performed the induced-fit refinement method to consider the flexibility of the protein, which is always ignored by most of the docking programs. However, the induced-fit refinement method only considering the sidechain flexibility of the binding site residues within the protein. Therefore, the protein conformational ensemble as described above was necessary to further consider the flexibility of the entire protein. I executed 15 ns-length MD simulations to refine the protein/compound complexes. To ensure only the stable ligands were selected, I utilized three parameters to filter the complexes, including the RMSDs of the ligands, the dynamicity of the complexes and the binding free energy of each system. In this way, the optimal complexes were successfully filtered. The results revealed one binding site, however two binding orientations of inhibitor 1 within hB7-1. This binding site located between two loops at the lower part of the IgV domain of hB7-1, far away from the hB7-1/hCTLA-4 protein/protein binding site. Analyzing the H-bond interactions and decomposing the binding free energies of these protein/compound complexes allowed us to identify the most significant residues for their binding. Interestingly, I identified a completely different binding site for inhibitor 2 within hB7-1, which located at the upper part of the IgV domain of hB7-1, occupied the β sheets. This binding site may overlap with the hB7-1/hCTLA-4 protein/protein binding site as supported by some conserved residues (Arg29, Tyr31, Met43) presented in both the protein/protein and protein/compound binding site.[58] The success of finding the binding sites and

mode(s) of action of hB7-1 small-molecule inhibitors provide clues for the future development of hB7-1 modulators more scientifically and efficiently.

To confirm the predicted binding sites in the experimental level, I decided to prepare the wild type extracellular domain of hB7-1 and if possible, also prepare the mutated proteins with the modelling work identified binding site residues (*e.g.* Arg29, Tyr31, Met42, Met43, Asn48, Asp55, Arg56, Leu70, Arg73, and Glu160 of hB7-1) mutated through mutagenesis assays. Moreover, two hCTLA-4 binding site residues Tyr31 and Met38 on hB7-1 were demonstrated to disrupt the interactions of hB7-1 with both CD 28 and CTLA-4 after mutations.[296] This attracts extra attention to amino acid Met38. To prepare the recombinant hB7-1, first of all, I need to decide which expression system to use. The biggest difference between expressing a protein in the mammalian expression system and bacterial expression system is the ability to induce post-translational modification, which is always important for protein folding and protein function.[280] One research team attempted to generate non-glycosylated hB7-1 and discovered that these glycans in hB7-1 were not necessary for receptor binding.[278] Furthermore, expressing a protein in a mammalian expression system requires long-expression period and has relatively low expression yield. Therefore, I decided to express the extracellular domain of hB7-1 in the *E. coli* expression system, which is faster and usually has a higher protein expression yield. To match the model used in the modelling work, the same sequence of the target protein (the extracellular domain of hB7-1) was used. For purification, a hexahistidine tag was added to the C-termini of the protein. A TEV tag was inserted in between, in case of the cleavage of the histidine tag is required. Overexpressing the recombinant eukaryotic protein hB7-1 in a prokaryotic *E. coli* expression system, leading to the formation of inclusion bodies where the misfolded or unfolded protein aggregations are stored. In some scenarios, researchers avoid forming insoluble inclusion bodies. However, in this project, I took advantage of the inclusion body, where about 90% pure recombinant protein was contained.[286] I expressed the recombinant hB7-1 by denaturing the protein and then refolding it *in vitro*. Two purification steps were utilized to obtain the pure hB7-1, including the Ni-NTA affinity chromatography and the size exclusion chromatography. I optimized the parameters to improve the expression amount by reducing the expression temperature from 37 ° to 24 °, extending the expression time from 3 hours to 5 hours and using induce agent IPTG of 1 mM. The most challenging part of expressing the recombinant protein from inclusion bodies is to refold the protein properly. I optimized the refolding systems using different combinations of chemical

additives and try to reduce the protein aggregations. Then the activity of the purified recombinant hB7-1 was detected through binding assays. I compared the ability of the recombinant hB7-1 proteins to bind a natural ligand hCTLA-4 with the commercial recombinant hB7-1. As shown in Chapter 3 Figure 3.7, the recombinant proteins have limited hCTLA-4 binding ability compared to that of the commercial hB7-1. If the glycans don't influence the binding activity of the recombinant proteins, then it could be the lack of mammalian chaperones that causing the misfolding and limited activity of the recombinant proteins.

CHAPTER 5: FUTURE PERSPECTIVES

In this thesis, I established a workflow to predict the binding sites and mode(s) of action of two hB7-1 small-molecule inhibitors. To confirm the accuracy of the prediction, I expressed the extracellular domain of hB7-1 using the bacterial expression system in the form of inclusion bodies. However, the limited binding activity of the recombinant protein indicated that the produced recombinant protein may not be properly folded. Therefore, as a future direction, I will express hB7-1 in a mammalian expression system. I expect that the mammalian chaperons and the post-translational modifications, in principle, to help B7-1 fold correctly. In addition to preparing the wild type recombinant hB7-1, constructing the mutated recombinant hB7-1 proteins is also required. I plan to include the mutations of hB7-1 residues Asp55, Arg56, Leu70, Arg73, Glu160 to confirm the mode of action of inhibitor 1 and also residues Arg29, Tyr31, Met42, Met43, and Asn48 to confirm the mode of action of inhibitor 2. Comparing the binding ability of the commercial hB7-1 with the recombinant wild type hB7-1 will confirm if the recombinant proteins are correctly folded. Comparing the binding activity of the wild type hB7-1 with the mutated proteins will confirm the accuracy of the modelling findings. Previously, I detected the binding activity of the recombinant hB7-1 to hCTLA-4, in the future, I will also perform the hB7-1/hCD28 binding assay. If the mutation of any residue has different binding affinities to hCD28 and hCTLA-4, I can discover the binding propensity of hB7-1 residues towards CD28 and CTLA-4. In the long run, such discoveries can guide the development of pathway-specific hB7-1 small-molecule modulators.

Except for the structures of small-molecule compounds inhibitor 1 and inhibitor 2 as shown in Figure 2.2, other tautomers also exist due to the delocalization of the lone pairs on nitrogen or oxygen atom. In different tautomers, the roles of some atoms in H-bond networking may change because of the H-bond donor turns into H-bond acceptor and vice versa. H-bond networking plays an essential role in protein/compound interaction. Different tautomers of the same compound may form different interactions with the same target protein. On classical simulations, all atoms will preserve their initial protonation states in the course of the simulation, the conversion between compound tautomers is not allowed. Therefore, considering the tautomers of the compounds will generate more accurate modelling results. Beyond the two hB7-1 small-molecule inhibitors I tested in this thesis, there are other hB7-1 small-molecule compounds with high binding specificities and

nanomolar binding affinities. First of all, I will detect if these compounds also specifically bind to hB7-1 through SPR assays. Then I will study the mode(s) of action of these compounds using the same protocol established by this thesis. Through comparing the chemical structures and the mode(s) of action of a series of these compounds, one can identify the important structural fragments for the protein/compound interactions. This information can provide important insights towards rationally design selective and potent hB7-1 small-molecule modulators.

BIBLIOGRAPHY:

1. Strutt TM, McKinstry KK, Swain SL. Control of innate immunity by memory CD4 T cells. *Adv Exp Med Biol.* 2011;780:57-68.
2. Pardoll DM. The blockade of immune checkpoints in cancer immunotherapy. *Nat Rev Cancer.* 2012;12(4):252-264.
3. Śledzińska A, Menger L, Bergerhoff K, Peggs KS, Quezada SA. Negative immune checkpoints on T lymphocytes and their relevance to cancer immunotherapy. *Molecular Oncology.* 2015;9(10):1936-1965.
4. Bluestone JA, Bour-Jordan H, Cheng M, Anderson M. T cells in the control of organ-specific autoimmunity. *The Journal of Clinical Investigation.* 2015;125(6):2250-2260.
5. Wolchok JD, Chiarion-Sileni V, Gonzalez R, et al. Overall Survival with Combined Nivolumab and Ipilimumab in Advanced Melanoma. *N Engl J Med.* 2017;377(14):1345-1356.
6. Hodi FS, Chiarion-Sileni V, Gonzalez R, et al. Nivolumab plus ipilimumab or nivolumab alone versus ipilimumab alone in advanced melanoma (CheckMate 067): 4-year outcomes of a multicentre, randomised, phase 3 trial. *Lancet Oncol.* 2018;19(11):1480-1492.
7. Sharpe AH, Freeman GJ. The B7–CD28 superfamily. *Nature Reviews Immunology.* 2002;2:116.
8. Curtsinger JM, Mescher MF. Inflammatory cytokines as a third signal for T cell activation. *Curr Opin Immunol.* 2010;22(3):333-340.
9. Curtsinger JM, Schmidt CS, Mondino A, et al. Inflammatory cytokines provide a third signal for activation of naive CD4+ and CD8+ T cells. *J Immunol.* 1999;162(6):3256-3262.
10. Harris NL, Ronchese F. The role of B7 costimulation in T-cell immunity. *Immunol Cell Biol.* 1999;77(4):304-311.
11. Paust S, Lu L, McCarty N, Cantor H. Engagement of B7 on effector T cells by regulatory T cells prevents autoimmune disease. *Proceedings of the National Academy of Sciences of the United States of America.* 2004;101(28):10398.
12. Azuma M, Ito D, Yagita H, et al. B70 antigen is a second ligand for CTLA-4 and CD28. *Nature.* 1993;366(6450):76-79.
13. Freeman GJ, Freedman AS, Segil JM, Lee G, Whitman JF, Nadler LM. B7, a new member of the Ig superfamily with unique expression on activated and neoplastic B cells. *J Immunol.* 1989;143(8):2714-2722.
14. Ikemizu S, Gilbert RJ, Fennelly JA, et al. Structure and dimerization of a soluble form of B7-1. *Immunity.* 2000;12(1):51-60.
15. Linsley PS, Brady W, Grosmaire L, Aruffo A, Damle NK, Ledbetter JA. Binding of the B cell activation antigen B7 to CD28 costimulates T cell proliferation and interleukin 2 mRNA accumulation. *J Exp Med.* 1991;173(3):721-730.
16. Taylor PA, Lees CJ, Fournier S, Allison JP, Sharpe AH, Blazar BR. B7 Expression on T Cells Down-Regulates Immune Responses through CTLA-4 Ligation via R-T Interactions. *The Journal of Immunology.* 2004;172(1):34.
17. Freeman GJ, Gribben JG, Boussiotis VA, et al. Cloning of B7-2: a CTLA-4 counter-receptor that costimulates human T cell proliferation. *Science.* 1993;262(5135):909-911.
18. Klaus SJ, Pinchuk LM, Ochs HD, et al. Costimulation through CD28 enhances T cell-dependent B cell activation via CD40-CD40L interaction. *J Immunol.* 1994;152(12):5643-5652.

19. Snanoudj R, Frangié C, Deroure B, et al. The blockade of T-cell co-stimulation as a therapeutic stratagem for immunosuppression: Focus on belatacept. *Biologics : targets & therapy.* 2007;1(3):203-213.
20. Freeman GJ, Boussiotis VA, Gribben JG, Sharpe AH, Nadler LM. B7 (CD80 and CD86). In: Delves PJ, ed. *Encyclopedia of Immunology (Second Edition).* Oxford: Elsevier; 1998:304-308.
21. Boise LH, Minn AJ, Noel PJ, et al. CD28 costimulation can promote T cell survival by enhancing the expression of Bcl-xL. *Immunity.* 1995;3(1):87-98.
22. Lindstein T, June CH, Ledbetter JA, Stella G, Thompson CB. Regulation of lymphokine messenger RNA stability by a surface-mediated T cell activation pathway. *Science.* 1989;244(4902):339.
23. Boonen GJJC, van Dijk AMC, Verdonck LF, van Lier RAW, Rijksen G, Medema RH. CD28 induces cell cycle progression by IL-2-independent down-regulation of p27kip1 expression in human peripheral T lymphocytes. *European Journal of Immunology.* 1999;29(3):789-798.
24. Kovalev GI, Franklin DS, Coffield VM, Xiong Y, Su L. An Important Role of CDK Inhibitor $p18^{INK4c}$ in Modulating Antigen Receptor-Mediated T Cell Proliferation. *The Journal of Immunology.* 2001;167(6):3285.
25. Cannons JL, Lau P, Ghumman B, et al. 4-1BB ligand induces cell division, sustains survival, and enhances effector function of CD4 and CD8 T cells with similar efficacy. *J Immunol.* 2001;167(3):1313-1324.
26. Oh HS, Choi BK, Kim YH, et al. 4-1BB Signaling Enhances Primary and Secondary Population Expansion of CD8+ T Cells by Maximizing Autocrine IL-2/IL-2 Receptor Signaling. *PLoS One.* 2015;10(5):e0126765.
27. Hutloff A, Dittrich AM, Beier KC, et al. ICOS is an inducible T-cell co-stimulator structurally and functionally related to CD28. *Nature.* 1999;397(6716):263-266.
28. Swallow MM, Wallin JJ, Sha WC. B7h, a novel costimulatory homolog of B7.1 and B7.2, is induced by TNFalpha. *Immunity.* 1999;11(4):423-432.
29. Wang S, Zhu G, Chapoval AI, et al. Costimulation of T cells by B7-H2, a B7-like molecule that binds ICOS. *Blood.* 2000;96(8):2808-2813.
30. Yao S, Zhu Y, Zhu G, et al. B7-h2 is a costimulatory ligand for CD28 in human. *Immunity.* 2011;34(5):729-740.
31. Yoshinaga SK, Zhang M, Pistillo J, et al. Characterization of a new human B7-related protein: B7RP-1 is the ligand to the co-stimulatory protein ICOS. *Int Immunol.* 2000;12(10):1439-1447.
32. Croft M. Costimulation of T cells by OX40, 4-1BB, and CD27. *Cytokine Growth Factor Rev.* 2003;14(3-4):265-273.
33. Godfrey WR, Fagnoni FF, Harara MA, Buck D, Engleman EG. Identification of a human OX-40 ligand, a costimulator of CD4+ T cells with homology to tumor necrosis factor. *J Exp Med.* 1994;180(2):757-762.
34. Gramaglia I, Weinberg AD, Lemon M, Croft M. Ox-40 ligand: a potent costimulatory molecule for sustaining primary CD4 T cell responses. *J Immunol.* 1998;161(12):6510-6517.
35. Paterson DJ, Jefferies WA, Green JR, et al. Antigens of activated rat T lymphocytes including a molecule of 50,000 Mr detected only on CD4 positive T blasts. *Mol Immunol.* 1987;24(12):1281-1290.

36. Triebel F, Jitsukawa S, Baixeras E, et al. LAG-3, a novel lymphocyte activation gene closely related to CD4. *J Exp Med.* 1990;171(5):1393-1405.
37. Baixeras E, Huard B, Miossec C, et al. Characterization of the lymphocyte activation gene 3-encoded protein. A new ligand for human leukocyte antigen class II antigens. *J Exp Med.* 1992;176(2):327-337.
38. Xu F, Liu J, Liu D, et al. LSECtin expressed on melanoma cells promotes tumor progression by inhibiting antitumor T-cell responses. *Cancer Res.* 2014;74(13):3418-3428.
39. Kouo T, Huang L, Pucsek AB, et al. Galectin-3 Shapes Antitumor Immune Responses by Suppressing CD8+ T Cells via LAG-3 and Inhibiting Expansion of Plasmacytoid Dendritic Cells. *Cancer Immunol Res.* 2015;3(4):412-423.
40. Monney L, Sabatos CA, Gaglia JL, et al. Th1-specific cell surface protein Tim-3 regulates macrophage activation and severity of an autoimmune disease. *Nature.* 2002;415(6871):536-541.
41. Zhu C, Anderson AC, Schubart A, et al. The Tim-3 ligand galectin-9 negatively regulates T helper type 1 immunity. *Nat Immunol.* 2005;6(12):1245-1252.
42. Chiba S, Baghdadi M, Akiba H, et al. Tumor-infiltrating DCs suppress nucleic acid-mediated innate immune responses through interactions between the receptor TIM-3 and the alarmin HMGB1. *Nat Immunol.* 2012;13(9):832-842.
43. Huang YH, Zhu C, Kondo Y, et al. CEACAM1 regulates TIM-3-mediated tolerance and exhaustion. *Nature.* 2015;517(7534):386-390.
44. Linsley PS, Brady W, Urnes M, Grosmaire LS, Damle NK, Ledbetter JA. CTLA-4 is a second receptor for the B cell activation antigen B7. *J Exp Med.* 1991;174(3):561-569.
45. Ishida Y, Agata Y, Shibahara K, Honjo T. Induced expression of PD-1, a novel member of the immunoglobulin gene superfamily, upon programmed cell death. *EMBO J.* 1992;11(11):3887-3895.
46. Latchman Y, Wood CR, Chernova T, et al. PD-L2 is a second ligand for PD-1 and inhibits T cell activation. *Nat Immunol.* 2001;2(3):261-268.
47. Kwon BS, Tan KB, Ni J, et al. A newly identified member of the tumor necrosis factor receptor superfamily with a wide tissue distribution and involvement in lymphocyte activation. *J Biol Chem.* 1997;272(22):14272-14276.
48. Montgomery RI, Warner MS, Lum BJ, Spear PG. Herpes simplex virus-1 entry into cells mediated by a novel member of the TNF/NGF receptor family. *Cell.* 1996;87(3):427-436.
49. Sedy JR, Gavrieli M, Potter KG, et al. B and T lymphocyte attenuator regulates T cell activation through interaction with herpesvirus entry mediator. *Nat Immunol.* 2005;6(1):90-98.
50. Watanabe N, Gavrieli M, Sedy JR, et al. BTLA is a lymphocyte inhibitory receptor with similarities to CTLA-4 and PD-1. *Nat Immunol.* 2003;4(7):670-679.
51. Boles KS, Vermi W, Facchetti F, et al. A novel molecular interaction for the adhesion of follicular CD4 T cells to follicular DC. *Eur J Immunol.* 2009;39(3):695-703.
52. Stanietsky N, Simic H, Arapovic J, et al. The interaction of TIGIT with PVR and PVRL2 inhibits human NK cell cytotoxicity. *Proc Natl Acad Sci U S A.* 2009;106(42):17858-17863.
53. Yu X, Harden K, Gonzalez LC, et al. The surface protein TIGIT suppresses T cell activation by promoting the generation of mature immunoregulatory dendritic cells. *Nat Immunol.* 2009;10(1):48-57.
54. Elahi S, Dinges WL, Lejarcegui N, et al. Protective HIV-specific CD8+ T cells evade Treg cell suppression. *Nat Med.* 2011;17(8):989-995.

55. Okoye IS, Houghton M, Tyrrell L, Barakat K, Elahi S. Coinhibitory Receptor Expression and Immune Checkpoint Blockade: Maintaining a Balance in $CD8^+$ T Cell Responses to Chronic Viral Infections and Cancer. *Front Immunol.* 2017;8:1215.
56. van der Merwe PA, Bodian DL, Daenke S, Linsley P, Davis SJ. CD80 (B7-1) Binds Both CD28 and CTLA-4 with a Low Affinity and Very Fast Kinetics. *Journal of Experimental Medicine.* 1997;185(3):393-404.
57. Schwartz J-CD, Zhang X, Fedorov AA, Nathenson SG, Almo SC. Structural basis for co-stimulation by the human CTLA-4/B7-2 complex. *Nature.* 2001;410:604.
58. Stamper CC, Zhang Y, Tobin JF, et al. Crystal structure of the B7-1/CTLA-4 complex that inhibits human immune responses. *Nature.* 2001;410:608.
59. Intlekofer AM, Thompson CB. At the Bench: Preclinical rationale for CTLA-4 and PD-1 blockade as cancer immunotherapy. *Journal of Leukocyte Biology.* 2013;94(1):25-39.
60. Lee JY, Lee HT, Shin W, et al. Structural basis of checkpoint blockade by monoclonal antibodies in cancer immunotherapy. *Nature Communications.* 2016;7:13354.
61. Tsai H-F, Hsu P-N. Cancer immunotherapy by targeting immune checkpoints: mechanism of T cell dysfunction in cancer immunity and new therapeutic targets. *Journal of Biomedical Science.* 2017;24(1):35.
62. Leach DR, Krummel MF, Allison JP. Enhancement of Antitumor Immunity by CTLA-4 Blockade. *Science.* 1996;271(5256):1734.
63. Abrams JR, Kelley SL, Hayes E, et al. Blockade of T Lymphocyte Costimulation with Cytotoxic T Lymphocyte–Associated Antigen 4–Immunoglobulin (Ctla4ig) Reverses the Cellular Pathology of Psoriatic Plaques, Including the Activation of Keratinocytes, Dendritic Cells, and Endothelial Cells. *Journal of Experimental Medicine.* 2000;192(5):681-694.
64. Keir ME, Sharpe AH. The B7/CD28 costimulatory family in autoimmunity. *Immunological Reviews.* 2005;204(1):128-143.
65. Lenschow DJ, Walunas TL, Bluestone JA. CD28/B7 SYSTEM OF T CELL COSTIMULATION. *Annual Review of Immunology.* 1996;14(1):233-258.
66. Zheng XX, Sayegh MH, Zheng XG, et al. The role of donor and recipient B7-1 (CD80) in allograft rejection. *The Journal of Immunology.* 1997;159(3):1169.
67. Butte MJ, Keir ME, Phamduy TB, Sharpe AH, Freeman GJ. Programmed death-1 ligand 1 interacts specifically with the B7-1 costimulatory molecule to inhibit T cell responses. *Immunity.* 2007;27(1):111-122.
68. Dakappagari N, Ho SN, Gascoyne RD, Ranuio J, Weng AP, Tangri S. CD80 (B7.1) is expressed on both malignant B cells and nonmalignant stromal cells in non-Hodgkin lymphoma. *Cytometry B Clin Cytom.* 2012;82(2):112-119.
69. Ni X, Song Q, Cassady K, et al. PD-L1 interacts with CD80 to regulate graft-versus-leukemia activity of donor CD8+ T cells. *J Clin Invest.* 2017;127(5):1960-1977.
70. Chaudhri A, Xiao Y, Klee AN, Wang X, Zhu B, Freeman GJ. PD-L1 Binds to B7-1 Only In Cis on the Same Cell Surface. *Cancer Immunol Res.* 2018;6(8):921-929.
71. Sugiura D, Maruhashi T, Okazaki IM, et al. Restriction of PD-1 function by cis-PD-L1/CD80 interactions is required for optimal T cell responses. *Science.* 2019;364(6440):558-566.
72. Tseng SY, Otsuji M, Gorski K, et al. B7-DC, a new dendritic cell molecule with potent costimulatory properties for T cells. *J Exp Med.* 2001;193(7):839-846.

73. Dong H, Zhu G, Tamada K, Chen L. B7-H1, a third member of the B7 family, co-stimulates T-cell proliferation and interleukin-10 secretion. *Nat Med.* 1999;5(12):1365-1369.
74. Freeman GJ, Long AJ, Iwai Y, et al. Engagement of the Pd-1 Immunoinhibitory Receptor by a Novel B7 Family Member Leads to Negative Regulation of Lymphocyte Activation. *The Journal of Experimental Medicine.* 2000;192(7):1027.
75. Chapoval AI, Ni J, Lau JS, et al. B7-H3: a costimulatory molecule for T cell activation and IFN-gamma production. *Nat Immunol.* 2001;2(3):269-274.
76. Suh WK, Gajewska BU, Okada H, et al. The B7 family member B7-H3 preferentially down-regulates T helper type 1-mediated immune responses. *Nat Immunol.* 2003;4(9):899-906.
77. Prasad DV, Richards S, Mai XM, Dong C. B7S1, a novel B7 family member that negatively regulates T cell activation. *Immunity.* 2003;18(6):863-873.
78. Sica GL, Choi IH, Zhu G, et al. B7-H4, a molecule of the B7 family, negatively regulates T cell immunity. *Immunity.* 2003;18(6):849-861.
79. Flies DB, Wang S, Xu H, Chen L. Cutting edge: A monoclonal antibody specific for the programmed death-1 homolog prevents graft-versus-host disease in mouse models. *J Immunol.* 2011;187(4):1537-1541.
80. Wang L, Rubinstein R, Lines JL, et al. VISTA, a novel mouse Ig superfamily ligand that negatively regulates T cell responses. *J Exp Med.* 2011;208(3):577-592.
81. Mager DL, Hunter DG, Schertzer M, Freeman JD. Endogenous retroviruses provide the primary polyadenylation signal for two new human genes (HHLA2 and HHLA3). *Genomics.* 1999;59(3):255-263.
82. Flajnik MF, Tlapakova T, Criscitiello MF, Krylov V, Ohta Y. Evolution of the B7 family: co-evolution of B7H6 and NKp30, identification of a new B7 family member, B7H7, and of B7's historical relationship with the MHC. *Immunogenetics.* 2012;64(8):571-590.
83. Zhao R, Chinai JM, Buhl S, et al. HHLA2 is a member of the B7 family and inhibits human CD4 and CD8 T-cell function. *Proc Natl Acad Sci U S A.* 2013;110(24):9879-9884.
84. Zhu Y, Yao S, Iliopoulou BP, et al. B7-H5 costimulates human T cells via CD28H. *Nat Commun.* 2013;4:2043.
85. Janakiram M, Chinai JM, Fineberg S, et al. Expression, Clinical Significance, and Receptor Identification of the Newest B7 Family Member HHLA2 Protein. *Clin Cancer Res.* 2015;21(10):2359-2366.
86. Greaves P, Gribben JG. The role of B7 family molecules in hematologic malignancy. *Blood.* 2013;121(5):734-744.
87. Zang X, Allison JP. The B7 Family and Cancer Therapy: Costimulation and Coinhibition. *Clinical Cancer Research.* 2007;13(18):5271.
88. Scarpa M, Scarpa M, Castagliuolo I, et al. CD80 down-regulation is associated to aberrant DNA methylation in non-inflammatory colon carcinogenesis. *BMC Cancer.* 2016;16:388.
89. Tirapu I, Huarte E, Guiducci C, et al. Low surface expression of B7-1 (CD80) is an immunoescape mechanism of colon carcinoma. *Cancer Res.* 2006;66(4):2442-2450.
90. Matulonis U, Dosiou C, Freeman G, et al. B7-1 is superior to B7-2 costimulation in the induction and maintenance of T cell-mediated antileukemia immunity. Further evidence that B7-1 and B7-2 are functionally distinct. *J Immunol.* 1996;156(3):1126-1131.
91. Van Gool SW, Delabie J, Vandenberghe P, Coorevits L, De Wolf-Peeters C, Ceuppens JL. Expression of B7-2 (CD86) molecules by Reed-Sternberg cells of Hodgkin's disease. *Leukemia.* 1997;11(6):846-851.

92. Zhang Q, Vignali Dario AA. Co-stimulatory and Co-inhibitory Pathways in Autoimmunity. *Immunity.* 2016;44(5):1034-1051.
93. Chang TT, Jabs C, Sobel RA, Kuchroo VK, Sharpe AH. Studies in B7-deficient mice reveal a critical role for B7 costimulation in both induction and effector phases of experimental autoimmune encephalomyelitis. *J Exp Med.* 1999;190(5):733-740.
94. Kinoshita K, Tesch G, Schwarting A, Maron R, Sharpe AH, Kelley VR. Costimulation by B7-1 and B7-2 is required for autoimmune disease in MRL-Faslpr mice. *J Immunol.* 2000;164(11):6046-6056.
95. Nocentini G, Giunchi L, Ronchetti S, et al. A new member of the tumor necrosis factor/nerve growth factor receptor family inhibits T cell receptor-induced apoptosis. *Proc Natl Acad Sci U S A.* 1997;94(12):6216-6221.
96. Gurney AL, Marsters SA, Huang RM, et al. Identification of a new member of the tumor necrosis factor family and its receptor, a human ortholog of mouse GITR. *Curr Biol.* 1999;9(4):215-218.
97. Kwon B, Yu KY, Ni J, et al. Identification of a novel activation-inducible protein of the tumor necrosis factor receptor superfamily and its ligand. *J Biol Chem.* 1999;274(10):6056-6061.
98. Kwon BS, Weissman SM. cDNA sequences of two inducible T-cell genes. *Proc Natl Acad Sci U S A.* 1989;86(6):1963-1967.
99. Pollok KE, Kim YJ, Zhou Z, et al. Inducible T cell antigen 4-1BB. Analysis of expression and function. *J Immunol.* 1993;150(3):771-781.
100. Saoulli K, Lee SY, Cannons JL, et al. CD28-independent, TRAF2-dependent costimulation of resting T cells by 4-1BB ligand. *J Exp Med.* 1998;187(11):1849-1862.
101. Bigler RD, Bushkin Y, Chiorazzi N. S152 (CD27). A modulating disulfide-linked T cell activation antigen. *J Immunol.* 1988;141(1):21-28.
102. Camerini D, Walz G, Loenen WA, Borst J, Seed B. The T cell activation antigen CD27 is a member of the nerve growth factor/tumor necrosis factor receptor gene family. *J Immunol.* 1991;147(9):3165-3169.
103. de Jong R, Loenen WA, Brouwer M, et al. Regulation of expression of CD27, a T cell-specific member of a novel family of membrane receptors. *J Immunol.* 1991;146(8):2488-2494.
104. Goodwin RG, Alderson MR, Smith CA, et al. Molecular and biological characterization of a ligand for CD27 defines a new family of cytokines with homology to tumor necrosis factor. *Cell.* 1993;73(3):447-456.
105. Spriggs MK, Fanslow WC, Armitage RJ, Belmont J. The biology of the human ligand for CD40. *J Clin Immunol.* 1993;13(6):373-380.
106. Stamenkovic I, Clark EA, Seed B. A B-lymphocyte activation molecule related to the nerve growth factor receptor and induced by cytokines in carcinomas. *EMBO J.* 1989;8(5):1403-1410.
107. Grewal IS, Flavell RA. The role of CD40 ligand in costimulation and T-cell activation. *Immunol Rev.* 1996;153:85-106.
108. Michot JM, Bigenwald C, Champiat S, et al. Immune-related adverse events with immune checkpoint blockade: a comprehensive review. *Eur J Cancer.* 2016;54:139-148.
109. Postow MA, Sidlow R, Hellmann MD. Immune-Related Adverse Events Associated with Immune Checkpoint Blockade. *N Engl J Med.* 2018;378(2):158-168.

110. Genovese MC, Becker J-C, Schiff M, et al. Abatacept for Rheumatoid Arthritis Refractory to Tumor Necrosis Factor α Inhibition. *New England Journal of Medicine.* 2005;353(11):1114-1123.
111. Vincenti F, Larsen C, Durrbach A, et al. Costimulation Blockade with Belatacept in Renal Transplantation. *New England Journal of Medicine.* 2005;353(8):770-781.
112. Fleischer J, Soeth E, Reiling N, Grage-Griebenow E, Flad HD, Ernst M. Differential expression and function of CD80 (B7-1) and CD86 (B7-2) on human peripheral blood monocytes. *Immunology.* 1996;89(4):592-598.
113. Hathcock KS, Laszlo G, Pucillo C, Linsley P, Hodes RJ. Comparative analysis of B7-1 and B7-2 costimulatory ligands: expression and function. *J Exp Med.* 1994;180(2):631-640.
114. Esensten JH, Helou YA, Chopra G, Weiss A, Bluestone JA. CD28 Costimulation: From Mechanism to Therapy. *Immunity.* 2016;44(5):973-988.
115. Elloso MM, Scott P. Expression and contribution of B7-1 (CD80) and B7-2 (CD86) in the early immune response to Leishmania major infection. *J Immunol.* 1999;162(11):6708-6715.
116. Linsley PS, Greene JL, Brady W, Bajorath J, Ledbetter JA, Peach R. Human B7-1 (CD80) and B7-2 (CD86) bind with similar avidities but distinct kinetics to CD28 and CTLA-4 receptors. *Immunity.* 1994;1(9):793-801.
117. Sigal LJ, Reiser H, Rock KL. The role of B7-1 and B7-2 costimulation for the generation of CTL responses in vivo. *J Immunol.* 1998;161(6):2740-2745.
118. Suresh M, Whitmire JK, Harrington LE, et al. Role of CD28-B7 interactions in generation and maintenance of CD8 T cell memory. *J Immunol.* 2001;167(10):5565-5573.
119. Okano M, Azuma M, Yoshino T, et al. Differential role of CD80 and CD86 molecules in the induction and the effector phases of allergic rhinitis in mice. *Am J Respir Crit Care Med.* 2001;164(8 Pt 1):1501-1507.
120. Grujic M, Bartholdy C, Remy M, Pinschewer DD, Christensen JP, Thomsen AR. The role of CD80/CD86 in generation and maintenance of functional virus-specific CD8+ T cells in mice infected with lymphocytic choriomeningitis virus. *J Immunol.* 2010;185(3):1730-1743.
121. Zhang P, Martin M, Yang QB, Michalek SM, Katz J. Role of B7 costimulatory molecules in immune responses and T-helper cell differentiation in response to recombinant HagB from Porphyromonas gingivalis. *Infect Immun.* 2004;72(2):637-644.
122. Subauste CS, de Waal Malefyt R, Fuh F. Role of CD80 (B7.1) and CD86 (B7.2) in the immune response to an intracellular pathogen. *J Immunol.* 1998;160(4):1831-1840.
123. Lumsden JM, Roberts JM, Harris NL, Peach RJ, Ronchese F. Differential requirement for CD80 and CD80/CD86-dependent costimulation in the lung immune response to an influenza virus infection. *J Immunol.* 2000;164(1):79-85.
124. Sabzevari H, Kantor J, Jaigirdar A, et al. Acquisition of CD80 (B7-1) by T cells. *J Immunol.* 2001;166(4):2505-2513.
125. Tatari-Calderone Z, Semnani RT, Nutman TB, Schlom J, Sabzevari H. Acquisition of CD80 by human T cells at early stages of activation: functional involvement of CD80 acquisition in T cell to T cell interaction. *J Immunol.* 2002;169(11):6162-6169.
126. Schwartz RH. Costimulation of T lymphocytes: the role of CD28, CTLA-4, and B7/BB1 in interleukin-2 production and immunotherapy. *Cell.* 1992;71(7):1065-1068.

127. Pedicord VA, Montalvo W, Leiner IM, Allison JP. Single dose of anti-CTLA-4 enhances CD8+ T-cell memory formation, function, and maintenance. *Proc Natl Acad Sci U S A.* 2011;108(1):266-271.
128. Eagar TN, Karandikar NJ, Bluestone JA, Miller SD. The role of CTLA-4 in induction and maintenance of peripheral T cell tolerance. *Eur J Immunol.* 2002;32(4):972-981.
129. Fecteau S, Basadonna GP, Freitas A, Ariyan C, Sayegh MH, Rothstein DM. CTLA-4 up-regulation plays a role in tolerance mediated by CD45. *Nat Immunol.* 2001;2(1):58-63.
130. Blackburn SD, Shin H, Haining WN, et al. Coregulation of CD8+ T cell exhaustion by multiple inhibitory receptors during chronic viral infection. *Nat Immunol.* 2009;10(1):29-37.
131. Kaufmann DE, Walker BD. PD-1 and CTLA-4 inhibitory cosignaling pathways in HIV infection and the potential for therapeutic intervention. *J Immunol.* 2009;182(10):5891-5897.
132. Wherry EJ. T cell exhaustion. *Nat Immunol.* 2011;12(6):492-499.
133. Baitsch L, Legat A, Barba L, et al. Extended co-expression of inhibitory receptors by human CD8 T-cells depending on differentiation, antigen-specificity and anatomical localization. *PLoS One.* 2012;7(2):e30852.
134. Chambers CA, Sullivan TJ, Allison JP. Lymphoproliferation in CTLA-4-deficient mice is mediated by costimulation-dependent activation of CD4+ T cells. *Immunity.* 1997;7(6):885-895.
135. Takahashi T, Tagami T, Yamazaki S, et al. Immunologic self-tolerance maintained by CD25(+)CD4(+) regulatory T cells constitutively expressing cytotoxic T lymphocyte-associated antigen 4. *J Exp Med.* 2000;192(2):303-310.
136. Walker LS, Sansom DM. Confusing signals: recent progress in CTLA-4 biology. *Trends Immunol.* 2015;36(2):63-70.
137. Callahan MK, Wolchok JD, Allison JP. Anti-CTLA-4 antibody therapy: immune monitoring during clinical development of a novel immunotherapy. *Semin Oncol.* 2010;37(5):473-484.
138. Egen JG, Allison JP. Cytotoxic T lymphocyte antigen-4 accumulation in the immunological synapse is regulated by TCR signal strength. *Immunity.* 2002;16(1):23-35.
139. Peggs KS, Quezada SA, Chambers CA, Korman AJ, Allison JP. Blockade of CTLA-4 on both effector and regulatory T cell compartments contributes to the antitumor activity of anti-CTLA-4 antibodies. *J Exp Med.* 2009;206(8):1717-1725.
140. Tang F, Du X, Liu M, Zheng P, Liu Y. Anti-CTLA-4 antibodies in cancer immunotherapy: selective depletion of intratumoral regulatory T cells or checkpoint blockade? *Cell Biosci.* 2018;8:30.
141. Bertrand A, Kostine M, Barnetche T, Truchetet ME, Schaeverbeke T. Immune related adverse events associated with anti-CTLA-4 antibodies: systematic review and meta-analysis. *BMC Med.* 2015;13:211.
142. Fecher LA, Agarwala SS, Hodi FS, Weber JS. Ipilimumab and its toxicities: a multidisciplinary approach. *Oncologist.* 2013;18(6):733-743.
143. Tarhini A. Immune-mediated adverse events associated with ipilimumab ctla-4 blockade therapy: the underlying mechanisms and clinical management. *Scientifica (Cairo).* 2013;2013:857519.

144. Anderson DE, Bieganowska KD, Bar-Or A, et al. Paradoxical inhibition of T-cell function in response to CTLA-4 blockade; heterogeneity within the human T-cell population. *Nat Med.* 2000;6(2):211-214.
145. Chaperot L, Plumas J, Jacob MC, et al. Functional expression of CD80 and CD86 allows immunogenicity of malignant B cells from non-Hodgkin's lymphomas. *Exp Hematol.* 1999;27(3):479-488.
146. Pope B, Brown RD, Gibson J, Yuen E, Joshua D. B7-2-positive myeloma: incidence, clinical characteristics, prognostic significance, and implications for tumor immunotherapy. *Blood.* 2000;96(4):1274-1279.
147. Suvas S, Singh V, Sahdev S, Vohra H, Agrewala JN. Distinct Role of CD80 and CD86 in the Regulation of the Activation of B Cell and B Cell Lymphoma. *Journal of Biological Chemistry.* 2002;277(10):7766-7775.
148. Czuczman MS, Thall A, Witzig TE, et al. Phase I/II study of galiximab, an anti-CD80 antibody, for relapsed or refractory follicular lymphoma. *J Clin Oncol.* 2005;23(19):4390-4398.
149. Karandikar NJ, Vanderlugt CL, Eagar T, Tan L, Bluestone JA, Miller SD. Tissue-specific up-regulation of B7-1 expression and function during the course of murine relapsing experimental autoimmune encephalomyelitis. *J Immunol.* 1998;161(1):192-199.
150. Herold KC, Vezys V, Koons A, Lenschow D, Thompson C, Bluestone JA. CD28/B7 costimulation regulates autoimmune diabetes induced with multiple low doses of streptozotocin. *J Immunol.* 1997;158(2):984-991.
151. Yeung MY, Najafian N, Sayegh MH. Targeting CD28 to prevent transplant rejection. *Expert Opin Ther Targets.* 2014;18(2):225-242.
152. Popp F, Semela D, von Kempis J, Mueller RB. Improvement of primary biliary cholangitis (PBC) under treatment with sulfasalazine and abatacept. *BMJ Case Rep.* 2018;2018.
153. Vincenti F, Blancho G, Durrbach A, et al. Five-year safety and efficacy of belatacept in renal transplantation. *J Am Soc Nephrol.* 2010;21(9):1587-1596.
154. Ford ML, Adams AB, Pearson TC. Targeting co-stimulatory pathways: transplantation and autoimmunity. *Nat Rev Nephrol.* 2014;10(1):14-24.
155. NULOJIX® (belatacept) [package insert]. Princeton, NJ: Bristol-Myers Squibb Company; 2011.
156. The UniProt Consortium. UniProt: the universal protein knowledgebase. *Nucleic Acids Research.* 2017;45(D1):D158-D169.
157. Williams AF, Barclay AN. The Immunoglobulin Superfamily—Domains for Cell Surface Recognition. *Annual Review of Immunology.* 1988;6(1):381-405.
158. Linsley PS, Peach R, Gladstone P, Bajorath J. Extending the B7 (CD80) gene family. *Protein Science.* 1994;3(8):1341-1343.
159. Bhatia S, Edidin M, Almo SC, Nathenson SG. Different cell surface oligomeric states of B7-1 and B7-2: Implications for signaling. *Proceedings of the National Academy of Sciences.* 2005;102(43):15569.
160. Zhang X, Schwartz J-CD, Almo SC, Nathenson SG. Crystal structure of the receptor-binding domain of human B7-2: Insights into organization and signaling. *Proceedings of the National Academy of Sciences.* 2003;100(5):2586.
161. Fargeas CA, Truneh A, Reddy M, Hurle M, Sweet R, Sékaly RP. Identification of residues in the V domain of CD80 (B7-1) implicated in functional interactions with CD28 and CTLA4. *Journal of Experimental Medicine.* 1995;182(3):667-675.

162. Metzler WJ, Bajorath J, Fenderson W, et al. Solution structure of human CTLA-4 and delineation of a CD80/CD86 binding site conserved in CD28. *Nature Structural Biology.* 1997;4:527.
163. Peach RJ, Bajorath J, Naemura J, et al. Both Extracellular Immunoglobin-like Domains of CD80 Contain Residues Critical for Binding T Cell Surface Receptors CTLA-4 and CD28. *Journal of Biological Chemistry.* 1995;270(36):21181-21187.
164. Wang S, Veldman GM, Stahl M, Xing Y, Tobin JF, Erbe DV. Antibodies to B7.1 define the GFCC′C″ face of the N-terminal domain as critical for co-stimulatory interactions. *Immunology Letters.* 2002;83(2):77-83.
165. Girard T, Gaucher D, El-Far M, Breton G, Sékaly R-P. CD80 and CD86 IgC domains are important for quaternary structure, receptor binding and co-signaling function. *Immunology Letters.* 2014;161(1):65-75.
166. Evans EJ, Esnouf RM, Manso-Sancho R, et al. Crystal structure of a soluble CD28-Fab complex. *Nature Immunology.* 2005;6:271.
167. Ganesan A, Moon TC, Barakat KH. Revealing the atomistic details behind the binding of B7–1 to CD28 and CTLA-4: A comprehensive protein-protein modelling study. *Biochimica et Biophysica Acta (BBA) - General Subjects.* 2018;1862(12):2764-2778.
168. Collins AV, Brodie DW, Gilbert RJC, et al. The Interaction Properties of Costimulatory Molecules Revisited. *Immunity.* 2002;17(2):201-210.
169. Sanchez-Lockhart M, Rojas AV, Fettis MM, et al. T Cell Receptor Signaling Can Directly Enhance the Avidity of CD28 Ligand Binding. *PLOS ONE.* 2014;9(2):e89263.
170. Korhonen R, Moilanen E. Abatacept, a Novel CD80/86–CD28 T Cell Co-stimulation Modulator, in the Treatment of Rheumatoid Arthritis. *Basic & Clinical Pharmacology & Toxicology.* 2009;104(4):276-284.
171. Archdeacon P, Dixon C, Belen O, Albrecht R, Meyer J. Summary of the US FDA Approval of Belatacept. *American Journal of Transplantation.* 2012;12(3):554-562.
172. Gardner D, Jeffery LE, Sansom DM. Understanding the CD28/CTLA-4 (CD152) Pathway and Its Implications for Costimulatory Blockade. *American Journal of Transplantation.* 2014;14(9):1985-1991.
173. Poirier N, Blancho G, Vanhove B. A more selective costimulatory blockade of the CD28-B7 pathway. *Transplant International.* 2011;24(1):2-11.
174. Davis PM, Abraham R, Xu L, Nadler SG, Suchard SJ. Abatacept binds to the Fc receptor CD64 but does not mediate complement-dependent cytotoxicity or antibody-dependent cellular cytotoxicity. *The Journal of Rheumatology.* 2007;34(11):2204.
175. Nüßlein HG, Alten R, Galeazzi M, et al. Real-world effectiveness of abatacept for rheumatoid arthritis treatment in European and Canadian populations: a 6-month interim analysis of the 2-year, observational, prospective ACTION study. *BMC Musculoskeletal Disorders.* 2014;15(1):14.
176. Melvin G, Sandhiya S, Subraja K. Belatacept: A worthy alternative to cyclosporine? *Journal of Pharmacology and Pharmacotherapeutics.* 2012;3(1):90-92.
177. Ville S, Cantarovich D. Belatacept and Autoimmune Adverse Events. *Transplantation.* 2018;102(7).
178. Schwarz C, Mahr B, Muckenhuber M, Wekerle T. Belatacept/CTLA4Ig: an update and critical appraisal of preclinical and clinical results. *Expert Review of Clinical Immunology.* 2018;14(7):583-592.

179. Bhat S, Czuczman MS. Galiximab: a review. *Expert Opinion on Biological Therapy.* 2010;10(3):451-458.
180. Gottlieb AB, Lebwohl M, Totoritis MC, et al. Clinical and histologic response to single-dose treatment of moderate to severe psoriasis with an anti-CD80 monoclonal antibody. *Journal of the American Academy of Dermatology.* 2002;47(5):692-700.
181. Czuczman MS, Leonard JP, Jung S, et al. Phase II trial of galiximab (anti-CD80 monoclonal antibody) plus rituximab (CALGB 50402): Follicular Lymphoma International Prognostic Index (FLIPI) score is predictive of upfront immunotherapy responsiveness. *Annals of Oncology.* 2012;23(9):2356-2362.
182. Leonard JP, Friedberg JW, Younes A, et al. A phase I/II study of galiximab (an anti-CD80 monoclonal antibody) in combination with rituximab for relapsed or refractory, follicular lymphoma. *Annals of Oncology.* 2007;18(7):1216-1223.
183. Patnaik A, Kang SP, Rasco D, et al. Phase I Study of Pembrolizumab (MK-3475; Anti-PD-1 Monoclonal Antibody) in Patients with Advanced Solid Tumors. *Clin Cancer Res.* 2015;21(19):4286-4293.
184. Vanella V, Festino L, Strudel M, Simeone E, Grimaldi AM, Ascierto PA. PD-L1 inhibitors in the pipeline: Promise and progress. *Oncoimmunology.* 2017;7(1):e1365209.
185. Ribas A. Clinical Development of the Anti–CTLA-4 Antibody Tremelimumab. *Seminars in Oncology.* 2010;37(5):450-454.
186. A Phase 1 Study of TSR-022, an Anti-TIM-3 Monoclonal Antibody, in Patients With Advanced Solid Tumors (AMBER). U.S. National Library of Medicine. https://ClinicalTrials.gov/show/NCT02817633. Accessed July 18, 2019.
187. MEDI9447 Alone and in Combination With MEDI4736 in Adult Subjects With Select Advanced Solid Tumors. U.S. National Library of Medicine. https://ClinicalTrials.gov/show/NCT02503774. Accessed July 18, 2019.
188. A Study of LY3321367 Alone or With LY3300054 in Participants With Advanced Relapsed/Refractory Solid Tumors. U.S. National Library of Medicine. https://ClinicalTrials.gov/show/NCT03099109. Accessed July 18, 2019.
189. Safety and Efficacy of MBG453 as Single Agent and in Combination With PDR001 in Patients With Advanced Malignancies. U.S. National Library of Medicine. https://ClinicalTrials.gov/show/NCT02608268. Accessed July 18, 2019.
190. An Investigational Immuno-therapy Study to Assess the Safety, Tolerability and Effectiveness of Anti-LAG-3 With and Without Anti-PD-1 in the Treatment of Solid Tumors. U.S. National Library of Medicine. https://ClinicalTrials.gov/show/NCT01968109. Accessed July 18, 2019.
191. Safety and Efficacy of LAG525 Single Agent and in Combination With PDR001 in Patients With Advanced Malignancies. U.S. National Library of Medicine. https://ClinicalTrials.gov/show/NCT02460224. Accessed July 18, 2019.
192. Safety Study of MGA271 in Refractory Cancer. U.S. National Library of Medicine. https://ClinicalTrials.gov/show/NCT01391143. Accessed July 18, 2019.
193. Intraperitoneal Radioimmunotherapy With 131I-8H9 for Patients With Desmoplastic Small Round Cell Tumors and Other Solid Tumors Involving the Peritoneum. U.S. National Library of Medicine. https://ClinicalTrials.gov/show/NCT01099644. Accessed July 18, 2019.
194. An Investigational Immuno-therapy Study of Experimental Medication BMS-986156, Given by Itself or in Combination With Nivolumab in Patients With Solid Cancers or

Cancers That Have Spread. U.S. National Library of Medicine. https://ClinicalTrials.gov/show/NCT02598960. Accessed July 18, 2019.
195. Phase 1/2 Study Exploring the Safety, Tolerability, and Efficacy of INCAGN01876 Combined With Immune Therapies in Advanced or Metastatic. U.S. National Library of Medicine. Malignancies. https://ClinicalTrials.gov/show/NCT03126110. Accessed July 18, 2019.
196. Phase I/Ib Study of GWN323 Alone and in Combination With PDR001 in Patients With Advanced Malignancies and Lymphomas. U.S. National Library of Medicine. https://ClinicalTrials.gov/show/NCT02740270. Accessed July 18, 2019.
197. Trial of TRX518 (Anti-GITR mAb) in Stage III or IV Malignant Melanoma or Other Solid Tumors. https://ClinicalTrials.gov/show/NCT01239134. Accessed July 18, 2019.
198. Study of MK-4166 and MK-4166 in Combination With Pembrolizumab (MK-3475) in Participants With Advanced Solid Tumors (MK-4166-001). https://ClinicalTrials.gov/show/NCT02132754. Accessed July 18, 2019.
199. Study Of OX40 Agonist PF-04518600 Alone And In Combination With 4-1BB Agonist PF-05082566. U.S. National Library of Medicine. https://ClinicalTrials.gov/show/NCT02315066. Accessed July 18, 2019.
200. A Phase 1/2, Open-Label, Dose-Escalation, Safety Study of INCAGN01949 in Subjects With Advanced or Metastatic Solid Tumors. U.S. National Library of Medicine. https://ClinicalTrials.gov/show/NCT02923349. Accessed July 18, 2019.
201. GSK3174998 Alone or With Pembrolizumab in Subjects With Advanced Solid Tumors (ENGAGE-1). U.S. National Library of Medicine. https://ClinicalTrials.gov/show/NCT02528357. Accessed July 18, 2019.
202. Phase 1 Study of Anti-OX40 in Patients With Advanced Cancer. U.S. National Library of Medicine. https://ClinicalTrials.gov/show/NCT01644968. Accessed July 18, 2019.
203. A Study to Evaluate MEDI0562 in Combination With Immune Therapeutic Agents in Adult Subjects With Advanced Solid Tumors. U.S. National Library of Medicine. . https://ClinicalTrials.gov/show/NCT02705482. Accessed July 18, 2019.
204. A Study to Assess the Safety and Pharmacokinetics of MOXR0916 and Atezolizumab (Also Known as MPDL3280A or Anti-PD-L1) in Participants With Locally Advanced or Metastatic Solid Tumors. U.S. National Library of Medicine. https://ClinicalTrials.gov/show/NCT02410512. Accessed July 18, 2019.
205. Marin-Acevedo JA, Dholaria B, Soyano AE, Knutson KL, Chumsri S, Lou Y. Next generation of immune checkpoint therapy in cancer: new developments and challenges. *J Hematol Oncol.* 2018;11(1):39.
206. Beck A, Wurch T, Bailly C, Corvaia N. Strategies and challenges for the next generation of therapeutic antibodies. *Nat Rev Immunol.* 2010;10(5):345-352.
207. Yang J, Hu L. Immunomodulators targeting the PD-1/PD-L1 protein-protein interaction: From antibodies to small molecules. *Med Res Rev.* 2019;39(1):265-301.
208. Suntharalingam G, Perry MR, Ward S, et al. Cytokine storm in a phase 1 trial of the anti-CD28 monoclonal antibody TGN1412. *N Engl J Med.* 2006;355(10):1018-1028.
209. Andrews A. Treating with Checkpoint Inhibitors—Figure $1 Million per Patient. *Health Economics.* 2015;8(special issue):9.
210. Scott AM, Wolchok JD, Old LJ. Antibody therapy of cancer. *Nat Rev Cancer.* 2012;12(4):278-287.

211. Huck BR, Kotzner L, Urbahns K. Small Molecules Drive Big Improvements in Immuno-Oncology Therapies. *Angew Chem Int Ed Engl.* 2018;57(16):4412-4428.
212. Zhu HF, Li Y. Small-Molecule Targets in Tumor Immunotherapy. *Nat Prod Bioprospect.* 2018;8(4):297-301.
213. Shih HP, Zhang X, Aronov AM. Drug discovery effectiveness from the standpoint of therapeutic mechanisms and indications. *Nat Rev Drug Discov.* 2018;17(1):19-33.
214. Waring MJ, Arrowsmith J, Leach AR, et al. An analysis of the attrition of drug candidates from four major pharmaceutical companies. *Nat Rev Drug Discov.* 2015;14(7):475-486.
215. Ganesan A, Barakat KH. Solubility: A speed–breaker on the drug discovery highway. *MOJ Bioequiv Availab.* 2017;3(3):56-58.
216. Bowes J, Brown AJ, Hamon J, et al. Reducing safety-related drug attrition: the use of in vitro pharmacological profiling. *Nat Rev Drug Discov.* 2012;11(12):909-922.
217. Erbe DV, Wang S, Xing Y, Tobin JF. Small Molecule Ligands Define a Binding Site on the Immune Regulatory Protein B7.1. *Journal of Biological Chemistry.* 2002;277(9):7363-7368.
218. Fine JS, Macosko HD, Justice L, et al. An Inhibitor of CD28–CD80 Interactions Impairs CD28-Mediated Costimulation of Human CD4 T Cells. *Cellular Immunology.* 1999;191(1):49-59.
219. Green NJ, Xiang J, Chen J, et al. Structure–activity studies of a series of dipyrazolo[3,4-b:3′,4′-d]pyridin-3-ones binding to the immune regulatory protein B7.1. *Bioorganic & Medicinal Chemistry.* 2003;11(13):2991-3013.
220. Hegde VR, Puar MS, Dai P, et al. Condensed aromatic peptide family of microbial metabolites, inhibitors of CD28–CD80 interactions. *Bioorganic & Medicinal Chemistry Letters.* 2003;13(3):573-575.
221. Jenh C-H, Zhang M, Wiekowski M, et al. Development of a CD28 Receptor Binding-Based Screen and Identification of a Biologically Active Inhibitor. *Analytical Biochemistry.* 1998;256(1):47-55.
222. Hida T. (Oxo-)xanthene derivatives, their preparation and their use as immunomodulators. *EP0795554A3.* Takeda ChemicalINdustries, Ltd.
223. Neal Jeffrey Green, Steve Yikkai Tam, Jason ShaoyunXiang, et al. Dihydrodipyrazolopyridinone inhibitors of B7-1. *US6900223B2.* Wyeth.
224. Uvebrant K, Da Graça Thrige D, Rosén A, et al. Discovery of Selective Small-Molecule CD80 Inhibitors. *Journal of Biomolecular Screening.* 2007;12(4):464-472.
225. Huxley P, Sutton DH, Debnam P, et al. High-Affinity Small Molecule Inhibitors of T Cell Costimulation: Compounds for Immunotherapy. *Chemistry & Biology.* 2004;11(12):1651-1658.
226. Per Axel BJÖRK, Tomas Fex, Lars Olof Göran Pettersson, Poul Sorensen, Thrige DDG. Novel immunomodulating compounds. *WO2003004495A1.* Active Biotech AB.
227. Matthews IR. Immunomodulating heterocyclic compounds. *US7276505B2.* Medigene AG.
228. Imaginot. Preliminary review of RhuDex® as a potential Surge Dose® candidate. http://www.imaginot.com.au/downloads/95301fbd-5a42-4036-8d0d-f5b3bfa947eb.pdf. Accessed July 18, 2019.
229. Medigine. RhuDex®: Outlicensed to Dr. Falk Pharma GmbH. https://www.medigene.com/pipeline/other-products/. Accessed July 18, 2019.
230. Matthews IR. Immunomodulating oxopyrrazolocinnolines as CD80 inhibitors. *US20090062289A1.* Avidex Limited.

231. Matthews IR. Salt of the CD80 antagonist. *US20120004237A1.* Medigene AG.
232. Guzik K, Zak KM, Grudnik P, et al. Small-Molecule Inhibitors of the Programmed Cell Death-1/Programmed Death-Ligand 1 (PD-1/PD-L1) Interaction via Transiently Induced Protein States and Dimerization of PD-L1. *J Med Chem.* 2017;60(13):5857-5867.
233. Waldner H. The role of innate immune responses in autoimmune disease development. *Autoimmunity Reviews.* 2009;8(5):400-404.
234. Sledzinska A, Menger L, Bergerhoff K, Peggs KS, Quezada SA. Negative immune checkpoints on T lymphocytes and their relevance to cancer immunotherapy. *Mol Oncol.* 2015;9(10):1936-1965.
235. Bluestone JA, Bour-Jordan H, Cheng M, Anderson M. T cells in the control of organ-specific autoimmunity. *J Clin Invest.* 2015;125(6):2250-2260.
236. Konig R, Huang LY, Germain RN. MHC class II interaction with CD4 mediated by a region analogous to the MHC class I binding site for CD8. *Nature.* 1992;356(6372):796-798.
237. Boussiotis VA, Freeman GJ, Gribben JG, Nadler LM. The role of B7-1/B7-2:CD28/CLTA-4 pathways in the prevention of anergy, induction of productive immunity and down-regulation of the immune response. *Immunol Rev.* 1996;153:5-26.
238. Freedman AS, Freeman GJ, Rhynhart K, Nadler LM. Selective induction of B7/BB-1 on interferon-γ stimulated monocytes: A potential mechanism for amplification of T cell activation through the CD28 pathway. *Cellular Immunology.* 1991;137(2):429-437.
239. Stack RM, Lenschow DJ, Gray GS, Bluestone JA, Fitch FW. IL-4 treatment of small splenic B cells induces costimulatory molecules B7-1 and B7-2. *J Immunol.* 1994;152(12):5723-5733.
240. Freeman GJ, Freedman AS, Segil JM, Lee G, Whitman JF, Nadler LM. B7, a new member of the Ig superfamily with unique expression on activated and neoplastic B cells. *The Journal of Immunology.* 1989;143(8):2714.
241. Zhang X, Schwartz JC, Almo SC, Nathenson SG. Crystal structure of the receptor-binding domain of human B7-2: insights into organization and signaling. *Proc Natl Acad Sci U S A.* 2003;100(5):2586-2591.
242. Linsley PS, Bradshaw J, Greene J, Peach R, Bennett KL, Mittler RS. Intracellular trafficking of CTLA-4 and focal localization towards sites of TCR engagement. *Immunity.* 1996;4(6):535-543.
243. van der Merwe PA, Bodian DL, Daenke S, Linsley P, Davis SJ. CD80 (B7-1) binds both CD28 and CTLA-4 with a low affinity and very fast kinetics. *J Exp Med.* 1997;185(3):393-403.
244. Pentcheva-Hoang T, Egen JG, Wojnoonski K, Allison JP. B7-1 and B7-2 selectively recruit CTLA-4 and CD28 to the immunological synapse. *Immunity.* 2004;21(3):401-413.
245. Bhatia S, Edidin M, Almo SC, Nathenson SG. Different cell surface oligomeric states of B7-1 and B7-2: implications for signaling. *Proc Natl Acad Sci U S A.* 2005;102(43):15569-15574.
246. Korhonen R, Moilanen aE. Abatacept, a Novel CD80/86–CD28 T Cell Co-stimulation Modulator, in the Treatment of Rheumatoid Arthritis. *Basic & Clinical Pharmacology & Toxicology.* 2009;104(4):276–284.
247. Zang X, Allison JP. The B7 family and cancer therapy: costimulation and coinhibition. *Clin Cancer Res.* 2007;13(18 Pt 1):5271-5279.
248. Chen R, Ganesan A, Okoye I, et al. Targeting B7-1 in immunotherapy. *Med Res Rev.* 2019.

249. Erbe DV, Wang S, Xing Y, Tobin JF. Small molecule ligands define a binding site on the immune regulatory protein B7.1. *J Biol Chem.* 2002;277(9):7363-7368.
250. Huxley P, Sutton DH, Debnam P, et al. High-affinity small molecule inhibitors of T cell costimulation: compounds for immunotherapy. *Chem Biol.* 2004;11(12):1651-1658.
251. Taddio MF, Mu L, Castro Jaramillo CA, et al. Synthesis and Structure-Affinity Relationship of Small Molecules for Imaging Human CD80 by Positron Emission Tomography. *J Med Chem.* 2019;62(17):8090-8100.
252. Ganesan A, Ahmed M, Okoye I, et al. Comprehensive in vitro characterization of PD-L1 small molecule inhibitors. *Sci Rep.* 2019;9(1):12392.
253. Genheden S, Ryde U. The MM/PBSA and MM/GBSA methods to estimate ligand-binding affinities. *Expert Opin Drug Discov.* 2015;10(5):449-461.
254. Buchan DWA, Jones DT. The PSIPRED Protein Analysis Workbench: 20 years on. *Nucleic Acids Res.* 2019;47(W1):W402-W407.
255. Sali A, Blundell TL. Comparative protein modelling by satisfaction of spatial restraints. *J Mol Biol.* 1993;234(3):779-815.
256. Pettersen EF, Goddard TD, Huang CC, et al. UCSF Chimera--a visualization system for exploratory research and analysis. *J Comput Chem.* 2004;25(13):1605-1612.
257. Dolinsky TJ, Nielsen JE, McCammon JA, Baker NA. PDB2PQR: an automated pipeline for the setup of Poisson-Boltzmann electrostatics calculations. *Nucleic Acids Res.* 2004;32(Web Server issue):W665-667.
258. Park SJ, Lee J, Qi Y, et al. CHARMM-GUI Glycan Modeler for modeling and simulation of carbohydrates and glycoconjugates. *Glycobiology.* 2019;29(4):320-331.
259. Case DA, Cheatham TE, 3rd, Darden T, et al. The Amber biomolecular simulation programs. *J Comput Chem.* 2005;26(16):1668-1688.
260. Phillips JC, Braun R, Wang W, et al. Scalable molecular dynamics with NAMD. *J Comput Chem.* 2005;26(16):1781-1802.
261. Roe DR, Cheatham TE, 3rd. PTRAJ and CPPTRAJ: Software for Processing and Analysis of Molecular Dynamics Trajectory Data. *J Chem Theory Comput.* 2013;9(7):3084-3095.
262. Ngan CH, Hall DR, Zerbe B, Grove LE, Kozakov D, Vajda S. FTSite: high accuracy detection of ligand binding sites on unbound protein structures. *Bioinformatics.* 2012;28(2):286-287.
263. _Molecular Operating Environment (MOE)_, 2019.01; Chemical Computing Group ULC, 1010 Sherbrooke St. West, Suite #910, Montreal, QC, Canada, H3A 2R7, **2019**.
264. Stamper CC, Zhang Y, Tobin JF, et al. Crystal structure of the B7-1/CTLA-4 complex that inhibits human immune responses. *Nature.* 2001;410(6828):608-611.
265. Kim S, Chen J, Cheng T, et al. PubChem 2019 update: improved access to chemical data. *Nucleic Acids Res.* 2019;47(D1):D1102-D1109.
266. Humphrey W, Dalke A, Schulten K. VMD: visual molecular dynamics. *J Mol Graph.* 1996;14(1):33-38, 27-38.
267. Shao J, Tanner SW, Thompson N, Cheatham TE. Clustering Molecular Dynamics Trajectories: 1. Characterizing the Performance of Different Clustering Algorithms. *J Chem Theory Comput.* 2007;3(6):2312-2334.
268. Davies DL, Bouldin DW. A cluster separation measure. *IEEE Trans Pattern Anal Mach Intell.* 1979;1(2):224-227.

269. Capra JA, Laskowski RA, Thornton JM, Singh M, Funkhouser TA. Predicting protein ligand binding sites by combining evolutionary sequence conservation and 3D structure. *PLoS Comput Biol.* 2009;5(12):e1000585.
270. Jendele L, Krivak R, Skoda P, Novotny M, Hoksza D. PrankWeb: a web server for ligand binding site prediction and visualization. *Nucleic Acids Res.* 2019;47(W1):W345-W349.
271. Yang J, Roy A, Zhang Y. Protein-ligand binding site recognition using complementary binding-specific substructure comparison and sequence profile alignment. *Bioinformatics.* 2013;29(20):2588-2595.
272. Wang Z, Sun H, Yao X, et al. Comprehensive evaluation of ten docking programs on a diverse set of protein-ligand complexes: the prediction accuracy of sampling power and scoring power. *Phys Chem Chem Phys.* 2016;18(18):12964-12975.
273. Greenwald RJ, Freeman GJ, Sharpe AH. The B7 family revisited. *Annu Rev Immunol.* 2005;23:515-548.
274. Ni L, Dong C. New B7 Family Checkpoints in Human Cancers. *Mol Cancer Ther.* 2017;16(7):1203-1211.
275. G J Freeman, A S Freedman, J M Segil GL, J F Whitman, Nadler LM. B7, a new member of the Ig superfamily with unique expression on activated and neoplastic B cells. *The Journal of Immunology.* 1989;143(8):2714-2722.
276. Sorensen HP, Mortensen KK. Advanced genetic strategies for recombinant protein expression in Escherichia coli. *J Biotechnol.* 2005;115(2):113-128.
277. Nagarajan S, Selvaraj P. Expression and characterization of glycolipid-anchored B7-1 (CD80) from baculovirus-infected insect cells: protein transfer onto tumor cells. *Protein Expr Purif.* 1999;17(2):273-281.
278. Chen A, Meyerson HJ, Salvekar A, Tykocinski ML. Non-glycosylated human B7-1(CD80) retains the capacity to bind its counter-receptors. *FEBS Lett.* 1998;428(3):127-134.
279. Kakoulidou M, Giscombe R, Zhao X, Lefvert AK, Wang X. Human Soluble CD80 is generated by alternative splicing, and recombinant soluble CD80 binds to CD28 and CD152 influencing T-cell activation. *Scand J Immunol.* 2007;66(5):529-537.
280. Hesketh AR, Chandra G, Shaw AD, et al. Primary and secondary metabolism, and post-translational protein modifications, as portrayed by proteomic analysis of Streptomyces coelicolor. *Mol Microbiol.* 2002;46(4):917-932.
281. Georgiou G, Valax P. Expression of correctly folded proteins in Escherichia coli. *Curr Opin Biotechnol.* 1996;7(2):190-197.
282. Tokmakov AA, Kurotani A, Takagi T, et al. Multiple post-translational modifications affect heterologous protein synthesis. *J Biol Chem.* 2012;287(32):27106-27116.
283. Rosano GL, Ceccarelli EA. Recombinant protein expression in Escherichia coli: advances and challenges. *Front Microbiol.* 2014;5:172.
284. Daegelen P, Studier FW, Lenski RE, Cure S, Kim JF. Tracing ancestors and relatives of Escherichia coli B, and the derivation of B strains REL606 and BL21(DE3). *J Mol Biol.* 2009;394(4):634-643.
285. Jia B, Jeon CO. High-throughput recombinant protein expression in Escherichia coli: current status and future perspectives. *Open Biol.* 2016;6(8).
286. Hoffmann D, Ebrahimi M, Gerlach D, Salzig D, Czermak P. Reassessment of inclusion body-based production as a versatile opportunity for difficult-to-express recombinant proteins. *Crit Rev Biotechnol.* 2018;38(5):729-744.

287. Gaberc-Porekar V, Menart V. Perspectives of immobilized-metal affinity chromatography. *J Biochem Biophys Methods.* 2001;49(1-3):335-360.
288. Turner P, Holst O, Karlsson EN. Optimized expression of soluble cyclomaltodextrinase of thermophilic origin in Escherichia coli by using a soluble fusion-tag and by tuning of inducer concentration. *Protein Expr Purif.* 2005;39(1):54-60.
289. Siller E, DeZwaan DC, Anderson JF, Freeman BC, Barral JM. Slowing bacterial translation speed enhances eukaryotic protein folding efficiency. *J Mol Biol.* 2010;396(5):1310-1318.
290. Okumura M, Saiki M, Yamaguchi H, Hidaka Y. Acceleration of disulfide-coupled protein folding using glutathione derivatives. *FEBS J.* 2011;278(7):1137-1144.
291. Hwang C, Sinskey AJ, Lodish HF. Oxidized redox state of glutathione in the endoplasmic reticulum. *Science.* 1992;257(5076):1496-1502.
292. Zak KM, Kitel R, Przetocka S, et al. Structure of the Complex of Human Programmed Death 1, PD-1, and Its Ligand PD-L1. *Structure.* 2015;23(12):2341-2348.
293. Hartl FU, Hlodan R, Langer T. Molecular chaperones in protein folding: the art of avoiding sticky situations. *Trends Biochem Sci.* 1994;19(1):20-25.
294. Larsen CP, Pearson TC, Adams AB, et al. Rational development of LEA29Y (belatacept), a high-affinity variant of CTLA4-Ig with potent immunosuppressive properties. *Am J Transplant.* 2005;5(3):443-453.
295. Uvebrant K, da Graca Thrige D, Rosen A, et al. Discovery of selective small-molecule CD80 inhibitors. *J Biomol Screen.* 2007;12(4):464-472.
296. Peach RJ, Bajorath J, Naemura J, et al. Both extracellular immunoglobin-like domains of CD80 contain residues critical for binding T cell surface receptors CTLA-4 and CD28. *J Biol Chem.* 1995;270(36):21181-21187.
297. Schasfoort RBM. Chapter 1 Introduction to Surface Plasmon Resonance. In: *Handbook of Surface Plasmon Resonance (2).* The Royal Society of Chemistry; 2017:1-26.
298. Abdulhalim I, Zourob M, Lakhtakia A. Surface Plasmon Resonance for Biosensing: A Mini-Review. *Electromagnetics.* 2008;28(3):214-242.

APPENDIX A: SURFACE PLASMON RESONANCE ANALYSES OF HUMAN B7-1 AND THREE SMALL-MOLECULE INHIBITORS

A.1 Introduction

Surface Plasmon Resonance (SPR) is a commonly used label-free assay system to evaluate the interaction between an immobilized ligand (usually a drug target) and injected analyte (*e.g.*, small molecules) in real-time. At certain light wavelength and certain angle (resonance angle), the photons of the incident light interact with the free electrons of the metal film, exciting the electromagnetic waves or the surface plasmons near the surface of the metal.[297] The incident light resonates with the surface plasmons, causing a dip in the intensity of the reflective light. The analytes are captured by the ligands immobilized on the chip surface after injection, this leading to the changing of the refractive index and the resonance angle, therefore allowing the measurement of the kinetics of the biomolecular interactions in real-time.

The SPR instruments primarily contain the light source, the sensor chip, and the signal detector. The systems employing the prism, where the metal thin layer is covered on top, to excite the surface plasmons are the most widely used.[298] After the P-polarized light beam is shone through the prism, the light is reflected by the metal surface to the detector. Plotting the sensorgram, one can observe the SPR response with time. Changing the types of the metal chips (*e.g.* CM5 chip, NTA chip, L1 chip, HPA chip), allows a variety of ligands to be immobilized to the metal surface through different coupling methods (*e.g.* amine coupling, thiol coupling).

SPR is well-known to detect the real-time kinetics of the biomolecular interactions, ranging from the protein-protein, protein-DNA, protein-small molecule, protein-lipid interactions, *etc*. The binding of the molecule to the immobilized ligand as well as the binding specificity of the binding partners can also be detected. Furthermore, the concentration or the mass of the bound analytes is proportional to the SPR response, this allows the measurement of the analyte concentrations.

A.2 Experimental Protocol

In this project, I aim to detect the binding of three small-molecule compounds (two known as human B7-1 inhibitors, namely inhibitor 1 and inhibitor 2 and a PD-L1 inhibitor or BMS-103) towards human B7-1 and the corresponding interaction kinetics and binding affinities. The kinetics for the interaction of small molecules with human B7-1 were performed on a Biacore T200 (GE

Healthcare Bio-sciences, Sweden) using Series S Sensor Chip Protein A (GE Healthcare Bio-sciences, Sweden, catalog # 29-1275-56). This recombinant protein A variant only binds to the heavy chain of the Fc domain, ensuring the specific orientation of the ligands. Basically, four steps were involved in a cycle, including the baseline phase (where the system buffer interacts with the sensor chip, generating the baseline), the association phase (where the analytes were injected to the flow cells or channels, forming the complexes), the dissociation phase (where the specific and/or the non-specific bound molecules dissociated from the ligands on the sensor chip) and the regeneration phase (where the remaining analytes were removed from the sensor chip).[297]

The Fc-B7-1 (B71-H5259, Acro Biosystems, MA, USA) was diluted using 1x PBS-P+ (phosphate-buffered saline 1×, Hyclone, Catalog number SH30256.01 enriched with 0.05% Tween-20) containing 2% DMSO (Sigma-Aldrich, ON, Canada) to 4 µg/ml. For the kinetic and affinity analysis, diluted Fc-B7-1 (4 ug/ml) was captured on the protein A chip surface through Fc capture. The contact time and flow rates for the ligand capture were 60 sec and 10 µl/min, respectively. Two channels (also known as flow cells) were used for each experiment, one having the ligand captured and the other without ligand functioning as a reference channel. The contact time and the flow rate of the analytes (three compounds) passing through both these two channels were set as 120 sec and 30 µl/min. These analytes were dissolved using DMSO as stock solutions of 10 µM. Each of the compounds was diluted 50x using 1x PBS-P+ buffer and then further diluted into serial dilutions using 1x PBS-P+ buffer with 2% DMSO. Finally, inhibitor 1, inhibitor 2 and inhibitor-3 were tested at concentrations of 0, 12.5, 50, and 200 nM. As a positive control, His-CTLA4 (Acro biosystem, CT4-H5229) was used as analyte at concentrations of 0, 8.12, 32.47 and 129.87 nM. In another experiment, Fc-PDL-1 (4 ug/ml) (Acro Biosystem, PD1-H5258) was captured on CM5-series S Protein-A chip according to the protocol described above and inhibitor-1, inhibitor-2 and inhibitor-3 were used as analytes to verify the specificity of interaction of inhibitor-1 and inhibitor-2 compounds with Fc-B7-1. The solvent correction was included to avoid the impact of DMSO on surface plasmon effect during binding analysis. The 50% DMSO in 1x PBS-P+ buffer was utilized to wash the channels and control carry-over effects. In order to regenerate the chip surface after each cycle (one-time ligand capture and binding of analyte at a single concentration), 10 mM glycine pH 1.5 (GE Healthcare Bio-sciences, Sweden) was used at a flow rate of 30 µl/min for 30 sec. Kinetic analysis was performed at room temperature (25 °C). Maximum binding response (Rmax) and equilibrium dissociation constant (K_D) values were

computed using Biacore T200 Evaluation software following the 1:1 Langmuir binding model with global fit parameters for solvent-corrected sensorgrams.

A.3 Results of the SPR Analyses

The results show both inhibitor-1 and inhibitor-2 bind with Fc-B7-1 with a R_{max} value of 30.14 RU and 21.95 RU, respectively. The K_D values for the steady-state affinity of binding for inhibitor-1 and inhibitor-2 were 4.87 nM and 15.34 nM, respectively. The positive control His-CTLA4 interacted with captured Fc-B7-1 with a Rmax of 159.8 RU and the K_D value was 1.71 nM. A PDL-1-specific inhibitor-3 did not exhibit interaction with Fc-B7-1.[252] To verify the specificity of binding of inhibitor-1 and inhibitor-2 with Fc-B7.1, we analyzed the binding of inhibitor-1 and inhibitor-2 with captured Fc-PDL-1 taking as an off-target ligand. The binding analysis revealed that inhibitor-1 and inhibitor-2 did not interact with captured Fc-PDL-1, whereas the inhibitor-3 showed binding with Fc-PDL-1 with a Rmax of 20.38 RU and a K_D value of 12.92 nM.[252] The results were shown in Figure A.1.

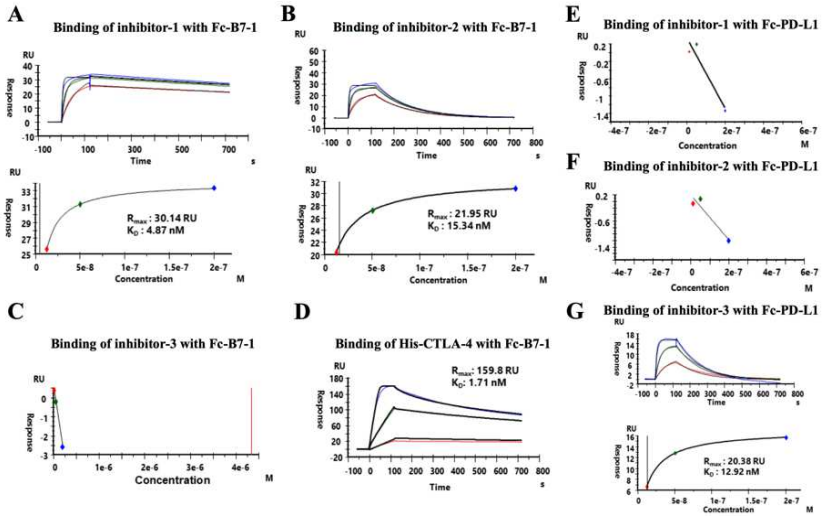

Figure A. 1 Binding of the selected molecules with Fc-B7-1 (A to D) or Fc-PD-L1 (E to F) measured using the SPR technique.

A to D, The Inhibitors 1 to 3, and His-CTLA-4 were allowed to flow over Fc-B7-1 captured on a flow cell as well as on a reference cell of Series S Sensor Chip Protein A at indicated concentrations; E to F, The Inhibitors 1 to 3 were allowed to flow over Fc-PD-L1 captured on Series S Protein A chip as well as on a blank reference cell on Biacore T200. The R_{max} and K_D values were determined by Biacore Evaluation software. The solvent-corrected sensorgrams were presented.